THE ZEBRAFISH *PANNEXIN1A* AND *PANNEXIN1B* OHNOLOGS CONTRIBUTE DIFFERENTIALLY TO SEIZURE PROPAGATION *IN VIVO*

DARIA TASKINA

A THESIS SUBMITTED TO THE FACULTY OF GRADUATE STUDIES IN PARTIAL FULFILLMENT OF THE REQUIREMENTS FOR THE DEGREE OF MASTER OF SCIENCE

GRADUATE PROGRAM IN BIOLOGY

YORK UNIVERSITY

TORONTO, ONTARIO

August 2021

Abstract

Seizures are a hallmark of epilepsy and are associated with many other diseases. However, their molecular determinants are not well understood. A membrane glycoprotein, Pannexin1, has been implicated in seizures for its overexpression in epileptic tissue and the channel's function of extracellular ATP release. Here, we investigated the mechanistic role of ohnologs *panx1a* and *panx1b in-vivo,* in a chemically induced zebrafish seizure model. *Panx1a* and *panx1b* knockout zebrafish lines, and treatment with a Panx1 channel blocker were evaluated for seizure phenotypes across behavioral, molecular, computational, and electrophysiological analyses. Pharmacologically blocking the channel suppressed seizures, while genetic targeting showed both pro- and anti-seizure properties. We propose the involvement of ATP and purinoceptor P2rx7 that drive the two Panx1 channels' differential effects on seizures. By identifying the critical players and their associated molecular processes, we present the Panx1 zebrafish model as a robust platform for seizure investigation in antiepileptic drug discovery.

I dedicate this thesis, my education, and my growth in academia and in life
to my family who are my heart, my strength and my everything

Acknowledgements

I have known for a long time that I wanted to pursue a master's degree, to dive into the field of neuroscience as I have always admired the drive and passion my parents have for research. Looking back to when I have just started, I think of all the people that have gifted me with unconditional support and strength to grow and move forward, to whom I would like to express my utmost gratitude.

First and foremost, I would like to express the sincerest appreciation I have for my supervisor Dr. Zoidl, for his continued and dedicated mentorship for the past few years. I could not have grown as an academic if not for your wholehearted support, ongoing encouragement, and constantly reminding me of the excitement of research. I sincerely believe I could not have had a better mentor in these earliest stages of my academic career, I respect and admire you and I hope to follow your outlook on research in the future.

I am very grateful to have had such a supportive advisor, Dr. Connor. I am thankful for the many times you have provided thorough guidance and teaching me how to think critically about my work. I am utterly grateful to Christiane for her constant guidance, for passing on her vast technical expertise and for aiding me in the lab in many ways I probably do not even fully realize. The lab team, Ryan, Nickie, Paige, Cherie, Ksenia, Anna, Georg S. and Sarah who are amazing colleagues to have, who have provided me with much advice and cherished times.

A special thanks to Paige, with whom I have worked closely on the epilepsy project. You have been a great academic to look up to. I have always admired your intellect and work ethic, and I cherish the guidance you have given me over the last few years.

I am incredibly thankful for Janet F.-M. and Veronica S. for their support at the vivarium. I cannot count the times I have been in debt to your knowledge, help and kindness, and I feel very fortunate to have had the pleasure of working with you.

To my friend Grace, whom I have counted on for emotional support and great friendship throughout my degree, I feel very lucky to have gained you as a close friend.

The Jclub: Becky, Caroline, Harpreet, Katie, and Shir I am utterly grateful for, as you are an amazing, smart, kindhearted and all-around great group of friends I am so lucky to have met during my masters and to have for a long time. Finally, I am utmost thankful for those who are closest to me, Daulton, Arimi and my family who undeniably are my foundation and reason for anything that I do. Thank you.

Table of Contents

List of Abbreviations

µM	micromolar
95%CI	95% Confidence Interval
Å	Angstrom
A43	A-438079 Hydrochloride hydrate
aa	Amino Acid
ATP	Adenosine 5'-triphosphate
AUC	Area Under the Curve
BLAST	Basic Local Alignment Search Tool
C (cys)	Cysteine
Ca^{2+}	Calcium ion
Cl^-	Chloride ion
CNN	Convolutional Neural Network
CNS	Central Nervous System
Cryo-EM	Cryo-Electron Microscopy
CT	Cycle Threshold
C-terminus	carboxyl-terminus
DKO	Double knockout
dpf	Days Post Fertilization
dur	Duration
ECL	Extracellular linker (loop)
EtBr	Ethidium Bromide
fps	Frames Per Second
$GABA_A$	γ-aminobutyric acid type A receptor
GFP	Green Fluorescent Protein
HC	Horizontal Cell
IEG	Immediate Early Gene
ICL	Intracellular linker
IL-1β	Interleukin 1 beta
K^+	Potassium ion
kDa	kilodalton
KNN	K-Nearest Neighbour
LFP	Local Field Potential

min	minutes
ML	Machine Learning
mPanx1	mouse Pannexin1
N (asn)	Asparagine
NaCl	Sodium Chloride
NMDAR	N-Methyl-D-aspartate Receptor
NN	Neural Network
N-terminus	amino-terminus
OMR	Optomotor Response
Panx1	Pannexin1
Pb	Probenecid
PCA	Principal Component Analysis
PCR	Polymerase Chain Reaction
ppm	Parts Per Million (mg/L)
pS	picoSiemens
PTZ	Pentylenetetrazole
R (arg)	Arginine
RF	Random Forest
RM	Repeated Measurements
RO	Reverse Osmosis
RT-qPCR	Reverse Transcription - quantitative PCR
SD	Standard Deviation
sec	Seconds
SEM	Standard Error Mean
SLE	Seizure-Like Event
SOM	Self Organization Map
SVM	Support Vector Machine
TAE	Tris acetate EDTA
TALEN	Transcription Activator-Like Effector Nuclease
TL	Tupfel long fin
TM	Transmembrane
VPA	Valproic acid
W (trp)	Tryptophan
WT	Wild-type

List of Tables

List of Figures

1. Introduction

The dynamic communication between the neuronal and glial cells in the central nervous system (CNS) is vastly complex and multimodal. The intercellular interactions are achieved via autocrine/paracrine, endocrine, and cell-to-cell gap junction mediated signaling. Synaptic signaling through neurotransmitter release is well described in the nervous system, however, another mode of paracrine signaling involving membrane channels Pannexins is not well understood. Their omnipresent expression and multifaceted function have made the family of glycoproteins of interest in many physiological and pathological conditions. Here, the most extensively characterized member of the family, Pannexin1, is investigated for its unresolved contributing role to seizure propagation.

1.1 Pannexin1: from discovery to structure, localization, and function

1.1.1 Panx1 discovery

Pannexin1 (Panx1) is an integral membrane protein part of the Pannexin glycoprotein family. First identified in the 2000s in the search for human orthologous genes, the Pannexin family was discovered via BLAST search in the GenBank for limited sequence similarities with invertebrate gap junctions, innexins (Panchin et al., 2000). Due to their ubiquitous expression, the name ‘pannexin’ was given, as in ‘pan’ for Latin prefix meaning ‘all-inclusive’ and nexus for ‘connection’.

1.1.2 Panx1 protomer and channel structure

Pannexins were predicted to be homologs to innexins and share structural similarities of four transmembrane regions and conserved cysteine residues (Baranova et al., 2004). Located on human chromosome 11q14.3, the *Panx1* gene contains five exons and four introns. Panx1 protomer consists of four transmembrane helices (TM1 to 4), two extracellular linkers/loops (ECL1 and ECL2), one intracellular linker/loop (ICL1) and intracellular N and C termini (Baranova et al., 2004). Recently, the cryo-EM structure of human and frog Panx1’s were resolved (**Fig. 1**) (Jin et al., 2020; Michalski et al., 2020; Mou et al., 2020). The human Panx1 was measured to be ~105Å long and ~100Å wide and confirmed the previously described topological structure (Jin et al., 2020). Despite being predicted to form a hexameric channel due to Panx1’s similar membrane topology as other large-pore forming channels, single-channel recordings and negative stain electron microscopy (Boassa et al., 2007; Chiu et al., 2017), the

cryo-EM structures revealed that Panx1 assembles into a heptameric channel. The inter-subunit interactions at ECL1, TM1 to TM1 and TM2 to TM4, and N-termini are responsible for consecutively forming the seven protomers into an assembly (Michalski et al., 2020). The inner surface of the pore that constitutes the substrate conduction path, is comprised of TM1, E1H (α-helix of ECL1) and IH1 (one of the α-helices of ICL1) (Jin et al., 2020). The Tryptophan residue W74 on E1H is located on the narrowest part of the pore, creating a diameter of 9.4Å. W74 has been implicated to be involved in the channel's ATP release activity, due to its interaction with channel blocker carbenoxolone (Chekeni et al., 2010). Additionally, mutations in the W74 site disrupted the ion selectivity of the channel. The amino acids forming the surface of the pore are uncharged, except for an Arginine residue R75 located near W74. Positively charged R75 has been proposed to contribute to anion-selectivity, as mutations to the site diminished the selectivity (Michalski et al., 2020) or ATP inhibition during negative feedback (Qiu et al., 2012; Qiu & Dahl, 2009). W74 and R75 were found to be located 4Å apart and were suggested to form a cation-π interaction between Tryptophan's benzene ring and Arginine's positive charge based on experimental evidence of the two sites' co-dependency in the channel's proper ion selectivity (Michalski et al., 2020).

Fig. 1 Pannexin1 cryo-EM channel and protomer structures.

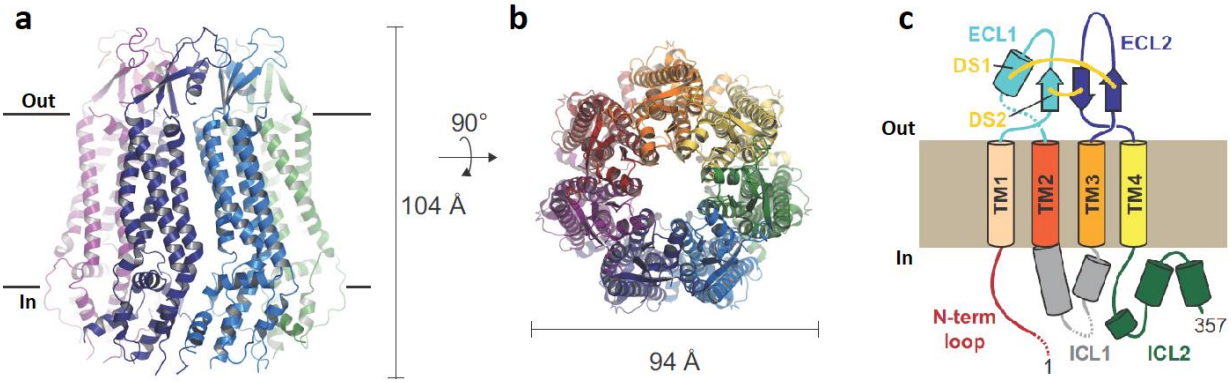

Xenopus Pannexin1 (frPanx1) cryo-EM structure was resolved. Depicted, the channel's side profile parallel to the membrane (**a**), heptameric structure viewed from the extracellular space (**b**), and protomer's topological structure (**c**). *Figures adapted from (Michalski et al., 2020).

1.1.3 Tissue expression and cell localization

Panx1 is ubiquitously expressed in several systems and tissue types; abundantly in the central nervous system, skeletal muscle, heart, skin, spleen, testis and ovary, moderately in the placenta, thymus, prostate and small intestine (Baranova et al., 2004; Barbe et al., 2003; Penuela et al., 2007). They are present in neuronal cells (Barbe et al., 2003), astrocytes (Suadicani et al., 2012), erythrocytes (Locovei, Bao, et al., 2006), evidence stemming from changes to electrophysiological data and ATP-release mechanism with modifications to or blockage of Panx1 in these cell types. Panx1 localizes in the plasma membrane as a non-junctional channel due to the glycosylation of the N254 site at ECL2 (Boassa et al., 2007; Penuela et al., 2007). Mutations to the site or non-glycosylated forms of the protein failed to reach the membrane, and pharmacological blocking of the site resulted in the accumulation of Panx1 in the cytoplasm. Although Pannexins were originally thought to belong to the gap junction family supported by scarce experimental evidence, it is now well accepted that Panx1 is not a part of the gap junction family and form a singular channel (Penuela et al., 2013). Panx1's plasma membrane position, localization in postsynaptic density that separates the channel from opposing membrane, and glycosylation on the extracellular surface structure discouraging docking of another oligomer, all provide compelling evidence (Boassa et al., 2007; Sosinsky et al., 2011).

1.1.4 Panx1 function and physiological relevance

Panx1 channels are stimulated by several physiological and pathological conditions including voltage, mechanical stress, oxygen deprivation, elevated Ca^{2+} and K^{+} concentrations, glutamate, and ligand-triggered via binding of ATP to associated pathways such as the purinergic receptors P2X and P2Y (Chiu et al., 2018; Iglesias et al., 2008; Locovei, Wang, et al., 2006; Weilinger et al., 2016). Through the various modes of activation, Panx1 is most predominantly characterized for its physiological role in the extracellular ATP release (Bao et al., 2004; Dahl, 2015; Locovei, Wang, et al., 2006; Narahari et al., 2021). Evidence for this mechanism includes the localized expression of Panx1 at the cell site of ATP release and in cell types with documented channel-mediated ATP release (Bao et al., 2004), knockouts and mutations of Panx1, or chemical targeting halt ATP release (Locovei, Bao, et al., 2006; Suadicani et al., 2012). Panx1 also exhibits high anion-selectivity to Cl^{-}, and when Panx1 is highly permeable to Cl^{-} it lacks the permeability to ATP (Wang et al., 2014). The findings from a resolved cryo-EM structure of

Panx1 have hypothesized a novel pathway for Cl^- transport (Ruan et al., 2020). Recent findings on Panx1 cryo-EM structure resolved by multiple groups did not provide sufficient evidence for a channel conformation suitable for ATP permeation (Mim et al., 2021). As such, Panx1 has been proposed to exhibit at least two distinct conformations depending on the type of stimuli and permeation substance (Wang et al., 2014). Panx1's multimodality of activation and function has been implicated in several physiological and pathological processes (Penuela et al., 2013, 2014). Panx1's involvement in the release of IL-1β via P2rx7 has been shown to trigger an inflammation response (Pelegrin & Surprenant, 2006). Activation by G protein-coupled receptors is associated with neuropathic pain (Weaver et al., 2017). Panx1 has been shown to contribute to the mechanism of cell death, irreversibly activated via the cleavage of C-terminus by caspase and releasing 'find-me' signals during apoptosis (Chekeni et al., 2010). The channel's ATP release with the association to astrocytic glutamate release and elevated K^+ levels has been proposed to play a critical role in epilepsy (Aquilino et al., 2017; Mylvaganam et al., 2014).

1.2 Pannexin1 in an epilepsy model

1.2.1 Panx1 expression in epilepsy

One of the most significant motives for investigating Panx1's role in epilepsy is the evidence of the protein's overexpression in human epileptic tissue. Some evidence of this in human patients includes, the region-specific overexpression of Panx1 in temporal lobe epilepsy (Jiang et al., 2013), upregulated *Panx1* mRNA in focal cortical dysplasia and a positive correlation between protein expression and seizure onset frequency (Li et al., 2017), and increased Panx1 and microglial activation in Rasmussen Encephalitis (Cepeda et al., 2015). Similarly in experimental investigation, Panx1 activation in epileptic tissue *ex vivo* promoted seizures and pharmacological blocking or genetic deletion of mouse Panx1 attenuated seizures (Dossi et al., 2018). In mouse hippocampal seizure models Panx1 transcriptome was shown to be upregulated (Mylvaganam et al., 2010). Compelling evidence in human and mouse epilepsy models suggest Panx1 is positively correlated with the occurrence and location of seizures and is actively involved in the mechanism.

1.2.2 Proposed mechanisms of Panx1 involvement in seizures

The mechanism under which Panx1 is associated with epilepsy has been largely debated (Aquilino et al., 2017; Carlen, 2012; Mylvaganam et al., 2014). Whether Panx1 has an excitatory or inhibitory effect on status epilepticus and seizure propagation, the channel's extracellular ATP release function in astrocytes and neurons is accepted as a probable, but not limited to, mechanism of contribution (Dahl, 2015). Seizures and pathogenic hyperexcitability often correspond with an increase in ATP and K^+ concentrations. Elevated K^+ concentrations are shown to activate Panx1, inducing a high conductance and ATP permeable state of the channel (Wang et al., 2014). Panx1's ATP permeability as a function of K^+ and P2X receptor activation was shown to contribute to seizure outcomes (Santiago et al., 2011). Moreover, Panx1's open state induces depolarization of the cell membrane, further contributing to electrochemical imbalance during seizures. Others have described Panx1's excitatory mechanism through NMDAR and Src kinase activation (Weilinger et al., 2016). Although arguably most research suggests an excitatory involvement of Panx1 in seizures, there is also a substantial amount of discrepancy in the field.

1.2.3 Contradictions in literature and points of consideration

Contradictions exist in the literature, as some studies indicate Panx1 increases seizure susceptibility, specifically with its interaction with P2rx7 (Kim et. al., 2011). The contrasting results reported for Panx1's involvement in seizures could be the result of varying experimental designs. Panx1 was found to induce seizure propagation when stimulated with elevated extracellular K^+ concentration in a kainic acid seizure induction model (Santiago et al., 2011). In contrast, Panx1 has been shown to attenuate seizures when the Panx1-P2rx7 complex is regulated by the muscarinic acetylcholine receptor M1 (Kim & Kang, 2011). Moreover, targeting of Panx1 on astrocytes or the neuronal cells results in the channel's opposing effect on seizures (Scemes et al., 2019). Even on the fundamental molecular level, contradicting mechanisms are present (**Fig. 2**). Panx1 can have an excitatory effect on seizures through the ATP mediated positive feedback and activation of P2X receptors and release of astrocytic glutamate. Panx1 can also have an inhibitory effect via negative feedback of excess ATP hydrolyzed to adenosine, in turn inhibiting glutamate release through the activation of presynaptic adenosine A1 receptors (Aquilino et al., 2017). Unresolved involvement of Panx1 in seizures and the presence of

contradictory data propel the need for further investigation. A new perspective on Panx1 and the seizure model may elucidate new mechanisms that would help to resolve the channel's role, and the zebrafish seizure model can provide just that.

Fig. 2 Proposed Panx1 involvement in the initiation or termination of seizure activity.

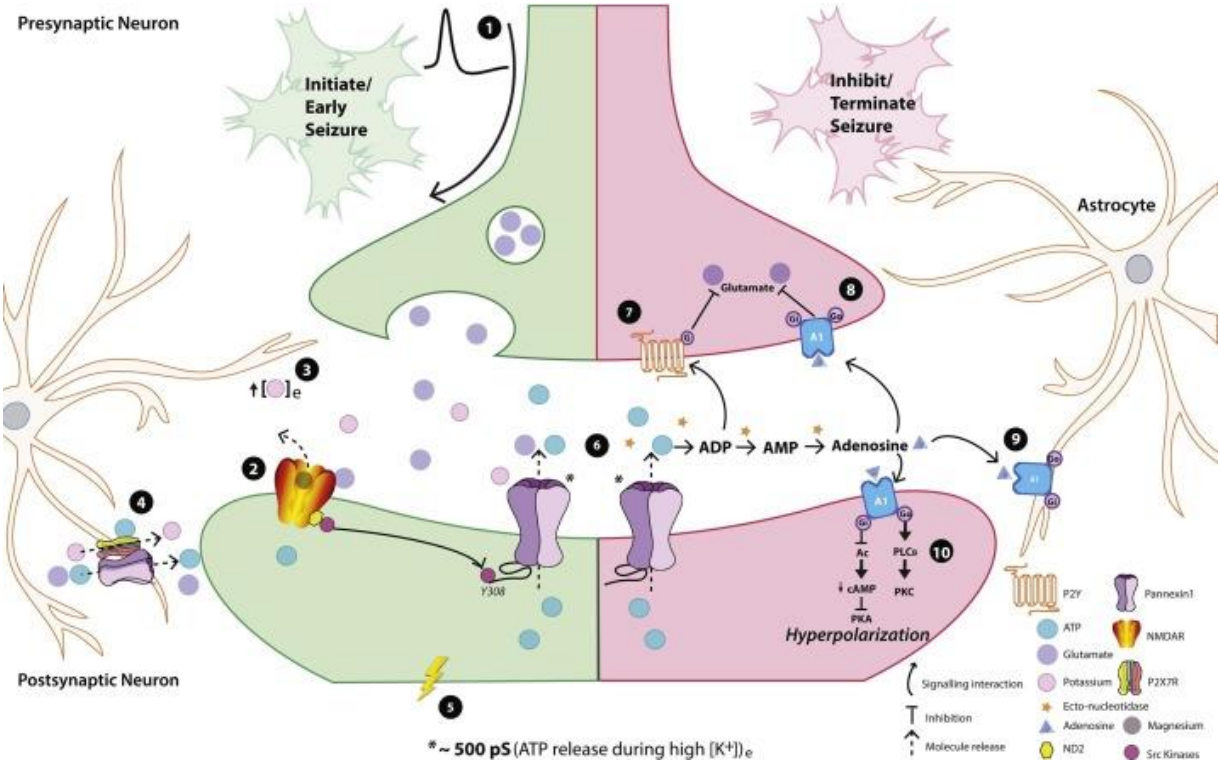

Panx1 involvement in seizure-associated mechanisms. **Left** – Proposed Panx1 involvement in the initiation and propagation of seizures via an elevation in extracellular K^+, Glutamate, NMDAR, Src kinase and ATP release. **Right** – Proposed Panx1 involvement in the inhibition or termination of seizures via hydrolyzation of ATP, Adenosine A1 receptor, and P2Y purinergic receptor. *Figure retrieved from Elsevier B.V. (Aquilino et al., 2017).

1.3 Zebrafish as an *in-vivo* animal model for epilepsy research

Zebrafish are a versatile high-throughput animal research model that has been widely utilized in disciplines ranging from genetic and molecular, to systems and whole organism characterization. Their sequenced genome, high fecundity and rapid physiological and cognitive development, availability in large quantity, transparency at the larval stage and rich behavioral repertoire; all these characteristics make the organism a highly compelling *in-vivo* animal model. Some of the widely investigated research areas in the zebrafish include genetics (Carpio & Estrada, 2006), development (Dodd et al., 2000), memory and learning (Best et al., 2008), visual processes (Bilotta & Saszik, 2001), optomotor and social behaviors (Kalueff et al., 2013), and disease models such as epilepsy and Parkinson's (Kari et al., 2007). Epilepsy research has gained traction in the world of zebrafish as strong evidence continued to emerge for the presence of seizure-like manifestations in the organism through genetic (Hortopan et al., 2010; Teng et al., 2010), pharmacological (Alfaro et al., 2011; Baraban et al., 2005; Kalueff & Stewart, 2012) or electrical interventions (Pineda et al., 2013). Depending on the form of induction, zebrafish display acute onset of seizures (Baraban et al., 2005), or reoccurring spontaneous seizures characteristic of status epilepticus (Paudel et al., 2020). Adults and larvae as young as 3 days old, exhibit the seizure phenotype through behavioral manifestations that resemble clonic and tonic-like locomotion, cellular and molecular responses similar to regulations and expressions observed in epilepsy patients and mouse models, and through an electrophysiological activity that shows ictal and inter-ictal like events in the brain.

For this study, seizures were chemically induced in the zebrafish larvae with an established convulsant. The acute model served to elucidate Panx1's role in seizures *in-vivo*.

1.3.1 PTZ induced zebrafish seizure model

To date, there are several well established chemically induced seizure models in the zebrafish, including treatment with kainite (Alfaro et al., 2011; Tiedeken & Ramsdell, 2009), picrotoxin (Wong et al., 2010), pilocarpine (Budaszewski Pinto et al., 2021; Paudel et al., 2020) and pentylenetetrazole (PTZ) (Afrikanova et al., 2013; Baraban et al., 2005; Mussulini et al., 2013). PTZ, a CNS convulsant inhibiting $GABA_A$ receptor complex (Huang et al., 2001), has been characterized most extensively in inducing both adult and larvae acute seizure models. Treatment

with PTZ manifests in a robust seizure phenotype across behavioral, molecular, tissue, and electrophysiological domains.

In behavioral phenotyping, the Baraban group pioneered the establishment of stages of seizure-associated behavior in PTZ treated larvae (Baraban et al., 2005). Stage I is characterized as an increased activity in response to the compound, starting almost immediately after treatment. Stage II manifests as rapid 'whirlpool-like' circling the edges of the larva's container, typically a well. Stage II begins around 10 minutes post-PTZ treatment and continues for 30 minutes. Final observable and quantifiable behavior, stage III, is described as uncontrolled twitching of the entire larva body, resembling convulsions, followed by prolonged loss of posture and balance. The onset of the last stage can differ between animal models, however, typically emerging 20 minutes post-treatment into over an hour following a normal distribution. Several independent groups have identified these stages in their PTZ-induced seizure models (**Table 1**) (Afrikanova et al., 2013; Baraban et al., 2007; Mussulini et al., 2013; Tiedeken & Ramsdell, 2007; Winter et al., 2008). Compartmentalization and characterization of behavioral outcomes in response to PTZ treatment have enabled standardized seizure investigation in the zebrafish larvae. Seizure-associated molecular responses have been shown in PTZ induced zebrafish models, through the upregulation of immediate early gene *c-fos* during the propagation of seizures (Baraban et al., 2005) and elevated cortisol levels (Wong et al., 2010). Evidence of robust calcium transients during seizure-like events in the larva brain have been characterized (Liu & Baraban, 2019). Electrophysiological evidence has shown seizure-like events in PTZ treated zebrafish brain, characterized as long duration and high amplitude bursts, polyspiking and changes to power frequency in adults' cerebellum (Pineda et al., 2011) or larvae's optic tectum and forebrain (Baraban et al., 2005; Hortopan et al., 2010).

Chemical induction with PTZ allows for an in-depth characterization of an acute seizure phenotype. An extensive body of work specifically on the zebrafish model, validated and standardized behavioral, molecular, and electrophysiological responses in PTZ-induced organisms *in-vivo*. As such, in this project, PTZ was chosen as a means of acute seizure induction in Panx1 targeted zebrafish larvae, as any shift from the expected phenotype can likely be attributed to the involvement of Panx1.

Table 1. PTZ-induced seizure-associated behavior in larvae and adult zebrafish characterized in stages.

Behavioral characterization in stages	(Baraban et al., 2005), (Berghmans et al., 2007)	(Desmond et al., 2012)	(Mussulini et al., 2013)
	Larvae	Adult	
Stage 0		Normal swimming	Short swimming at the bottom of the tank
Stage I	General hyperactivity	Initial freezing followed by hyperlocomotion	Increased activity
Stage II	'whirlpool-like' rapid circling	Spiral swimming, muscular contractions	Erratic bursts of swimming
Stage III	Uncontrolled twitching of the whole body followed by loss of posture		Circular movements
Stage IV			Clonic; rhythmic muscular contraction
Stage V		Rigid extension of body and loss of posture, sinking	Tonic; loss of posture
Stage VI		Death, immobility	Death

1.3.2 Machine learning methods in zebrafish models

In the last two decades, machine learning techniques have advanced immensely in almost all areas of technological development, including in animal research. Machine learning procedures provide a novel approach to data collection, extraction, and analysis. They can enhance existing research protocols by automatizing the process and standardizing data acquisition thus reducing experimenter error and bias. Moreover, an unsupervised machine learning approach can effectively characterize and group large data, uncover novel patterns within, and draw new conclusions. In small animal models such as the zebrafish, machine learning techniques can be utilized in behavioral characterization, phenotyping, tissue and cell segmentation, analysis of genetics and electric recordings (**Fig. 3**). Several studies have implemented supervised machine learning techniques in the investigation and advancement of these application areas. Support Vector Machine (SVM) and Convolutional Neural Network (CNN) were utilized for sex-classification of adult zebrafish and determining sex-linked phenotypic differences (Hosseini et al., 2019). Assessment of toxicity to the live organism is an essential element of drug screening protocols, and machine learning techniques such as SVM and CNN can provide a systematic approach to the identification and quantification of morphological anomaly (Ishaq et al., 2013, 2017). Others have utilized neuronal networks (NN) for tissue and cell type segmentation to characterize development and cell fate processes (Singh et al., 2018; Viader-Llargués et al., 2018). Automatic detection and analysis of electrical signals of interest in the brain or heart of zebrafish can be achieved with K-means clustering protocols that categorize data by similarity association (Cong et al., 2017; Lenning et al., 2018). These are several examples of supervised machine learning techniques utilized in the investigation of zebrafish disease models to date, which continues to expand.

The effects of stimulation or genetic and pharmacologic targeting of live zebrafish models most often manifest through changes to the organism's behavior and locomotor activity (Kalueff & Stewart, 2012). Presently, there are software that automatically track larvae or adult zebrafish behavior and generate behavioral outputs such as speed, time and direction of movement for the analysis of genetic or drug-associated phenotypes, optomotor response (OMR), prey capture and social interactions (Green et al., 2012; Guilbeault et al., 2021; Nath et al., 2019; Pérez-Escudero et al., 2014). In this thesis, ViewPoint ZebraLab (Scott et al., 2016), is utilized to automatically

record several basic behavioral attributes of larvae and make a phenotypic comparison between *panx1* genotypes. The advantages of these software allow a high-throughput, rapid and automatic characterization of the zebrafish model based on general behavioral attributes. However, they are limited in characterizing complex behaviors specific to a model, such as convulsive events seen in the zebrafish seizure model. Machine learning techniques help bridge this gap by providing a sophisticated method for automatically extracting specific behavioral attributes and characterizing a unique repertoire.

Software capable of breaking down zebrafish behavior into distinct and elementary locomotor outputs can be utilized in several machine learning techniques that require continuous numerical data as input, such as k-nearest neighbour (KNN), SVM, Random Forest (RF) or NN. These supervised techniques group and categorize data into complex behavioral outcomes specified by the experimenter. Several studies have utilized this approach to categories complex behaviors such as prey capture and social interactions (Breier & Onken, 2019; Semmelhack et al., 2014). Alternatively, unsupervised machine learning techniques, such as unsupervised K-mean clustering and Self-Organizing Maps (SOM), input basic unmarked behavioral parameters and cluster data without any further specifications. These methods allow for an unbiased clean approach to data characterization and potentiate the uncovering of new patterns in data. Studies that have implemented these methods have found novel ways of deciphering locomotor components to complex behaviors (Marques et al., 2018; Zhang et al., 2013), recreated 2D locomotor trajectories for the characterization of new behavioral patterns (Mearns et al., 2020).

Behavioral characterization is one of the key methods of identifying changes in a live zebrafish organism as many genetic, pharmacological, and physically stimulated models' effects to the organism manifest through behavioral changes. Zebrafish behavior is suited for a high-throughput investigation and collection of large amounts of data. Machine learning techniques can aid the utilization of these advantages by providing a platform for a systematic, and automatized method for data acquisition and analysis. Supervised techniques allow for manual manipulation and fine-tuning of data acquisition to acquire the desired output. Unsupervised techniques can provide a starting point to the characterization of data or a novel approach to analysis. In this project, two machine learning techniques are implemented in the characterization of *panx1* through behavioral phenotypes. SOM is utilized to unbiasedly cluster

behavioral data by similarity, ultimately characterizing seizure phenotypes based on basic behavioral attributes. Moreover, this method was used to correlate seizure phenotypes and identifying similarities in targeting Panx1 genetically or pharmacologically. A second method, CNN, was used to quantify seizure-associated convulsive behavior in treated zebrafish larvae and provide a systematic alternative to the manual acquisition of data. Here, image sequences of seizing larvae were processed through a constructed convolutional neural network to categorise images into ‘convulsing’ or ‘non-convulsing’, and sequences of categorized images were used to calculate the duration of seizing events, their total occurrence and frequency.

Fig. 3 Machine learning techniques and application areas in zebrafish disease models.

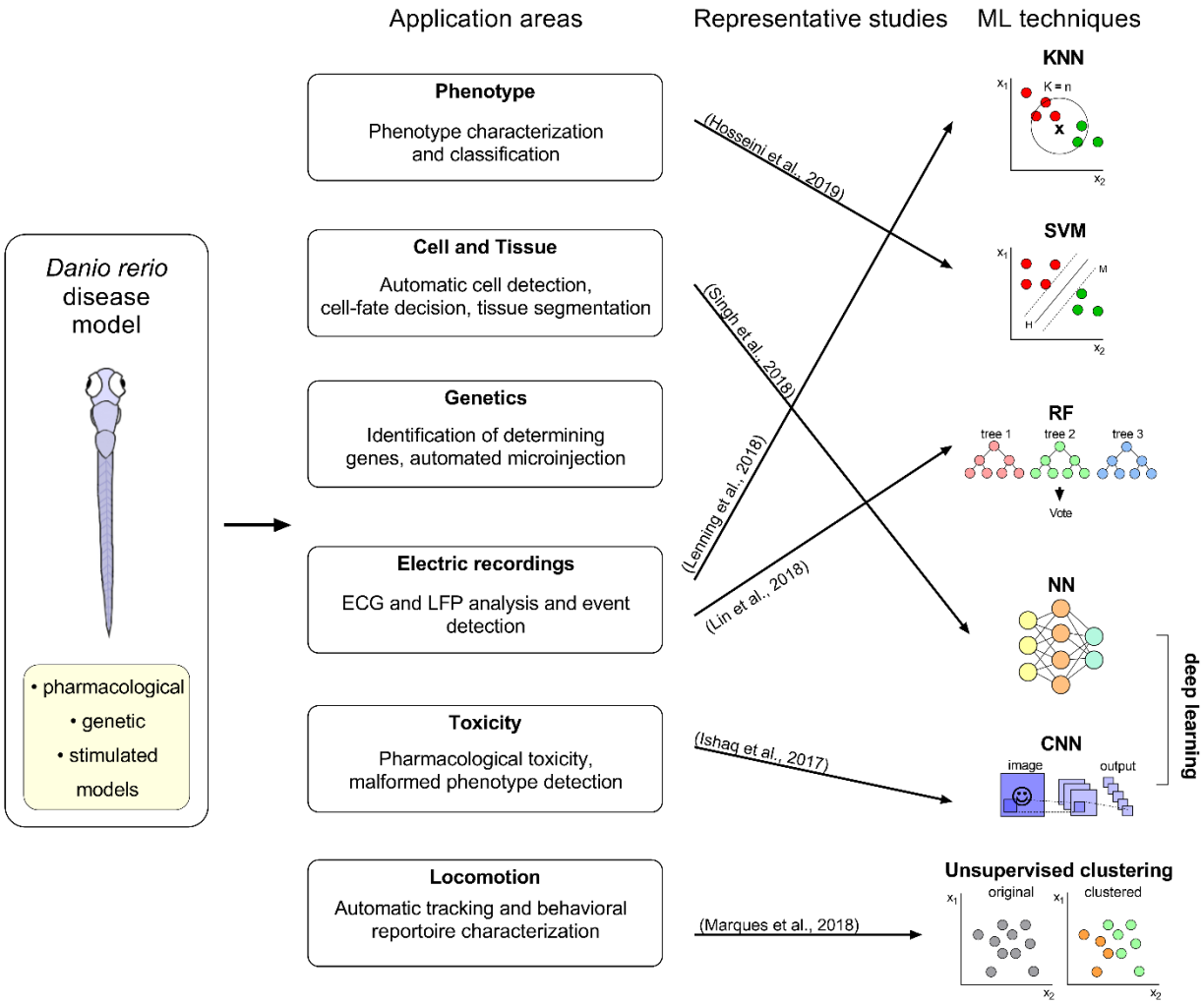

Diseases are investigated in live zebrafish via pharmacological, genetic and/or physical stimulation. Machine learning (ML) techniques can be applied to study the disease models in areas ranging from behavioral and physiological phenotyping to molecular and electrophysiological characterization. Some examples of ML techniques utilized in these areas include supervised classifiers such as K-Nearest Neighbour (KNN), Support Vector Machine (SVM; specifically, linear kernel SVM is depicted in the figure), decision tree-based Random Forest (RF); Deep learning algorithms such as Neural Networks (NN) and Convolutional Neural Networks (CNN); Unsupervised clustering methods. ML techniques utilized in listed application areas are connected with arrows with representative work. *The figure is included in the 'Automated Procedures and Machine Learning for Zebrafish Disease Models: A Neurobiologists Perspective' manuscript in prep. Constructed by D.T.*

1.4 *Pannexin1a* and *pannexin1b* ohnologs in the zebrafish

In addition to the anticipated advantages of the animal model, zebrafish provide a unique platform in examining Panx1's contribution to pharmacologically induced seizures, as they express two independent and functionally distinctive Panx1 channels.

A whole-genome duplication event in the teleost lineage 320 to 350 million years ago, followed by intrachromosomal exchange and activation/deletion of replicated genes, led to a rapid speciation of teleost (Jaillon et al., 2004). Although most duplicated genes are lost over time, some genes were retained as ohnologs, likely due to their neofunctionalization that resulted in evolutionary advantage. *Panx1* is among the genes that preserved both of its ohnologs, *pannexin1a* (*panx1a*) and *pannexin1b* (*panx1b*). The gene is proposed to have duplicated due to the almost identical exon structure of the paralogs (Bond et al., 2012). The two genes have been shown to form functional Panx1a or Panx1b channels sharing similarities and differences in their tissue expression pattern, cell localization (**Fig. 4**), key amino acids governing the channel pore, gating, and activation properties (**Table 2**).

Key structural and functional properties of Panx1 were conserved after the genome duplication. Both Panx1a and Panx1b are proposed to form heptameric hemichannels, each protomer conserved for TM1 through TM4, ECL1 and 2, and ICL1 with intracellular N and C termini. Between the two, protein sequence similarity reaches 68% and identity 55% (Bond et al., 2012), and sequence identity between Panx1a, Panx1b and mouse Panx1 (mPanx1) is in the range of 55 to 57% (Kurtenbach et al., 2013).

Panx1a gene is located on *Danio rerio* chromosome 15 and codes for 416 amino acid (aa) residues. The protein is 47.1kDa with high conservation in the TM domains and the highest variability in the C terminus compared to human Panx1 (Prochnow, Hoffmann, Vroman, et al., 2009). Panx1a channel is ubiquitously expressed in the CNS, retina, kidney and muscle and is similar in its expression pattern to Panx1 (Bond et al., 2012). *Panx1b* gene is located on chromosome 5, codes for 422 aa with a protein molecular weight of 47.8kDa. The Panx1b protein expression is centralized in the CNS and was found in the perinuclear region as well as the plasma membrane, as opposed to Panx1a found predominantly on the plasma membrane (Kurtenbach et al., 2013). In terms of gating and activation properties, Panx1a was comparable to

mPanx1 in conductance. Panx1b on the other hand exhibited delayed activation and requiring 10 to 20mV higher membrane potential than Panx1a for activation.

Panx1a contained a conserved N-glycosylation site on ECL2, N264, the mutation of which results in improper membrane docking and multimeric channel formation (Prochnow, Hoffmann, Vroman, et al., 2009). One of the earlier studies demonstrated the physiological relevance of Panx1a in the zebrafish retina, forming channels on the Horizontal cells (HC) folded into the cone pedicle adjacent to glutamate release location and activated by physiological membrane potentials and ion gradient (Prochnow, Hoffmann, Vroman, et al., 2009). The localization pattern was proposed as an indicator of Panx1a's involvement in the cone-HC feedback mechanism, either through ATP release or the ephaptic mechanism. The group also discovered that a cysteine mutation in TM4, C282W, altered the Panx1a gating mechanism (Prochnow, Hoffmann, Dermietzel, et al., 2009). Cells transfected with the mutated protein had reduced dye uptake and altered voltage sensitivity and subconducting states. The channel otherwise displayed no differences in its membrane insertion, proposing the residue's contribution to the proper gating of the channel, being one of the first reports tying Panx1a structure to function.

The differences between Panx1a and Panx1b in their expression and distribution patterns, gating and activation properties, have most likely evolved due to neofunctionalization of the two channels. This suggests that the two play distinctive roles in the organism's intercellular communication and thus can be speculated to contribute to seizure onset and propagation differentially. If targeting Panx1a or Panx1b in a seizure model results in distinct outcomes, the channels' structural and functional differences have the potential to indicate the mechanistic how of Panx1's contribution to seizures.

Table 2. Pannexin1a (Panx1a) and Pannexin1b (Panx1b) channels' expression, localization and gating properties identified in the literature to date.

Pannexin1a	*Pannexin1b*	*References*
Expressed in the retina, upregulated in muscle and kidney, downregulated in heart	-	(Zoidl et al., 2008)
Localized on HC near cone synaptic terminal, open under physiological membrane potential and elevated intracellular Ca^{2+}	-	(Prochnow, Hoffmann, Vroman, et al., 2009)
Gating properties of Panx1a altered with cysteine mutation in TM4	-	(Prochnow, Hoffmann, Dermietzel, et al., 2009)
Ubiquitous expression; high in brain and muscle tissue Panx1 expression alike 0-20mV activation, ~275 pS conductance	Expressed in CNS and spine, expressed in the cell membrane and intracellular vesicles. Longer delay (8sec) and higher voltage threshold (+10mV higher than Panx1a) for activation, channel conductance ~123pS	(Bond et al., 2012)
Ubiquitous expression in CNS, abundant in retina and HC	High expression in cerebellum, spinal cord and tectum opticum	(Kurtenbach et al., 2013)
Localized in the cell membrane	Localized in the plasma membrane and perinuclear region (mPanx1 similarity)	
Less sensitivity to ATP concentrations; pH = 6.93	Concentration dependent sensitivity to ATP (high ATP = excitatory); pH = 6.86	
Activation comparable to mPanx1	Longer open state, late and prolonged activation	
mPanx1 (N254) and Panx1a (N246) glycosylation sites	N71 (ECL1) and N246 (ECL2) as glycosylation sites	
panx1a knockout = CNS and visual system, development, P2X pathways and K^+ channels downregulated, phototransduction cascade and mRNA processing upregulated.	-	(Safarian et al., 2020)
Obstructed dopaminergic signaling; rescue with D2-like receptor or Panx1 blockers		

Higher threshold for electrically induced response in *panx1a*$^{-/-}$ than WT	-	(Khalili et al., 2019)
Trp123 and Tyr205 in TM 2 and 3 govern the assembly of Panx1a into a channel	-	(Timonina et al., 2020)
Involved in negative feedback from HC to cones	Involved in negative feedback from HC to cones	(Cenedese et al., 2017)

Fig. 4 Panx1a and Panx1b relative expression in the nervous system of zebrafish and cellular localization.

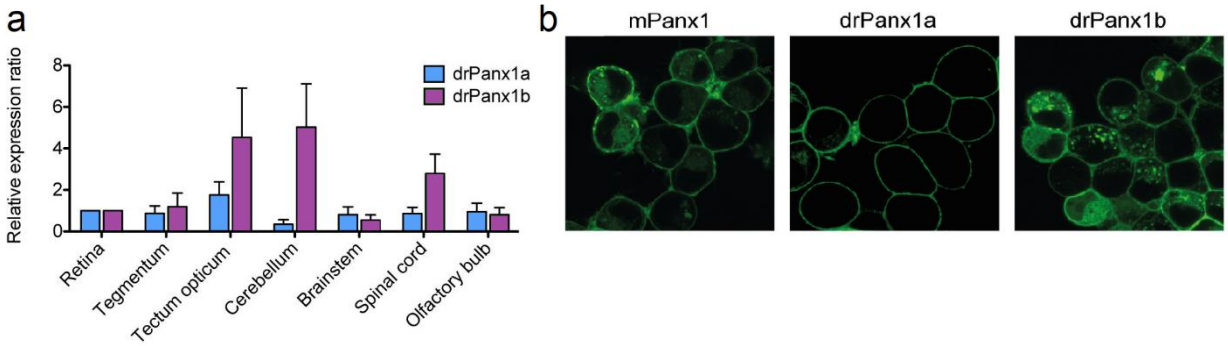

a Relative expression of Panx1a and Panx1b in the nervous tissue of zebrafish. **b** Cellular localization of the channels; mPanx1 and Panx1a localizes in the plasma membrane and Panx1b in the plasma membrane and perinuclear region. *Adapted from (Kurtenbach et al., 2013).

1.5 Investigating the role of pannexin1a/b in a zebrafish seizure model

The differential properties of Panx1a and Panx1b in an *in-vivo* zebrafish model can elucidate the mechanism under which Panx1 is involved in the molecular determinants of seizures. The differential localization and expression of the two channels may be an indication of their effect on varying molecular and cellular pathways. The channels' unique gating and open state properties can influence the sensitivity and activation timeline. In addition to expression of Panx1a and Panx1b, the zebrafish model provides a high-throughput platform for screening of genetics and pharmacological treatments *in-vivo*. It is a comprehensive animal model for the characterization of Panx1's mechanistic involvement in seizures with the ability to elucidate the effect on intact systems of the organism.

2. Aim of the thesis and research design

The research project described in this thesis aims to characterize the involvement of Panx1a and Panx1b in seizure manifestations for an *in-vivo* zebrafish model. Seizures were chemically induced with Pentylenetetrazole. The compound has been established as an experimental convulsant in animal research and validated in the zebrafish model (Afrikanova et al., 2013). The compound induces a robust and comprehensive response in the organism, ranging from molecular to whole system behavioral and electrophysiological outcomes.

The investigation of the two *panx1* ohnologs in this animal seizure model is achieved in two ways. Genetic deletion of the *panx1a* and *panx1b* genes established three transgenic knockout zebrafish lines; *panx1a*$^{-/-}$, *panx1b*$^{-/-}$ and Double Knockout (DKO). Pharmacological treatment with a Panx1 blocker, Probenecid, elucidated the effects of targeting the Panx1 channel. The two methods investigate the lack of functioning Panx1 from distinct angles, bearing differential effects on the molecular and physiological properties of the organism.

The seizure phenotype, based on extensive literature description (Baraban et al., 2005), was evaluated in live zebrafish larvae through several procedures. Signs of seizure-related hyperactivity was examined first, to uncover any primary and global changes to the organism. Specific seizure-associated behaviors, survival of PTZ-induced larvae, and computational analysis on phenotype similarities were examined next to further evaluate the behavioral phenotype. Differential expression of seizure-affiliated molecular markers was examined and

potentially interacting molecular pathways were identified. Electrophysiological recordings from seizing larvae were obtained as Local Field Potential (LFP) signals, coupled with Ca^{2+} imaging in the brain. The extensive characterization of Panx1 in a zebrafish seizure model aimed to identify key channel properties and interacting partners in the context of seizures.

2.1 Manuscripts and contributions

- The results presented in this thesis are included in the manuscript:

*"***Panx1 channels promote both anti- and pro-seizure-like activities in the zebrafish via p2rx7 receptors and ATP signaling***"*
Paige Whyte-Fagundes, Daria Taskina, Nickie Safarian, Christiane Zoidl, Peter L Carlen, Logan W Donaldson, Georg R Zoidl.
BioRxiv at https://doi.org/10.1101/2021.06.03.446992.

Data that was obtained and analyzed by Paige Whyte-Fagundes and Dr. Logan W Donaldson are indicated in the figure captions.

- Introduction and discussion partially discuss the review in preparation:

"**Automated Procedures and Machine Learning for Zebrafish Disease Models: A Neurobiologists Perspective**"
Daria Taskina, Georg S Zoidl, Georg R Zoidl.

3. Materials

3.1 Organism annotations and abbreviations

Pannexin1 (panx1) knockout transgenic zebrafish lines are referred to in-text as: *panx1a*$^{-/-}$ for *panx1a* gene knockout lines (*panx1a*$^{-/-}$ *: 1b*$^{+/+}$), *panx1b*$^{-/-}$ for *panx1b* gene knockout lines (*panx1a*$^{+/+}$ *: 1b*$^{-/-}$), DKO for both *panx1a* and *panx1b* gene knockout lines (*panx1a*$^{-/-}$ *: 1b*$^{-/-}$).

Panx1 knockouts refers to all three transgenic lines.

GCaMP6 TL refers to TL larvae with the GCaMP6 genetically encoded. GCaMP6 *panx1b*$^{-/-}$ refers to *panx1b*$^{-/-}$ knockout with GCaMP6 encoded.

Genes and transgenic lines are italicised, proteins are capitalized in-text.

Full terms for abbreviations appearing in-text can be found on page **ix-x**.

3.2 Biosafety

All experiments were conducted in a containment level 2 laboratory in accordance with federal, provincial, and institutional safety standards. Prior to experimentation, WHMIS II, general and laboratory specific biosafety and autoclave training were completed. Experiments involving live animals were conducted after the certification for animal care and training in the vivarium in accordance with the regulations set by the Canadian Council for Animal Care and after the approval of the protocol by the Animal Care Committee (GZ: 2019-7-R2 and GZ: 2020-7-R3).

3.3 Organism

Zebrafish (*Danio rerio*) Tupfel long fin (TL) strain was utilized. Unmodified TL strain served as the Wild-type (WT) line.

3.3.1 Generation of transgenic lines

The *panx1* knockout lines (*panx1a*$^{-/-}$, *panx1b*$^{-/-}$ and double *panx1a*$^{-/-}$ and *panx1b*$^{-/-}$ knockout a.k.a. DKO) were generated in house by Nickie Safarian (Safarian et al., 2020, 2021), where *panx1* was knocked out via TALEN technology. The knockout lines were bred to at least the 3rd generation before testing on their larvae.

GCaMP6 transgenic lines were generated to express calcium indicator GCaMP6 under pan-neuronal *elavl3* promotor (Chen et al., 2013; Vladimirov et al., 2014). GCaMP6 TL's F2 generation was tested for homozygous GCaMP6 expression before use. GCaMP6 *panx1b*$^{-/-}$ F0 generation with mosaic expression were used.

3.4 Solutions and Chemicals

3.4.1 Solutions for larvae handling

Solution	*Composition*	*Source*
E3 medium	60ppm of Instant Ocean® Sea Salt mixed in RO water (pH 7.2~7.4)	Instant Ocean®

3.4.2 Solutions for molecular biology

Procedure	*Solutions*	*Source*
Tissue lysis and RNA extraction	RLT Plus Lysis Buffer, βME, RW1 Wash Buffer, RPE Wash Buffer, 70% Ethanol, RNase-free water	QIAGEN (RNeasy plus mini kit)
RNA/DNA visualization	Formaldehyde, Agar, 1x TAE buffer, EtBr, 100bp DNA Ladder	ThermoFisher Scientific, etc.
cDNA synthesis	5x iScript Reaction Mix, iScript Reverse Transcriptase, Nuclease-free water	Bio-Rad
18s product PCR	HotStarTaq DNA Polymerase, 1x PCR Buffer, dNTPs, 10mM 18s FP and RP solution, Nuclease-free water	QIAGEN (HotStar Taq Pol Kit)
RT-qPCR	Ssofast™ EvaGreen® Supermix	Bio-Rad

3.4.3 Solutions for electrophysiology

Procedure	*Solution*	*Source*
Extracellular solution	2M NaCl	-

3.4.4 Chemicals applied on larvae

Solution	*In-text appearance and final concentration*	*Source*
A-438079 hydrochloride hydrate	A43; 100µM	cat#A9736
Pancuronium bromide	Panc; 300µM	cat#P1918
Pentylenetetrazole	PTZ; 15mM	cat#P6500
Probenecid	Pb; 75µM	cat#P8761
Valproic acid	VPA; 5mM	cat#P4543

*All chemicals were purchased from Sigma-Aldrich (Mississauga, Canada).

3.5 Oligonucleotides

3.5.1 Primers for RT-qPCR

Gene sequences were retrieved from NCBI (https://www.ncbi.nlm.nih.gov/nucleotide/) via their accession number. Forward and reverse primer pairs were designed in IDT software Real-Time qPCR tool (https://www.idtdna.com/scitools/Applications/RealTimePCR/) and confirmed for length, Guanine/Cytosine content, melting temperature, lack of complementary regions and location in SnapGene software (https://www.snapgene.com/).

Table 3. Genes analyzed in RT-qPCR, their accession number, forward and reverse primer sequences.

Gene	Gene Accession Number	Forward Primer (5'-3')	Reverse Primer (5'-3')
actb2 (ref)	NM_181601	GCCCCTAGCACAATGAAGATC	GACTCATCGTACTCCTGCTTG
adora1b	NM_001128584	GGAACAATTTACACAGCCTGC	ACGAGCATGAAAAGCAGAGG
bdnf	NM_001308648	ACAAGCGGCACTATAACTCG	ACTATCTGCCCCTCTTAATGG
cacna1da	NM_203484	GGATGAGAAGGATAATGCCGAG	GGGTTTGTGTTGCTGAAGATG
egr1	NM_131248	TCAACATATCCCAGTGCCAAG	TGTGTCTGGATGGGTTTCTG
egr2a	NM_001328404	CTTCTCCTGTGACTTCTGCG	GCTTTCTGTCCTTATGTCTCTGG
egr2b	NM_130997	GATGCGGAGAGGTCTATCAAG	AGGAGTAGGATGGCGGAG
egr4	NM_001114453	ACAGCACCTCAAAGACTACAG	ACGACAAGGTAAAAGACTGGAG
eif4ebp2	NM_212803	AGTGACGGGCAAGAACATC	GTTGTTCACGTAGGTTCCTCTTC

entpd1	NM_001003545	ACCTGACCAACATGATTCCG	GCTGTTTTAGTAAAGCGACGG
fosab	NM_205569	GTGAACGAAACAAGATGGCTG	TTTCATCCTCAAGCTGGTCAG
grin2bb	NM_001128337	ATGAGGGACAGGGATAGAGG	AGGTTGGGATGAATGGGTTC
il1b	NM_212844	GTTCAGATCCGCTTGCAATG	TGCTTCATTCTGTTCAGGGC
jun	NM_199987	CACAAGGCTCTGAAACACAAC	TGATGCCAGTTTGAGAAGTCC
kcnc3a	NM_001195240	CCATGATAGGGCCTGCTTC	AGAGATGTTATTGAGGCTGCG
kcnf1a	NM_001082811	GCTGATTCTTACGCATTTGGG	GTTTGTAGACCTGACGAGTGG
nt5e	NM_200932	CAAACGGAAATGTGCTGGAG	GTCTGTCCCACTTGCTGAG
p2rx7	NM_198984	GTGTCATTTGTGGACGAGGAC	CACTCAACAGAGTCTTCATGCTG
p2ry12	NM_001308557	TCTTCGGTTTGATCAGCATCG	TCAGGATTACATTTGGGAGCG
scn4bb	NM_001077573	ACCTATGCCAGCTGTATTGG	CGCTCACGGTAAATTTGCAC
sema6ba	NM_001366315	TGATGGAGGGCTGTTTGTG	CGTTTGCGTGTTTGGGATC
slc8a1a	NM_001037102	TGAAGCCATCACTGTCAACTC	AACAGAACCTTCCAGAATACCG
slc8a1b	NM_001039144	GGAGGGACCAGTTTATTGAGG	GGCACGAAAGCAAAGAGAAC
slc8a2b	NM_001123284	TCACCAATGACCAGACAACTC	TGCACTCAACTGACCTTCTG
slco2b1	NM_001037678	AGATGGATTGGTGCTTGGTG	TTCTCAGTTGATGGCTCCAC
snap25b	NM_131434	TGAGAATTTGGAGCAGGTCG	TGTTGGAGTCAGCCATGTC
trpv6	NM_001001849	CGCTCAAGTGGAATCTGTATGG	GCCTGCTTTGGTGTAATTCTC
vcp	NM_201481	GACCAACTCATCTACATCCCAC	CAGCACCTGAAAAGCCATTG
tuba1a (ref)	AF029250	GAGCGTCCTACTTACACCAAC	AGGGAAGTGGATACGAGGATAG

3.6 Molecular Kits

Procedure	*Kit*
Tissue lysis and RNA extraction	QIAGEN QIAcube RNeasy Plus Mini Kit
cDNA synthesis	Bio-Rad iScript cDNA Synthesis Kit 170-8890
RNA and 18s cDNA visualization	Qiagen HotStar Taq Pol Kit
RT-qPCR	Ssofast™ EvaGreen® Supermix

3.7 Equipment

3.7.1 Equipment for behavioral and survival analyses

Procedure	*Equipment*	*Source*
Locomotor activity retrieval; automatically generated outputs and videos	ZebraBox monitoring enclosure	ViewPoint Behavior Technology, Lyon, France
Survival assay	Light Microscope (CKX41)	Olympus

3.7.2 Equipment for molecular RT-qPCR

Procedure	*Equipment*	*Source*
Tissue lysis	TissueLyser LT Adapter, 12-tube	QIAGEN
	Sorvall™ Legend™ Micro 21R Microcentrifuge	Thermo Scientific
RNA extraction	QIAcube	QIAGEN
cDNA PCR	Mastercycler® nexus	Eppendorf, Canada
RNA and cDNA visualization	Nanodrop 2000 Photospectrometer	Thermo Scientific
	Mini-Sub Cell GT System	Bio-Rad
	AlphaImager™ HP System	Alpha Innotech
RT-qPCR	CFX96™ Real-Time PCR Detection System	Bio-Rad

3.7.3 Equipment for computational analysis

Procedure	*Equipment*	*Source*
Model generation and analysis	VivoBook ASUS Laptop X512DA; AMD Ryzen™ 5 3500U processor	ASUSTeK

3.7.4 Equipment for electrophysiology

Procedure	*Equipment*	*Source*
Larvae storage	10-140 Analog Incubator	Quincy Lab
Capillary preparation	P-30 Vertical Micropipette Puller	Sutter Instrument
Agar preparation	VWR Analogue Heat Block	VWR Scientific
Embedding of larva	Light Microscope (CKX41)	Olympus
Wire soldering	Weller WES51	Apex Tool Group
Stage and electrode manipulation	Research Control Unit SM7	Luigs and Neumann
Light/Fluorescence source	Lumen 200 Fluorescence Illumination System	Prior Scientific
Imaging	Femto2D Resonant	Femtonics
LFP signal acquisition	Digidata® 1550A Digitizer MultiClamp 700B Microelectrode Amplifier	Molecular Devices

3.8 Software

3.8.1 Software for behavioral and survival analyses

Procedure	*Software*	*Application*
Behavioral (activity output and retrieval of videos) and survival assays	ZebraLab (ViewPoint, Life Technology, Lyon, France)	Locomotor outputs retrieval
	Fast Data Monitor (ViewPoint Biotechnology)	Assignment of groups
	SPSS	Data restructuring
	GraphPad Prism 9.0	PCA, statistical analysis and figure generation
	G*Power	Statistical power analysis

3.8.2 Software for RT-qPCR

Procedure	*Software*	*Application*
RNA and cDNA visualization	AlphaView	Agarose gel imaging
RT-qPCR	NCBI - nucleotide	Gene sequence retrieval
	IDT - RealTime qPCR tool	Primer design
	SnapGene	Primer location
	CFX Manager software™	RT-qPCR data acquisition
	REST 2009©	Relative expression analysis

3.8.3 Software for computational analysis

Procedure	*Software*	*Application*
CNN (via MATLAB®)	MathWorks® – Deep Learning Toolbox; Deep Learning Network for Classification (*MATLAB and Deep Learning Toolbox Release 2020a*, 2020)	Generation of CNN layers; convulsion classification
SOM (via MATLAB®)	MathWorks® – Deep Learning Toolbox; Self-Organizing Maps (*MATLAB and Deep Learning Toolbox Release 2020a*, 2020)	Unsupervised clustering; behavioral phenotyping

All statistical analyses and figures were generated in GraphPad Prism 9.0. Estimation of sample sizes required for sufficient power and final power calculations were conducted in G*Power software.

3.8.4 Software for electrophysiology

Procedure	*Software*	*Application*
LFP signal acquisition	pCLAMP Clampex 11.1	Recording and visualization of LFP signals
	MultiClamp Commander	Microelectrode signal amplification
Imaging of larva	Femto2D powered by MATLAB®	Microscope
Larva monitoring and image generation	HCImage Live	Visualization of larvae
LFP signal analysis	pCLAMP Clampfit 11.1	Visualization and analysis of LFP signals
Image processing and analysis	ImageJ	Fluorescence detection and analysis

4. Methods

4.1 Animal Handling

4.1.1 Adult zebrafish maintenance and breeding

Animal work was conducted at York University's zebrafish vivarium or containment level 2 laboratory, in accordance with the regulations set by the Canadian Council for Animal Care and after the approval of the protocol by the Animal Care Committee (GZ: 2019-7-R2 and GZ: 2020-7-R3). *Panx1* transgenic lines were generated in house (Safarian et al., 2020, 2021). Adult zebrafish were maintained in the vivarium's recirculation system (Aquaneering Inc., San Diego, CA) and kept at 28ºC on a 14-hour light and 10-hour dark cycle. Zebrafish were separated by sex a week before breeding and placed in the same tank separated by a transparent divider a day before breeding. Adults were bred in the morning and eggs were washed and submerged in an E3 medium.

4.1.2 Maintenance of larvae

Larvae were kept in the E3 medium from 0 days post fertilization (dpf) to 7dpf. All use of larvae was kept to a minimum. Larvae were sacrificed after the 7th day according to the Animal Care Protocol guidelines. Behavioral and molecular assays were conducted on 7dpf larvae. Electrophysiology was conducted on larvae from 5 to 7dpf.

4.2 Behavioral Assays

4.2.1 Acquisition of behavioral data

Larvae were submerged in an E3 medium in a 96-well plate individually and were set to rest in a 28°C incubator for at least half-hour. Next, the plate was placed in the ZebraBox chamber (ViewPoint, Lyon, France) maintained at 27.5°C under 30% light intensity. Locomotor activity was tracked, and behavioral outputs were automatically generated by the ZebraLab™ software. Eight of the behavioral outputs generated by the software were extracted for principal component analysis (PCA) to select one output for further investigation. Videos of larvae and their tracks were recorded under infrared light illumination at 30fps. Videos were utilized for manual scoring of stages II and III of seizure-associated behavior.

4.2.2 Principal component analysis

Eight behavioral parameters obtained from the locomotor activity of PTZ treated TL and *panx1* knockout larvae were extracted from the ZebraLab software and evaluated via PCA. The analyzed parameters included total activity score (Δpixel), indicative of the total change in pixel values due to larvae movement, total duration of movement (sec), freezing activity (0 mm/sec movement) occurrence (count) and duration (sec), normal swimming activity (0 – 20 mm/sec) occurrence and duration, and burst activity (≥ 20 mm/sec) occurrence and duration. The first two Principal Components with the highest contribution to data variance were extracted for further analysis. Eigenvector maps of the two Principal Components were plotted to visualize the individual contributions of the eight behavioral parameters to data variance. Lastly, each genotype's data was plotted against the rest, to visualize data distribution within genotypes and identify preliminary variance between genotypes.

4.2.3 Activity output

A behavioral output 'Activity integral' was chosen to examine larvae's locomotor behavior. The output calculates total pixel change (Δpixel) in a well during a specified time interval (1 minute) and is representative of the total change in movement per larva. The output is referred to as 'activity score' in text. The activity score was recorded for larvae (n = 36 per group) placed in a 96-well plate in the ZebraBox for three types of activity. Rest activity was recorded for 25 minutes for larvae that have not been interfered with for over half-hour before the beginning of the recording. Next, an E3 medium was added to each well to account for larvae's activity changes induced by the addition of any medium. The activity was referred to as Baseline and recorded for 30 minutes. Lastly, PTZ was added for a final concentration of 15mM, and larvae were recorded for another hour.

In a pharmacological model, TL larvae were treated before the application of PTZ, for the investigation of known anticonvulsant (VPA), Panx1 blocker (Pb) and P2rx7 blocker (A43). All anticonvulsants and blockers were added into the medium 30 minutes before PTZ application; thus, these groups' baseline activity reflected activity influenced by the compounds. TL larvae treated with PTZ were examined on the same plate as the *panx1* knockouts or pharmacologically treated TL to control for variations. Each treatment group was examined across at least three individual plates.

Area Under the Curve (AUC) analysis was conducted on the activity plots and contrasted between baseline and PTZ induced activity and between genotypes/treatments. Baseline AUC was taken in the last 15 minutes of stabilized baseline activity and PTZ AUC was taken over the hour of PTZ treatment. 'PTZ – Base Mean' AUC was taken by subtracting mean baseline activity from the PTZ AUC to extract the effect of PTZ independently of the genotype/treatments' baseline.

4.2.4 Seizure-associated stage II and stage III behavior

Videos of treated larvae were recorded via ZebraLab software under infrared light illumination using a Point Grey Research Dragonfly2 DR2-HIBW at 30 fps. Videos were used to blindly and manually score seizure-associated stage II and stage III activity in PTZ induced larvae (n = 18 per group) based on the descriptions available in the literature (Baraban et al., 2005). Stage II manifests as 'whirlpool-like' rapid circling of the well and stage III as an uncontrolled twitching of the body resembling a convulsion, followed by a loss of upright posture. Stages II and III were scored at 2-minute intervals for a total of one hour after the PTZ application.

4.3 Survival Assay

7dpf TL and *panx1* knockout larvae were examined for several physical signs of fitness and survival after treatment with 15mM PTZ (n = 80 per genotype). Larvae were placed in a 96-well plate and administered PTZ as per behavioral tests and monitored every hour under a bright field microscope for 10 consecutive hours, and once at 24 hours. Larvae's fitness and survival manifested in three distinct categories: signs of movement or response to stimulation, the clear presence of circulation and/or heartbeat, and signs of degradation of the body. The presence of circulation was chosen as the metric for survival, as movement of larvae would often be observed intermittently after 3 to 5 hours post-PTZ treatment, and not all larvae underwent degradation within 24 hours. Movement was examined as an overall indicator of larvae's health and degradation for signs of an excessive toll on the larva's body from treatment. *Panx1* knockouts' survival rates were analyzed with a log-rank (Mantel-Cox) test against TL and plotted as Kaplan Meier curves.

Survival of VPA (n = 24) and Pb (n = 76) treated TL larvae were examined 24 hours after PTZ treatment and analyzed against the TL group treated with only PTZ via the Barnard test.

4.4 Molecular Assay (RT-qPCR)

After the experimental endpoint of behavioral assays was reached, larvae treated with 15mM PTZ for one hour were collected to be analyzed for differential gene expression via RT-qPCR.

4.4.1 Tissue lysis and RNA extraction

After the behavioral assays, 30 larvae per genotype (TL and *panx1* knockouts) and per treatment (nontreated control and PTZ) were pooled into one sample, three samples per group were obtained in total (3 biological replicates, n = 90 larvae per genotype/treatment) and frozen at -80ºC. Next, frozen samples' tissue was lysed to prepare for RNA extraction. 350 µM RLT and 3.5µM βME were added to samples and shaken in the TissueLyser with a metal ball at 50Hz for 3 minutes. Samples were then centrifuged at 13rpm for 2 minutes, the supernatant was collected and centrifuged at 13rpm for 3 minutes. The lysates were placed in QIAcube for automatic total RNA extraction via RNeasy Plus Mini Kit and Protocol (Qiagen). Obtained RNA samples were measured for concertation, 260/280 and 260/230 wavelengths using a nanometer. In addition, to confirm RNA presence, samples were visualized on an agarose gel. 1µl of RNA was treated with formaldehyde (50% of the sample) at 55ºC for 10 minutes, treated with EtBr and ran under gel electrophoresis at 90V for 20 minutes, and visualized via AlphaImager.

4.4.2 cDNA synthesis

1µg of total RNA was reverse transcribed using the iScript Reverse Transcription Supermix (Bio-Rad Laboratories, Mississauga, Canada) and PCR protocol for cDNA synthesis (**Table 4**).

Table 4. PCR protocol for cDNA synthesis

5 min	25ºC
30 min	42ºC
5 min	85ºC
∞	4ºC

4.4.3 cDNA 18s PCR product visualization

Uniform concentrations of cDNA across samples were confirmed by the visualization of 18s product via gel electrophoresis. 1µl of synthesized cDNA was used to amplify the 18s product

via Taq polymerase in a PCR protocol (**Table 5**). 5µl of the PCR product and 1µl of loading dye were run on an agarose gel containing EtBr at 90V for 20 minutes. Obtained gel bands were visualized in AlphaImager and contrasted against a 100bp DNA ladder.

Table 5. PCR protocol for 18s product

15 min	95ºC	
30 sec	94ºC	x 17
30 sec	52ºC	
1 min	72ºC	
10min	72ºC	
∞	4ºC	

4.4.4 RT-qPCR

The equivalent of 130ng of cDNA per sample was analyzed in Reverse Transcription quantitative PCR (RT-qPCR). SsoAdvanced SybrGreen PCR mix (50%), PCR-grade water (47.5%) and forward and reverse primer mixes (2.5%; **Table 3**) comprised a 30µl solution to which 1µl of cDNA was added and split into triplicates for the analysis of technical replicates. Samples were run on a 96-well plate in a Bio-Rad CFX96 real time PCR system under the SyberGreen Protocol. Nontreated controls and PTZ treated samples were paired on each run with the inclusion of references genes *actb2* and *tuba1a*. CT values were analyzed in the Relative Expression Software Tool (REST-2009) and gene expression ratios were obtained by comparing the expression in non-treated controls to PTZ treated (**Equation 1**) (Pfaffl et al., 2002). The statistical significance was tested by a Pair Wise Fixed Reallocation Randomisation Test©.

Equation 1. Relative quantification of expression in RT-qPCR

$$R = \frac{(E_{target})^{\Delta CT\ target(control-sample)}}{(E_{ref})^{\Delta CT\ ref(control-sample)}}$$

R = relative expression ratio

E = RT-qPCR efficiency

CT = Cycle Threshold

4.5 Computational Analysis

4.5.1 CNN model

4.5.1.1 Preprocessing of videos

Videos of PTZ treated TL and *panx1* knockout larvae (n = 6 per group) used in activity and seizure-associated behavioral scoring were retrieved from the ZebraLab software. Individual frames during peak activity (20 to 40 minutes post-PTZ treatment) were extracted in MATLAB® (30fps) and each well was automatically cropped out of the frames, creating a continuous sequence of images for individual larva. A subset of images (0.4%) was selected and manually categorized into either a 'non-convulsing' group with normal swimming behavior or 'convulsing' group with signs of twitching and loss of posture described for stage III seizure-associated activity. Training images for the 'non-convulsing' category were selected randomly, with a mixture of images of larvae in-between convulsions and nontreated controls. The labelled images were used as input for the training on the Convolutional Neural Network (CNN).

4.5.1.2 CNN architecture

The CNN architecture was constructed in the Deep Learning Network module on MATLAB® ("Create Simple Deep Learning Network for Classification," 2020; *MATLAB and Deep Learning Toolbox Release 2020a*, 2020). It consisted of 17 layers in total, with the first and last layers processing the input or output of image data. The layers in-between consisted of a combination of Convolution2D layers, ReLu layers, MaxPooling layers and BatchNormalization layers. The CNN model was constructed for maximal accuracy of training, without overfitting of the data.

`Convolution2dLayer` – convolves an input image for its unique features and assigns a value (weight). Convolutional layers deeper into the CNN are more detailed and specific to the category (**Fig. 5** grey scale images are a representation of features extracted in each layer).

Example of controlled and learnable parameters (Conv1 layer)

Hyperparameters	Learnable Parameters
`FilterSize: [2 2]`	`Weights: [2 x 2 x 3 x 40]`
`NumChannels: 'auto'`	`Bias: [1 x 1 x 40]`

```
NumFilters: 40
Stride: [1 1]
DilationFactor: [1 1]
PaddingMode: 'same'
PaddingSize: []
```

`reluLayer` – applies a non-linearity equation to the processed weights, by converting negative weight values to 0 (*f(x) = max(0, x)).* Assists with speed and complexity of training.

`batchNormalizationLayer` – normalizes weights of a small section of the image with that area's mean and standard deviation values. Aids with the speed of training and sensitivity.

`maxPooling2dLayer` – down-sampling of the input; pools values of a specified region and creates a single output of the maximum value.

Example of controlled parameters

Hyperparameters

```
PoolSize: [2 2]
Stride: [2 2]
PaddingMode: 'manual'
PaddingSize: [0 0 0 0]
```

A subset of images was categorized for either 'non-convulsing' or 'convulsing' and applied to the CNN structure described above. Learning conditions were specified:

Learning rate - 0.001; representative of the number of weights updated at a time, based on the error gradient estimation in the current state of the network.
Max Epochs – 20; the number of times the entire training dataset is passed through the network.
Iterations – 31 per epoch; the number of smaller batch of data the epoch is divided to.
Validation frequency – 30; testing frequency of the network, at every 30 epoch a set of data is tested for accuracy of the network

4.5.1.3 Training of data

During training, a set of labeled images were continuously tested for the accuracy of the network. Post-training, a confusion chart identified the error rate for each category individually and assessed for false positives. Additionally, images of nontreated controls were processed through the network to evaluate its sensitivity.

4.5.1.4 Testing of data

The Trained CNN was applied on the unlabelled images of seizing larvae to individually classify them as ‘convulsing’ or ‘non-convulsing’. A consecutive sequence of ‘convulsing’ images per larva was scored as a single convulsive event. The events were quantified and time spent convulsing (% frequency) and duration of convulsing events (sec) were analyzed.

Fig. 5 Convolutional Neural Network (CNN) structure for the categorization of convulsive events in PTZ treated larvae.

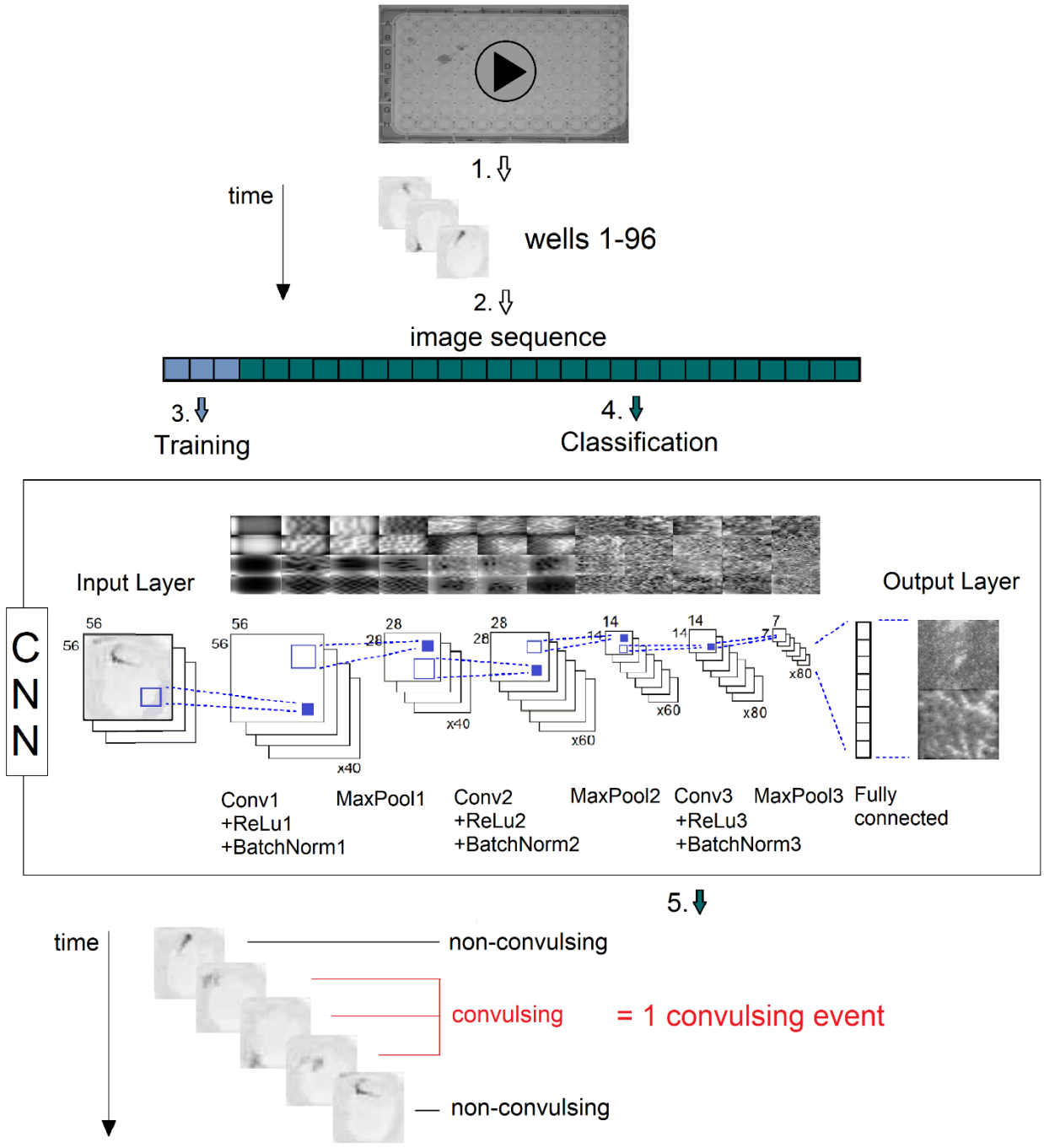

1. ZebraLab videos of PTZ treated TL and *panx1* knockout larvae were processed to extract a time sequence of images for induvial larva. **2.** The image sequences were applied to the CNN to categorize into 'convulsing' or 'non-convulsing' groups. **3.** A small subset was used for training through the 17 layers of the CNN model that create a feature map identifying each category. **4.** The model was used to classify unlabelled images. **5.** Categorized image sequences were analyzed for convulsive events, where a consecutive sequence identified as 'convulsing' was scored as a single convulsive event.

4.5.2 Unsupervised clustering model

4.5.2.1 Data acquisition

An unsupervised clustering method was applied to TL and *panx1* knockout larvae's behavioral data to identify similarities between PTZ induced phenotypes. Larvae were treated with 15mM PTZ and recorded for one hour at 1-minute intervals. Time series data of the same behavioral parameters captured by the ZebraLab software and analysed in the PCA were used as input values in the Self-Organizing Map (SOM) function in MATLAB® (*MATLAB and Deep Learning Toolbox Release 2020a*, 2020).

4.5.2.2 Unsupervised clustering method

The Self-Organizing Method (SOM) was used to cluster behavioral data based on their similarities and generate 'neurons' that act as the best representation for a group of data.

```
net = selforgmap([dimension1 dimension2]);

% Training of data
[net,tr] = train(net,DATA);
```

Each larva was categorized for a representative 'neuron' that clusters most of the larva's data around it.

```
% Testing of data, y is the representative 'neuron' output
y = net(DATA);

% extract representative 'neuron's
rep_neuron=vec2ind(y);
```

4.5.2.3 Data processing

Each larva was assigned a 'neuron' that best represented its behavioral data, creating fractions of larvae that were represented by 'neurons' one through four for each behavioral parameter. Next, the fraction values were used to visualize the relationship between genotypes via heatmaps. The relationships were visualized by analysing how far removed each genotype is from one another in each neuronal cluster by calculating the differences in fraction values (difference in %). Heatmaps of similarity scores between genotypes for each behavioral feature were plotted. The heatmaps reveal information about the feature-specific similarity between genotypes.

4.6 Electrophysiology

4.6.1 Preparation of larvae

Individual GCaMP6 larva (5 to 7dpf) was anaesthetized with 300µM Pancuronium Bromide (Panc) for 5 minutes or until larva showed no signs of movement and intact circulation. The larva was positioned dorsally and fixed on the experimental stage with 2% noble agar. The stage was placed under the Femto2D microscope, the larva was checked for viability and 1ml of E3 medium was added over the top of the agar.

4.6.2 Equipment set-up

MES electrophysiology system was used. Femto2D microscope and HC Image Live software were used to visualize larva, Multiclamp for amplification of the electrical single and 1550A digitizer for reduction of background noise. After the stage with the fixed larva was placed under the microscope, a reference wire of 2.5-3MΩ resistance was fixed on the stage with agar as well. The recording electrode was inserted into a capillary containing 2M NaCl solution. The capillary was placed into the egg water on top of the fixed larva and reference wire to check for stable signal and appropriate resistance. Once a stable signal of < 0.05mV has been established, the set-up is complete, and the larva is ready for insertion of the capillary.

4.6.3 LFP recording in larvae

Capillary was inserted into the right optic tectum of larva and recorded for baseline activity for a minimum of 5 minutes. Images of the larva's head under bright field light and the GFP filter were taken. 20mM final concentration PTZ was applied, and images were taken again. LFP signal was recorded for an hour post-treatment and seizure-like events (SLE), that manifest as excessive polyspiking, were monitored in real-time. During SLEs, GCaMP6 fluorescence activity in the brain was imaged under the GFP filter at 1fps.

4.6.4 Post-recording processing of data

Images of GCaMP6 fluorescence obtained during SLEs were processed in ImageJ software. LUT filter, differentially coloring the fluorescence activity based on intensity level, was applied to the

image sequences for visualization of shift in brain activity during SLEs. Additionally, localization and changes to fluorescence during SLEs compared to baseline were derived using the threshold filter and setting the threshold at baseline activity.

4.7 Statistical Analysis

All statistical analyses were conducted in GraphPad Prism 9.0 unless specified otherwise. Each analysis was performed on $n \geq 3$ independent replicates and a p-value of ≤ 0.05 was deemed statistically significant. Refer to **Supplementary Table S4** for details on statistical tests and values.

4.7.1 Statistics in behavioral and survival assays

Locomotor behaviors detected by the ZebraLab software were extracted and analysed via Principal Component Analysis (PCA) to select a behavioral variable responsible for most of the variation in the data. Next, the chosen variable, activity score (Δpixel) was analyzed via Two-way Repeated Measurements (RM) ANOVA for the effects of genotype and time. Post-ANOVA, Bonferroni multiple comparisons test indicated the time points the *panx1* knockouts' activity significantly differed from TL. The areas under the activity curve (AUC) were generated in GraphPad for each of rest, base, and PTZ-induced activity plots. AUCs were compared between genotypes via One-way ANOVA, followed by Tukey's multiple comparison test. AUCs for Pb and A43 treatments against PTZ only controls were analyzed via two-tailed unpaired t test and Mann-Whitney U test (due to unmatched sample sizes), respectively. Seizure-associated stages II and III were manually scored at 2-minute intervals and analyzed with Two-way RM ANOVA, followed up by Bonferroni multiple comparison test in Pb and A43 treatment groups. TL and *panx1b*$^{-/-}$'s total stage III count was further examined with a two-tailed unpaired t test and average stage III count per 2 minutes with a two-tailed paired t test (paired across time). Survival rates were plotted on Kaplan-Meier plots and analyzed with Mantel-Cox (log-rank) test.

4.7.2 Statistics in RT-qPCR

CT values were obtained from the CFX Manager software after the completion of RT-qPCR. The CT values were analyzed in REST 2009 software to determine the differential expression of

target genes in PTZ-induced larvae to their non-treated controls. Pair Wise Fixed Reallocation Randomisation Test© was implemented to test for significance ($p < 0.05$) of gene regulation.

4.7.3 Statistics in computational analysis

In the CNN model, the time series of larvae images categorized as ‘convulsing’ or ‘non-convulsing’ were scored for occurrences of consecutive ‘convulsing’ frames. Continuous ‘convulsing’ frames in a row, neighboring ‘non-convulsing’ frames on both ends, were considered to represent an independent convulsion event. The length of these events (seconds), their frequency and total count, standard deviation (SD), standard error mean (SEM), 95 % confidence interval (95%CI), maximum and minimum length (seconds) were calculated using standard MATLAB® statistical functions.

5. Results

5.1 Genetically targeting *panx1* has a mixed effect on seizure-associated behavior, molecular and electrophysiological responses

5.1.1 PCA on behavioral attributes of TL and *panx1* knockout larvae

7dpf TL (Wild-type strain) and *panx1* knockout larvae were assessed for their behavioral response to treatment with an established convulsant, PTZ. Larvae were placed in a 96-well plate and PTZ-induced behavior was recorded for one hour. The ZebraLab software generated several behavioral parameters that break down larvae's locomotion. The parameters were categorized based on larvae's speed of movement and were counted for the number of occurrences (count) and duration (sec) of specified movement speed. Freezing, a state of immobility (0 mm/sec) was counted (freeze count) and timed (freeze dur), as well as, swimming at an average speed (0-20mm/sec; mid count and mid dur) and burst activity (≥ 20 mm/sec; burst count and burst dur). Additionally, the total duration of any movement (total dur) and activity score described as a total change in pixels (Δpixel) were generated by the software. The eight behavioral parameters were investigated under the Principal Component Analysis (PCA) for dimension reduction and determination of a parameter suitable for further analysis (**Fig. 6**). The first two Principal Components (PC) accounted for 94% of the variance in data (**Fig. 6a**). As such, further PCA was conducted in a 2-dimensional space of PC1 against PC2. The Eigenvector map depicted the relative contribution of the behavioral parameters to either of the PCs, with highly contributing parameters aligning with the horizontal plane (PC1) or vertical (PC2) (**Fig. 6b**). Parameters for total and freeze durations highly contributed to PC1 in opposite directions, followed by the activity score. Freeze count and burst duration contributed to PC2 the most, followed by the activity score. As the activity score contributed to both PCs, the parameter was chosen for further investigation of PTZ-induced behavior. Lastly, PC score maps uncovered that TL and DKO's behavioral data was most similarly distributed, and *panx1a*$^{-/-}$ and *panx1b*$^{-/-}$ data was most dissimilar (**Fig. 6c**). *Panx1a*$^{-/-}$ and *panx1b*$^{-/-}$'s data showed high variance in the negatively correlated direction for both PCs, justifying the activity score as the suitable parameter for visualizing differences between the two genotypes.

Fig. 6 PCA on PTZ treated TL and *panx1* knockout larvae's behavioral parameters.

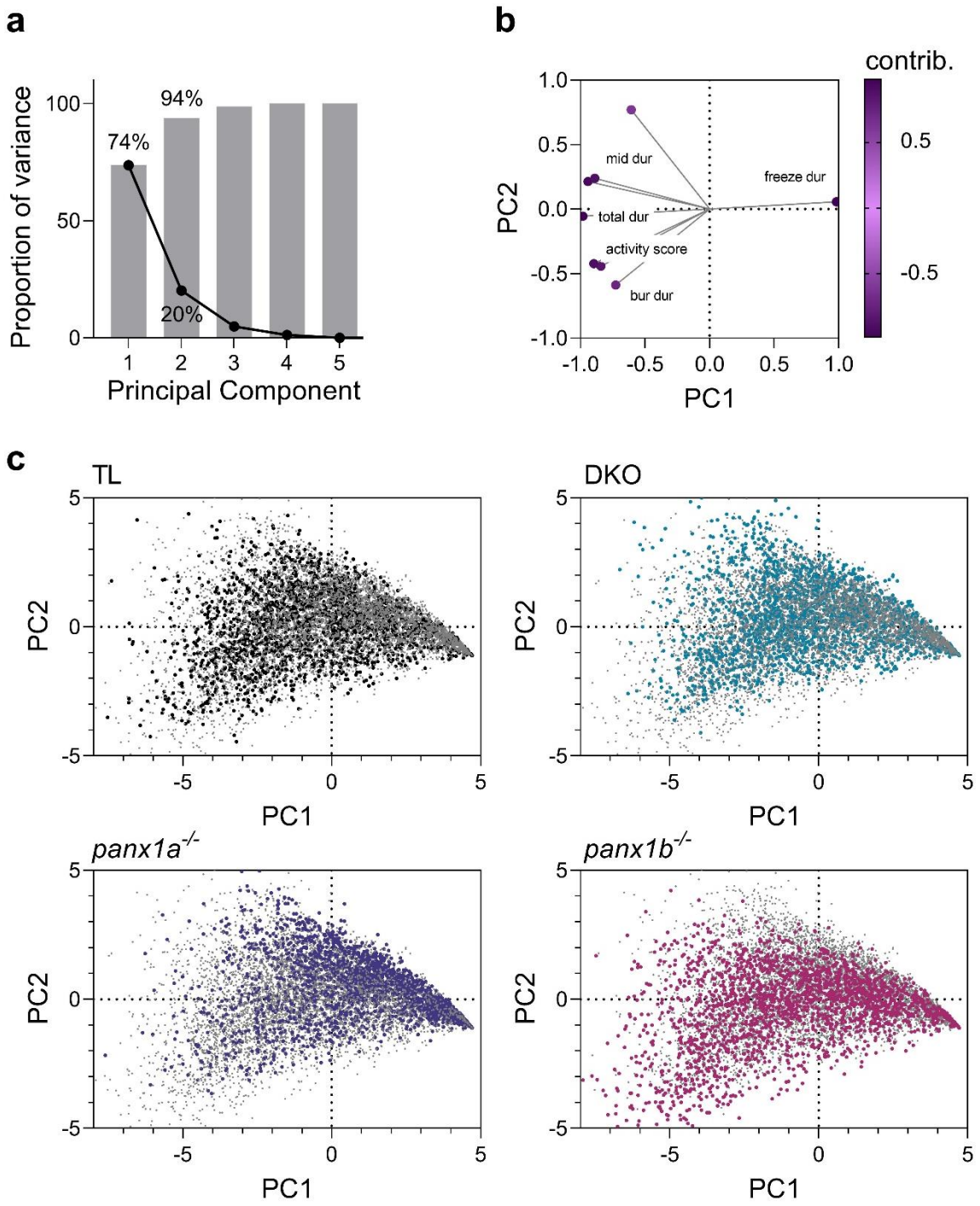

Eight behavioral parameters of PTZ treated TL and *panx1* knockout larvae generated by the ZebraLab software were analyzed for contribution to data variance via PCA. **a** Proportions (%) of Principal components' (PC) individual (point) and cumulative (bar) contributions to variance. **b** Eigenvector map of behavioral parameters' correlation with PC1 and PC2. Higher values indicate a positive correlation of the parameter with PCs, lower values indicate a negative correlation. Darker purple represents a larger influence on PC1. **c** PC score maps for genotypes' behavioral data. Colored data points indicate labelled genotype, grey color is attributed to the rest of the genotypes.

5.1.2 Seizure-related hyperactivity is reduced in *panx1a*$^{-/-}$ and increased in *panx1b*$^{-/-}$

Activity scores (Δpixel ± SEM; n = 36 per genotype), indicative of overall locomotor activity in larvae, were plotted for rest, baseline and PTZ induced behavior (**Fig. 7a**). Resting activity was recorded for 25 minutes and accounted for the undisturbed locomotor behavior of larvae. *Panx1b*$^{-/-}$'s locomotor activity at rest was significantly higher compared to TL ($p < 0.05$; 8-13 minutes). Next, baseline activity was recorded for 30 minutes after the E3 medium was applied to account for any behavioral changes due to an addition of a medium and disturbance to larvae. Application of the E3 medium caused a transient increase in activity for all genotypes that stabilized within 30 minutes. *Panx1b*$^{-/-}$'s baseline activity increased and stabilized at significantly higher levels compared to TL ($p < 0.05$; 1-9, 20-25 minutes). Lastly, 15mM PTZ was added, and larvae's behavior was recorded for one hour. All genotypes exhibited a continuous increase in activity for the first 10 minutes, a peak around 15 to 30 minutes and a gradual decline within the hour. The activity pattern corresponded with previously observed behavior for PTZ treated zebrafish larvae in literature (Ekkwill strain) (Afrikanova et al., 2013). DKO's activity curve did not significantly differ from TL (**Fig. 7b** second from the top), however, did not reach the maximum PTZ-induced activity in TL indicated by the dashed line. *Panx1a*$^{-/-}$'s PTZ-induced hyperactivity was reduced significantly compared to TL after its peak (**Fig. 7b** third from the top; $p < 0.05$; 22-49 minutes). *Panx1b*$^{-/-}$ exhibited a sharper and higher peak of activity than TL (**Fig. 7b** bottom; $p < 0.05$; 18-21 minutes) and displayed a steeper decline in activity after the peak.

To account for the contributions of varying baseline activities in *panx1* knockouts to their response to PTZ treatment, Areas Under the Curve (AUCs) were calculated for activity plots in **Fig. 7ab** (**Fig. 7c**). AUCs of the last 15 minutes of stabilized baseline activity were significantly different between *panx1b*$^{-/-}$ and TL only (**Fig. 7c** top, open points; $p < 0.0001$). AUCs for PTZ-induced activity plots were significantly lower in *panx1a*$^{-/-}$ (**Fig. 7c** top, closed points; $p < 0.0001$) and higher in *panx1b*$^{-/-}$ ($p < 0.01$) compared to TL. Means of stabilized baseline activity for each genotype were subtracted from their respective PTZ-induced activity curves and calculated as AUCs for the effect of PTZ (**Fig. 7c** bottom). As a result, only *panx1a*$^{-/-}$'s AUC was significantly lower than that of TL ($p < 0.001$).

In summary, general locomotor activity in PTZ treated *panx1* knockout larvae revealed *panx1a*$^{-/-}$ phenotype as the least susceptible to seizure-related hyperactivity and *panx1b*$^{-/-}$ as the most, whilst DKO displayed the most similar phenotype to TL.

Fig. 7 Genetic targeting of *panx1a* or *1b* differentially affects seizure-related hyperactivity.

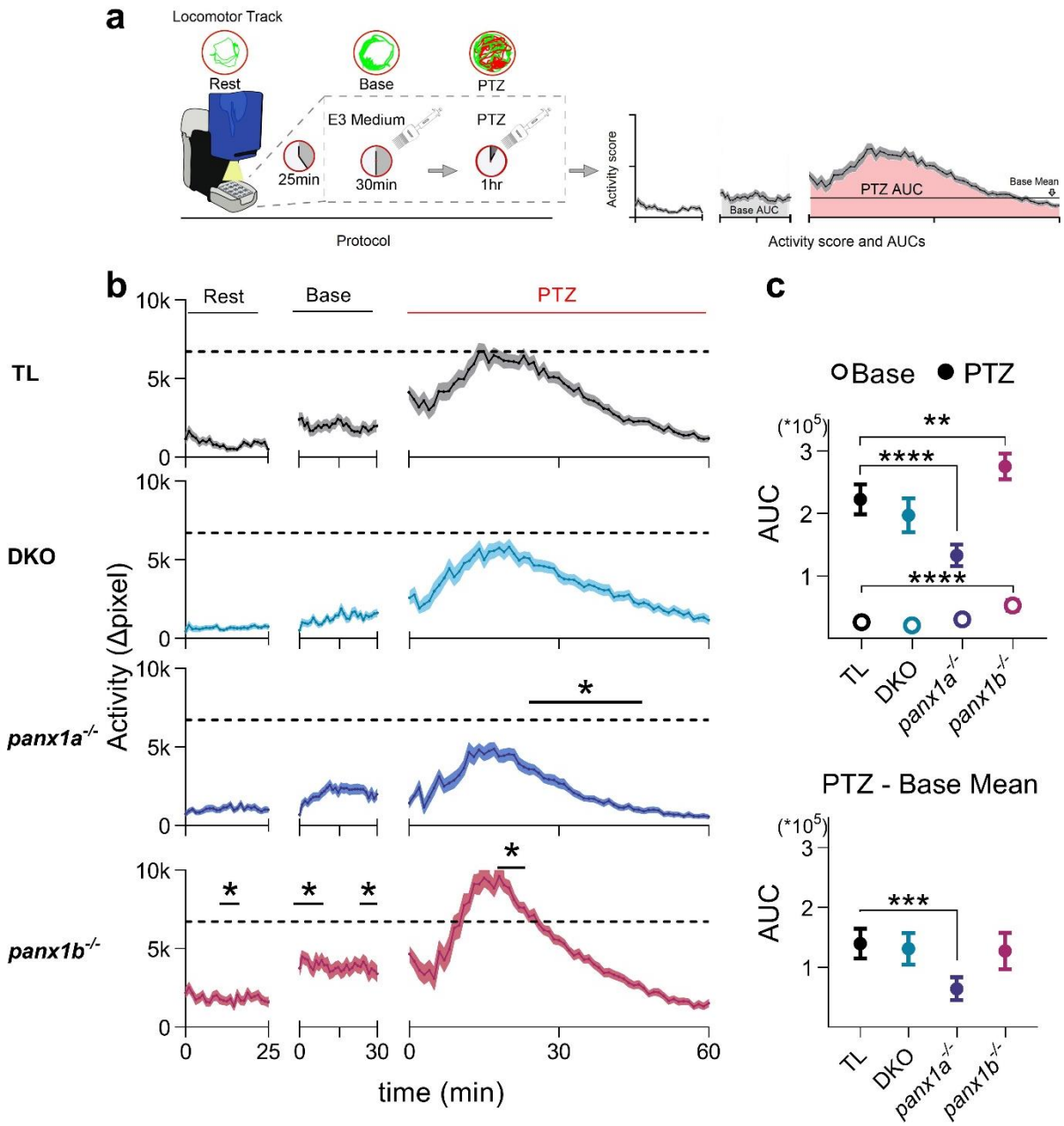

a Locomotor activity was recorded in 7dpf TL and *panx1* knockout larvae (n = 36) in the ZebraBox apparatus and treated with 15mM PTZ to observe for seizure-related behavior. **b** Activity score (Δpixel) was plotted for 25-minute rest, 30-minute baseline and 1-hour PTZ-induced behavior. At baseline, when an additional medium was added to the larvae, a transient peak of activity was observed that stabilized within 30 minutes. *Panx1b*$^{-/-}$*'s* (bottom; purple) rest and baseline activity significantly differed from TL (top; grey) ($p < 0.05$). Addition of PTZ induced hyperactivity in all genotypes. Activity score increased within the first 10 minutes of treatment, peaked from 15 to 30 minutes, and subsided within the hour. *Panx1a*$^{-/-}$ (third from the top; dark blue) had a significantly reduced hyperactivity (18-40 minutes, $p < 0,05$), whereas *panx1b*$^{-/-}$ exhibited an increase in activity (18-21min, $p < 0.05$). DKO (second from the top; light blue) did not significantly differ from TL. Max average activity score for TL is indicated with a dashed line. **c** AUCs of activity plots in (**b)** were compared between genotypes. Baseline AUC was higher for *panx1b*$^{-/-}$ than TL ($p < 0.0001$). Treatment resulted in a smaller PTZ-induced AUC for *panx1a*$^{-/-}$ than TL ($p < 0.0001$), and a larger AUC in *panx1b*$^{-/-}$($p < 0.01$). When genotypes' respective average baseline activity was subtracted from the PTZ AUC, *panx1b*$^{-/-}$ was not significantly different from TL. AUC of *panx1a*$^{-/-}$, however, remained significantly lower than TL ($p < 0.001$). * - $p < 0.05$, ** - $p < 0.01$, *** - $p < 0.001$, **** - $p < 0.0001$. *Data and graphs were generated by Daria Taskina and included in* (Whyte-Fagundes et al., 2021) *manuscript.*

5.1.3 SOM identify behavioral parameters that differentiate PTZ-induced *panx1* knockout larvae's behavior

An unsupervised clustering method, Self-Organizing Map (SOM) was employed to uncover behavioral parameters that foster similarities and differences between PTZ treated TL and *panx1* knockout larvae (n = 36 per group). Behavioral parameters generated by the ZebraLab software and used in the PCA were utilized for SOM generation. Behavioral data points were processed through the unsupervised clustering method and grouped to one out of four representative 'neurons' they identify with the most (**Fig. 8a**). The proportion of genotypes' larvae represented by a particular 'neuron' was plotted for each neuron and each behavioral parameter (**Fig. 8b**). For the activity score, PTZ treated TL and DKO share the most similarities in terms of how many of their larvae are represented by each neuron. Nearly 50% of larvae's data is represented by 'neuron 1' for both genotypes. 36% of DKO and 17% of TL are represented by 'neuron 2', 6% of DKO and 11% of TL by 'neuron 3', and 11% of DKO and 17% of TL by 'neuron 4'. Overall, the two genotypes are the closest in percentages across all neurons, compared to *panx1a*$^{-/-}$ and *panx1b*$^{-/-}$ genotypes, which display a unique distribution of neuron representation.

An unsupervised categorization of data has two main implications. One use for this type of analysis is to uncover which genotypes bear similarities in which behavioral categories. TL and DKO treated with PTZ share the most similarities in overall activity levels, burst count, and duration of average locomotion (mid dur). On the other hand, *panx1a*$^{-/-}$ and *panx1b*$^{-/-}$ share the least amount of similarities in terms of overall activity, number of average locomotor events (mid count), and burst durations. This is due to the fraction of their larvae that are represented by each 'neuron' in these parameters are furthest apart from each other and the rest of the genotypes. Another outcome of this analysis is behavioral features that successfully distinguish genotypes can be extracted for future investigation, similarly to a PCA method. In the case of PTZ treated TL and *panx1* knockout genotypes' activity, number of freezing (freeze count) and average swimming events (mid count) display the most variation in how data is distributed across genotypes for each 'neuron'.

Fig. 8 Fractions of larvae in the TL and *panx1* knockout groups represented by a 'neuron' in each behavioral parameter based on SOM clustering.

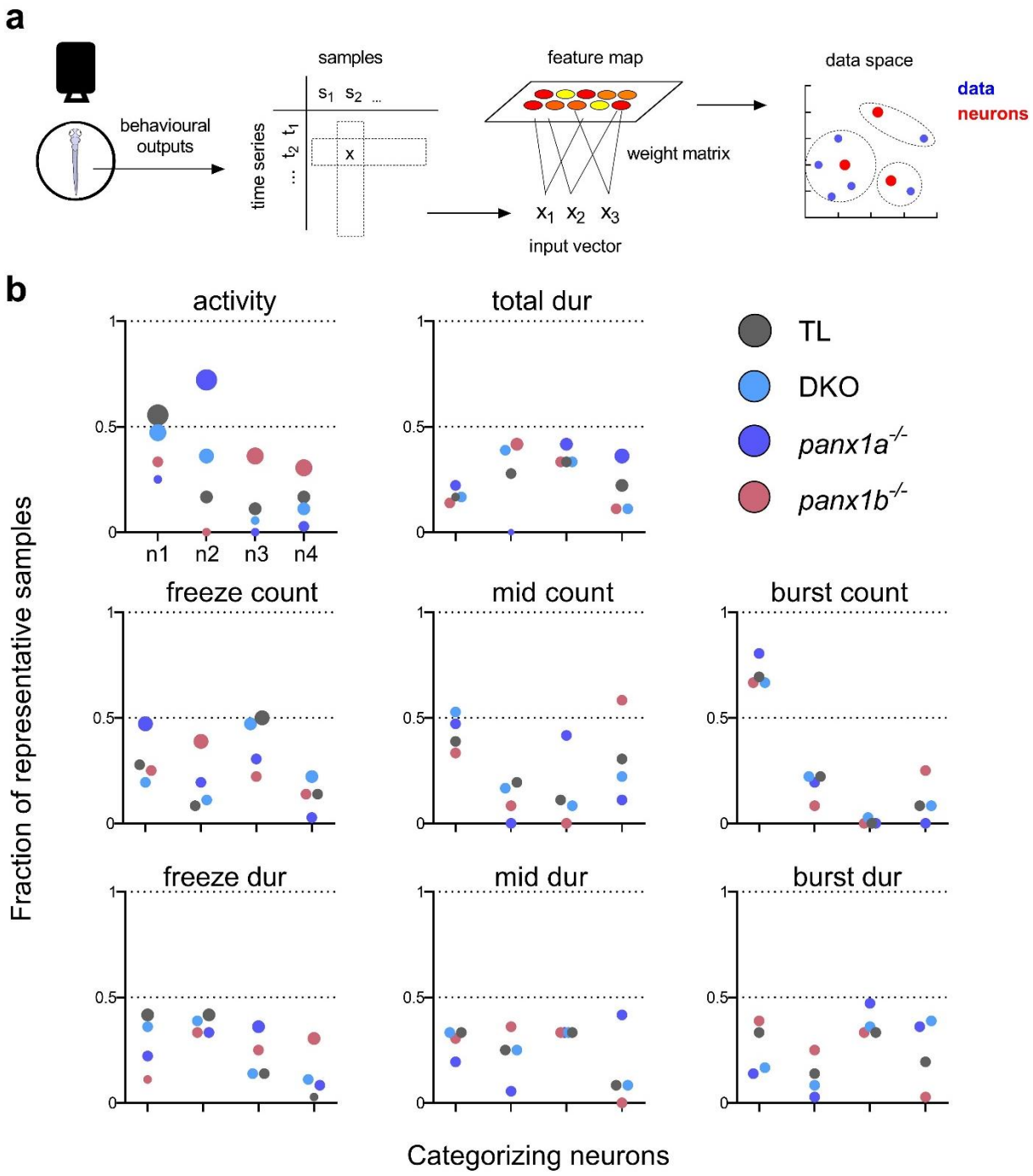

a Behavioral parameters' data was categorized into four representative 'neurons' via SOM. **b** Fractions (%; y-axis) of TL and *panx1* knockout larvae that hold data represented by one out of four 'neurons' (x-axis) in each of the eight behavioral parameters are plotted. Genotypes that are plotted closely together are highly similar in neuron representation. Parameters include activity (Δpixel), total duration of movement (sec), number of freezing events (freeze count) and their duration (sec), number of average movement events (mid count) and their duration (mid dur; sec), and number of burst events (burst count) and their duration (sec).

For further interpretation of the results, the clustering outcomes were graphed as heatmaps based on similarities between genotypes for each behavioral parameter (**Fig. 9**). Heatmaps were generated based on the distances between representative genotype fractions for each neuron. For example, in the activity category, 72% of *panx1a*$^{-/-}$ larvae are represented by 'neuron 2' which is much higher than the 3% of *panx1b*$^{-/-}$ represented by the same neuron, marking them as furthest apart from one another. The distances were pooled across all four neurons for each parameter and plotted as similarity heatmaps. Thus, higher similarity scored lower due to the shortest average distance between genotypes. The results indicated that PTZ treatment resulted in the most behavioral similarities between TL and DKO, specifically in the total duration of movement, freezing count and duration, average swimming duration and burst counts categories. In contrast, TL was most dissimilar to *panx1a*$^{-/-}$ in their activity, average swimming events and their duration, and burst duration. *Panx1a*$^{-/-}$ and *panx1b*$^{-/-}$ shared the least number of behavioral similarities in these categories as well, suggesting *panx1a*$^{-/-}$ larvae display the most unique phenotype with PTZ treatment.

Fig. 9 Heatmaps derived from SOM show similarities between TL and *panx1* knockouts' response to PTZ treatment in eight behavioral parameters.

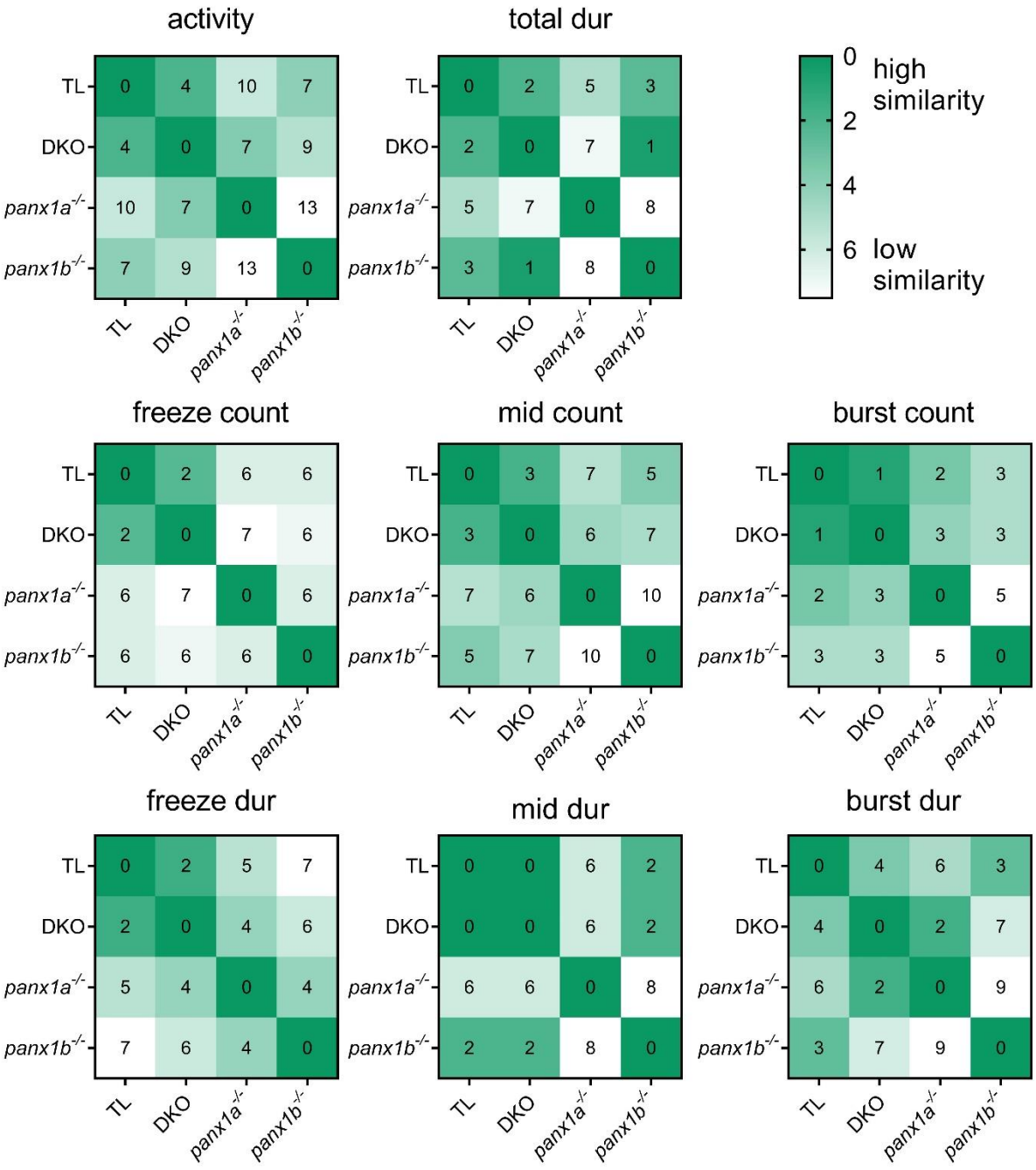

Heatmaps depict average distances between each genotype pooled for four representative SOM 'neurons' in each behavioral parameter. High behavioral similarity is in green with a lower number; 0 indicates maximum similarity or the same genotype. Behavioral parameters include general activity score (Δpixel), total duration of movement (total dur; sec), number of freezing events (freeze count) and their duration (freeze dur; sec), number of normal movement events (mid count) and their duration (mid dur; sec), and number of burst events (burst count) and their duration (burst dur; sec).

5.1.4 Seizure-associated stages II and III behavior manifest differentially in *panx1* knockouts

Changes in seizure-specific behaviors in *panx1* knockout larvae were scored next (**Fig. 10**). Stage II of PTZ-induced seizure-associated behaviors manifests as 'whirlpool-like' rapid circling around the wells (**Fig. 10a**). Stage III is detected as uncontrollable convulsions followed by a prolonged loss of balance (**Fig. 10b**) (Baraban et al., 2005). Stages II and III were manually and blindly scored at 2-minute intervals for a total of one-hour post-PTZ treatment (count/2min; n = 18 per genotype). Stage II events commenced a few minutes after treatment and lasted for 30 minutes (**Fig. 10a**). TL and *panx1b*$^{-/-}$'s stage II activity peaked earlier on, in the first 10 minutes, and subsided within 20 minutes. DKO and *panx1a*$^{-/-}$ peaked in stage II activity around 15 minutes after treatment, exhibiting a bell curve pattern. However, stage II activity did not significantly differ among genotypes in terms of onset or total count. Stage III convulsive activity began 10 minutes after PTZ treatment, peaked at 20 to 40 minutes and gradually declined until the experimental endpoint was reached (**Fig. 10b**). DKO and *panx1a*$^{-/-}$ had a reduced stage III count over time compared to TL ($p < 0.05$). *Panx1b*$^{-/-}$, although displaying a raised peak of stage III activity than TL, did not differ from TL in terms of count over time (**Fig. 10b**) or total sum for one hour (**Fig. 10c**; $p = 0.105$; *panx1b*$^{-/-}$ 74.9 ± 5 counts/hour and TL 63.2 ± 5 counts/hour). However, mean stage III count over time significantly differed between groups and indicated a delayed peak in stage III manifestation for *panx1b*$^{-/-}$ at 34 minutes compared to a peak at 26 minutes for TL (**Fig. 10d**; $p < 0.001$). Additionally, time points at which 50% or more larvae reached a particular stage III count (from 1 up to 5 counts per 2 minutes) revealed a delayed onset of higher stage III counts in *panx1b*$^{-/-}$ (**Fig. 10e**). In summary, PTZ-induced convulsive behavior was reduced in DKO and *panx1a*$^{-/-}$ genotypes in contrast to TL. *Panx1b*$^{-/-}$ had an increased and delayed peak of convulsive behavior than TL. The manifestation of these seizure-associated behaviors corresponded with the general hyperactivity patterns detailed previously.

Fig. 10 Stage III of seizure-associated convulsive behavior is reduced in DKO and *panx1a*$^{-/-}$ and delayed in *panx1b*$^{-/-}$.

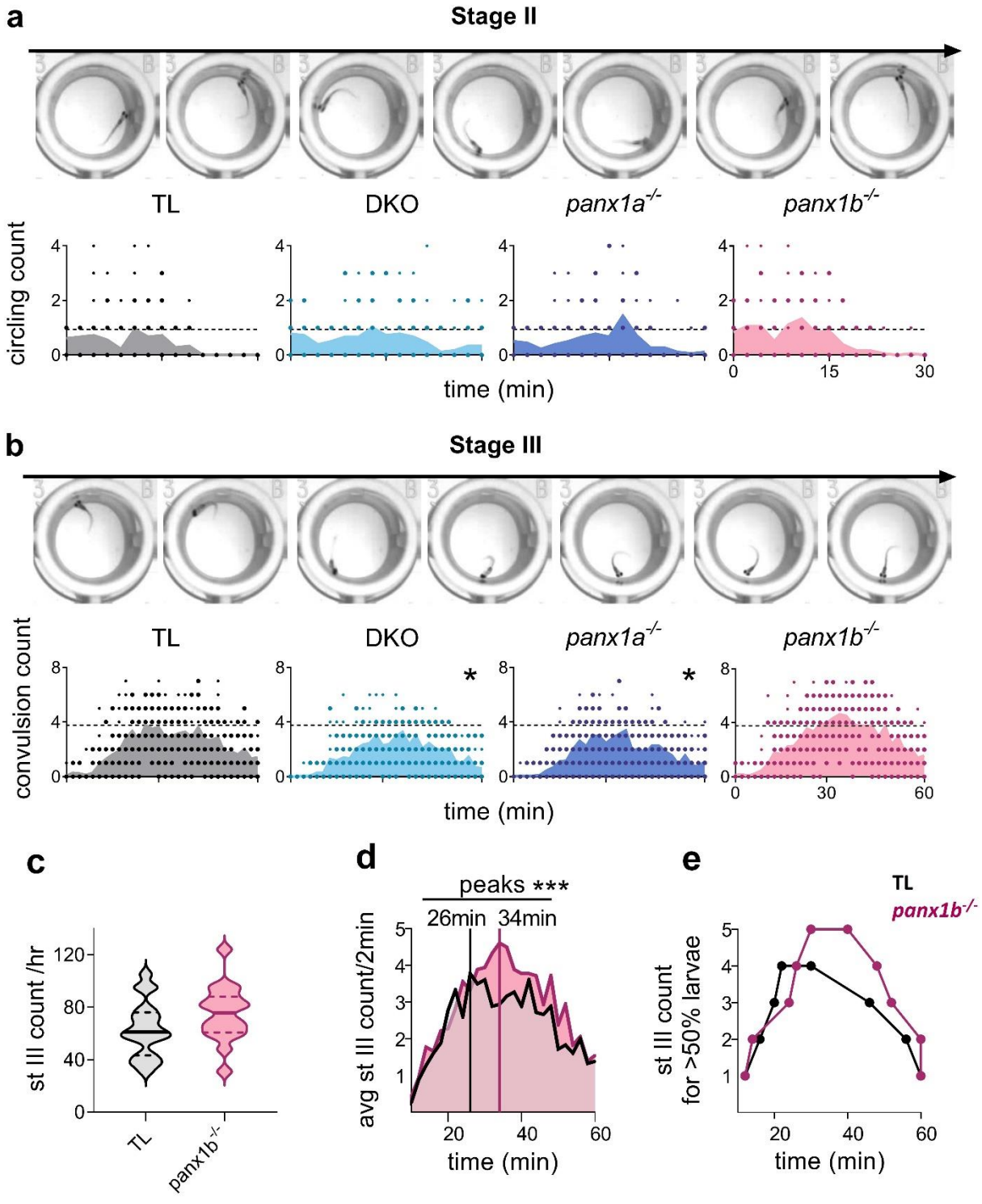

a Stage II, circling behavior depicted from left to right, was scored for TL and *panx1* knockout larvae (7dpf, n = 18) at 2-minute intervals for a total of 1 hour of PTZ treatment. None of the genotypes differed significantly in count over time or in the total count of stage II. TL and p*anx1b*$^{-/-}$ stage II events had an earlier onset (in the first 10 minutes), and DKO and *panx1a*$^{-/-}$'s stage II activity was uniform across the first 30 minutes. The grey dashed line represents max average stage II count in TL. **b** Stage III, convulsion count was significantly reduced for DKO and *panx1a*$^{-/-}$ larvae compared to TL ($p < 0.05$). The dashed line represents the max average stage III count in TL. **c** Total Stage III count over an hour did not differ between TL and *panx1b*$^{-/-}$. **d** Mean stage III activity overtime was delayed for *panx1b*$^{-/-}$, peaking at 34 minutes after PTZ treatment, compared to TL peaking at 26 minutes ($p < 0.001$). **e** 50% or more *panx1b*$^{-/-}$ larvae reached stage III counts of 1 through 5 later than TL larvae. * - $p < 0.05$, *** - $p < 0.001$. *Data and graphs were generated by Daria Taskina and included in* (Whyte-Fagundes et al., 2021) *manuscript.*

5.1.5 Convolutional Neural Network (CNN) for automated convulsion detection

A CNN model was utilized for automatic scoring and quantification of peak stage III seizure-associated behavior in PTZ induced TL and *panx1* knockout larvae (**Fig. 11,** n = 6 per group). Videos of treated larvae were extracted and categorized by frame for convulsive behavior. When the CNN model was trained on a subset of categorized images, accuracy of training reached 85%, with higher percentage of 'non-convulsing' images falsely categorized as 'convulsing'. Images of nontreated larvae were ran through the model to assess the rate of false positives. Out of the ten nontreated larvae examined, four were categorized to have 'convulsive' activity under 1.5%. Frames that were categorized as 'convulsing' in a row were identified as a single convulsing event. The amount of time larvae spent convulsing during peak stage III activity identified during manual scoring (20 to 40 minutes post-PTZ treatment) was plotted (**Fig. 11a**). *Panx1b*$^{-/-}$ had the highest convulsive frequency as per the analysis of the CNN model ($p < 0.001$), followed by TL, DKO and finally *panx1a*$^{-/-}$ ($p < 0.0001$). The overall high frequency across genotypes may be due to the presence of short 'convulsing' image sequences. The expected duration of convulsions would require to be standardized to filter out potential noise in data. Average duration of a convulsive behavior (sec; based on 30frames = 1sec) was computed to have a similar trend; *panx1b*$^{-/-}$ exhibited the longest duration among all other genotypes (**Fig. 11b**; $p < 0.0001$) and *panx1a*$^{-/-}$ the shortest ($p < 0.05$).

Fig. 11 Quantification of Stage III convulsive behavior in TL and *panx1* knockouts via CNN.

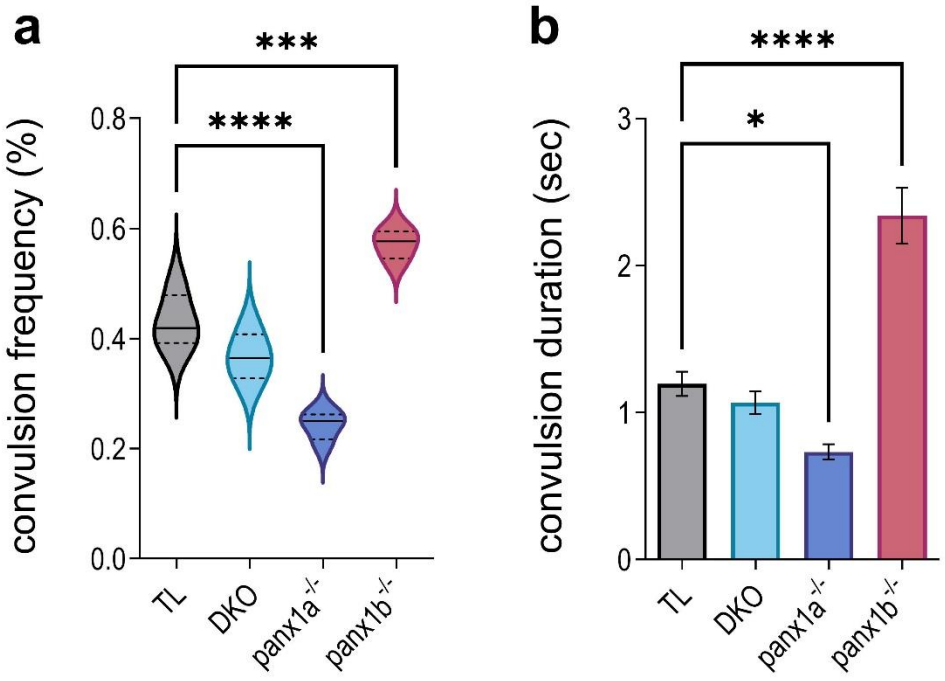

Stage III of seizure-associated convulsive behavior in PTZ-induced TL and *panx1* knockout larvae (n = 6) was extracted through a CNN model. **a** Convulsion frequency (% time) of larvae during peak stage III activity, 20-40 minutes post-PTZ treatment, was plotted. *panx1b*$^{-/-}$ had the highest frequency ($p < 0.001$), followed by TL. *Panx1a*$^{-/-}$ had the lowest convulsive frequency ($p < 0.0001$). **b** Average duration (sec) of an individual convulsive event during peak activity was plotted. *Panx1b*$^{-/-}$'s average event lasted the longest ($p < 0.0001$, ~2.5 sec) and *panx1a*$^{-/-}$ the shortest ($p < 0.05$). * - $p < 0.05$, *** - $p < 0.001$, **** - $p < 0.0001$.

5.1.6 RT-qPCR reveal the differential molecular response of PTZ treated *panx1* knockouts

Several Immediate Early Genes (IEG) were selected to observe for seizure-associated changes in *panx1* knockout larvae on a molecular level. The IEGs were selected based on evidence of strong activation in the zebrafish PTZ model (Baraban et al., 2005), in rodent models (Barkmeier et al., 2012; Lösing et al., 2017), and human epileptic cortical tissue (Rakhade et al., 2005) previously described in the literature. TL and *panx1* knockout larvae were collected for analysis via RT-qPCR after one hour of 15mM PTZ treatment and were contrasted to their respective non-treated controls for differential gene expression (**Fig. 12**; n = 30 per independent sample). *Fosab* (110.36) and *egr4* (120.54) exhibited the most robust upregulation among all tested IEGs, reaching over a 100-fold increase in expression for PTZ treated TL. The upregulation of these two genes was moderate in the *panx1* knockouts, about twice as low in DKO (*fosab* (67.62), *egr4* (63.68)) and *panx1b*$^{-/-}$ (*fosab* (57.72), *egr4* (44.53)) compared to TL. Overall DKO and *panx1b*$^{-/-}$ had the most modest upregulation of the IEGs compared to the other genotypes, having the lowest upregulation of *fosab, egr1, egr2b, egr4* and *bdnf*. TL had the highest upregulation in *fosab, eg4* and *bdnf* (6.13), while *panx1a*$^{-/-}$ in *egr1* (10.41), *egr2b* (7.59) and *jun* (9.38).

Fig. 12 Seizure-associated IEGs are differentially expressed in *panx1* knockouts

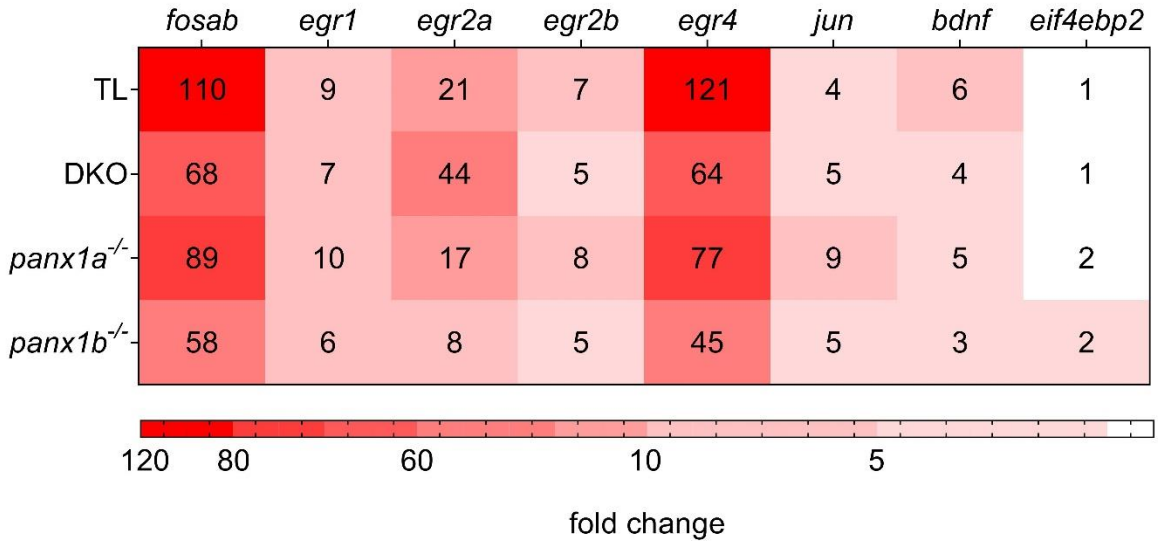

Eight seizure-associated IEGs were tested for differential expression via RT-qPCR in PTZ treated TL and *panx1* knockouts. Expression values represent fold change relative to the genotypes' respective non-treated controls. Red color represents significant upregulation ($p < 0.05$), no color depicts no significant upregulation of the gene. *Fosab* and *egr4* had the highest upregulation in TL and were moderate in the *panx1* knockouts. DKO and *panx1b*$^{-/-}$ exhibited the least amount of IEG upregulation. *Data and graphs were generated by Daria Taskina and included in* (Whyte-Fagundes et al., 2021) *manuscript.*

5.1.7 Fitness and survival improved in PTZ treated *panx1* knockouts

After reaching the experimental endpoint of behavioral tests, PTZ treated larvae were monitored for survival every hour for a total of 10 hours, and once again at 24 hours (**Fig. 13**; n = 80 per genotype). Larvae's fitness and survival were examined for three categories: evidence of movement or response to stimuli (**Fig. 13a;** fitness), presence of heartbeat and circulation (**Fig. 13b;** survival), and signs of degradation of the body (**Fig. 13c;** fitness). Each category for each genotype was graphed separately using Kaplan-Meier plots and contrasted to TL for differences in the survival curve via the Mantel-Cox test. DKO larvae ($p < 0.001$) displayed the sharpest decline in movement in the first 10 hours, followed by *panx1a*$^{-/-}$ ($p < 0.01$) as both had significantly lower movement rates compared to TL (**Fig. 13a**). At 24 hours post-PTZ treatment, none of the genotypes had any larvae that were still physically active or showed signs of mobility when stimulated. The presence of circulation declined most rapidly for *panx1a*$^{-/-}$ between 5 to 10 hours post-PTZ treatment, however, the group had the highest percentage with intact circulation at 24 hours (**Fig. 13b**; $p < 0.01$; 30%). *Panx1b*$^{-/-}$ had 13% of larvae show the presence of circulation at 24 hours ($p < 0.01$), and DKO had 11% but did not significantly differ from TL. Reduced to 1%, TL larvae had the lowest presence of circulation at 24 hours. Degradation of the body followed after the loss of movement and circulation but did not have a high occurrence in the first 10 hours (**Fig. 13c**). Most genotypes had a similar outcome at 24 hours (TL (46%), DKO (56%), *panx1a*$^{-/-}$ (51%)) and only *panx1b*$^{-/-}$ (68%, $p < 0.05$) exhibited significantly less degradation compared to TL. In summary, all genotypes lost movement after 24 hours from the start of the PTZ treatment, with the sharpest and fastest decline observed in DKO and *panx1a*$^{-/-}$. The presence of heartbeat and circulation was considered as the metric for survival, where *panx1a*$^{-/-}$ performed best, followed by *panx1b*$^{-/-}$ and DKO, TL having the lowest survival rate at 24 hours. Degradation of the body was observed at similar rates in all genotypes except *panx1b*$^{-/-}$ which performed the best in this category. The results suggest that genotypes such as DKO and *panx1a*$^{-/-}$ may respond to external stressors with inactivity, however, it does not correlate to their overall survival which is improved compared to TL.

Fig. 13 Fitness and survival after PTZ treatment are improved in *panx1* knockout larvae.

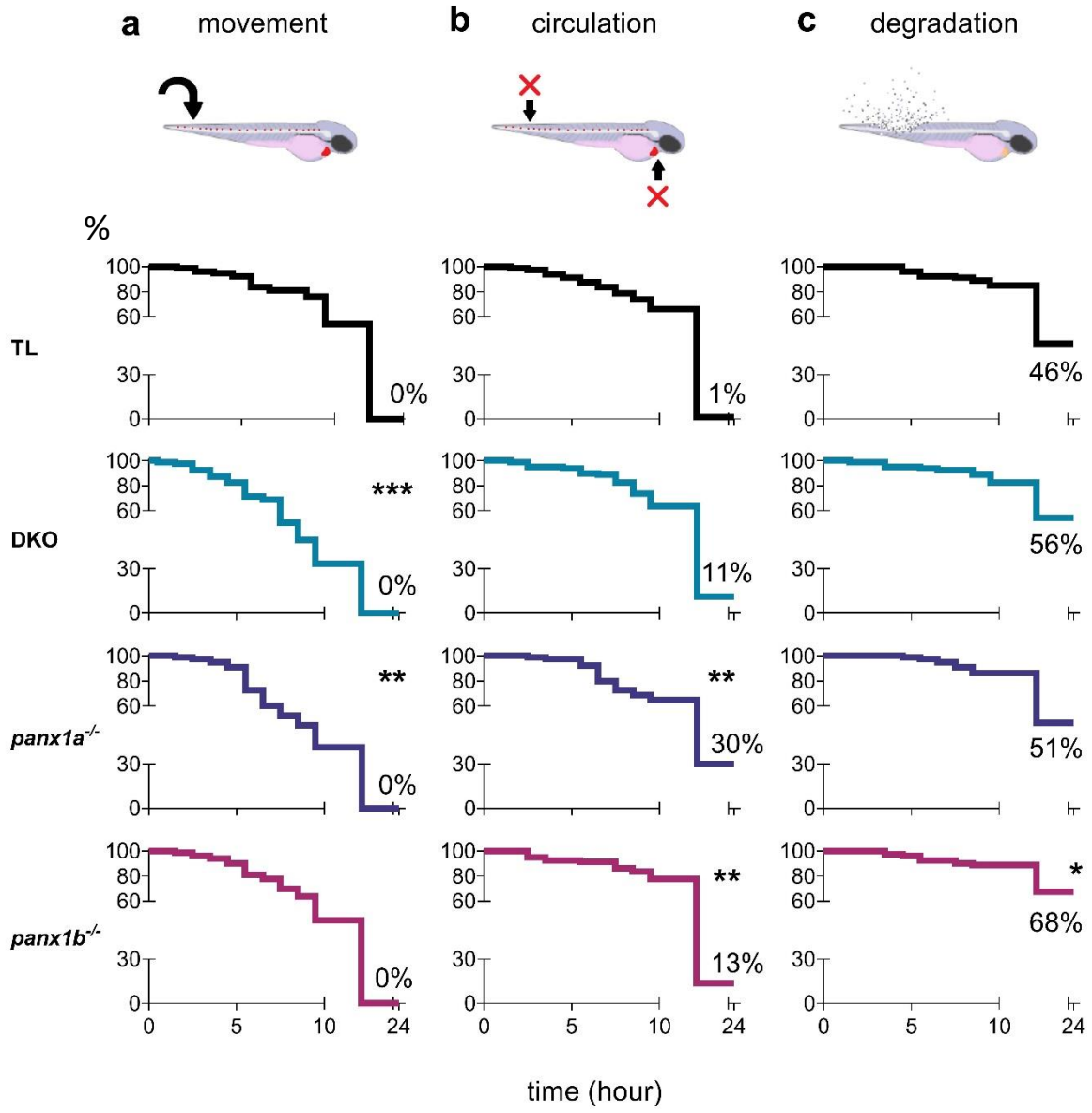

TL and *panx1* knockout larvae (7dpf, n = 80) were monitored after 15mM PTZ treatment every hour for 10 consecutive hours and once at 24 hours. Fitness and survival were characterized in three categories: **a** sign of movement, response to physical stimuli and upright posture, **b** presence of circulation and/or heartbeat, and **c** signs of degradation of the body. Survival rates (%) were graphed as Kaplan-Meier plots and analyzed for significant differences to TL's survival rate. DKO ($p < 0.001$) and *panx1a*$^{-/-}$ ($p < 0.01$) exhibited reduced movement compared to TL. *Panx1a*$^{-/-}$ and *panx1b*$^{-/-}$ had higher survival rates (presence of circulation) compared to TL ($p < 0.01$), and *panx1b*$^{-/-}$ had the lowest rate of degradation ($p < 0.05$). Percentages shown are fitness/survival rates at 24 hours. * - $p < 0.05$, ** - $p < 0.01$, *** - $p < 0.001$. *Circulation data and graphs were generated by Daria Taskina and included in* (Whyte-Fagundes et al., 2021) *manuscript.*

5.1.8 Seizure-like events in the Optic Tectum are reduced in DKO and *panx1a*$^{-/-}$

In-vivo Local Field Potential (ivLFP) was recorded from the right optic tectum of 7dpf TL and *panx1* knockout larvae (n = 5 to 12 per genotype) for detection and quantification of seizure-like events (SLE) after PTZ treatment (**Fig. 14**). SLEs are characterized in LFP recordings as an action potential spike followed by paroxysmal bursts typically lasting for several seconds. In this study, SLEs were extracted from the recordings based on the criteria that the event is three times the SD of the baseline recording, exhibits polyspiking with high amplitude and frequency, and is three seconds or longer. TL larvae exhibited SLEs throughout the hour of the recording with increased low and high frequency power (**Fig. 14a**). DKO and *panx1a*$^{-/-}$ had a reduced occurrence of SLEs and did not exhibit the same frequency patterns during SLEs (**Fig. 14bc**). *Panx1b*$^{-/-}$ displayed a high number of SLEs as in TL (**Fig. 14d**).

Quantification of SLEs highlighted TL as displaying the highest number of SLEs with the longest duration, highest seizing frequency, and the earliest onset of the first event (**Fig. 14efgh**). *Panx1b*$^{-/-}$ exhibited the most similar response to TL, with slightly less total SLEs ($p < 0.01$) and reduced seizing frequency ($p < 0.05$). DKO ($p < 0.0001$) and *panx1a*$^{-/-}$ ($p < 0.001$) were significantly reduced for these criteria compared to TL. Duration of SLEs did not significantly differ among the genotypes (**Fig. 14f**). Onset of the first SLE was delayed in DKO ($p < 0.01$) and in *panx1b*$^{-/-}$ ($p < 0.001$) (**Fig. 14g**). Overall, these results reinforced the findings for reduced susceptibility of *panx1a*$^{-/-}$ to the seizure phenotype, and the presence of robust seizure phenotype in *panx1b*$^{-/-}$.

Fig. 14 Seizure-like events (SLEs) and frequency power differentially manifested in the Optic Tectum of *panx1* knockouts *in-vivo.*

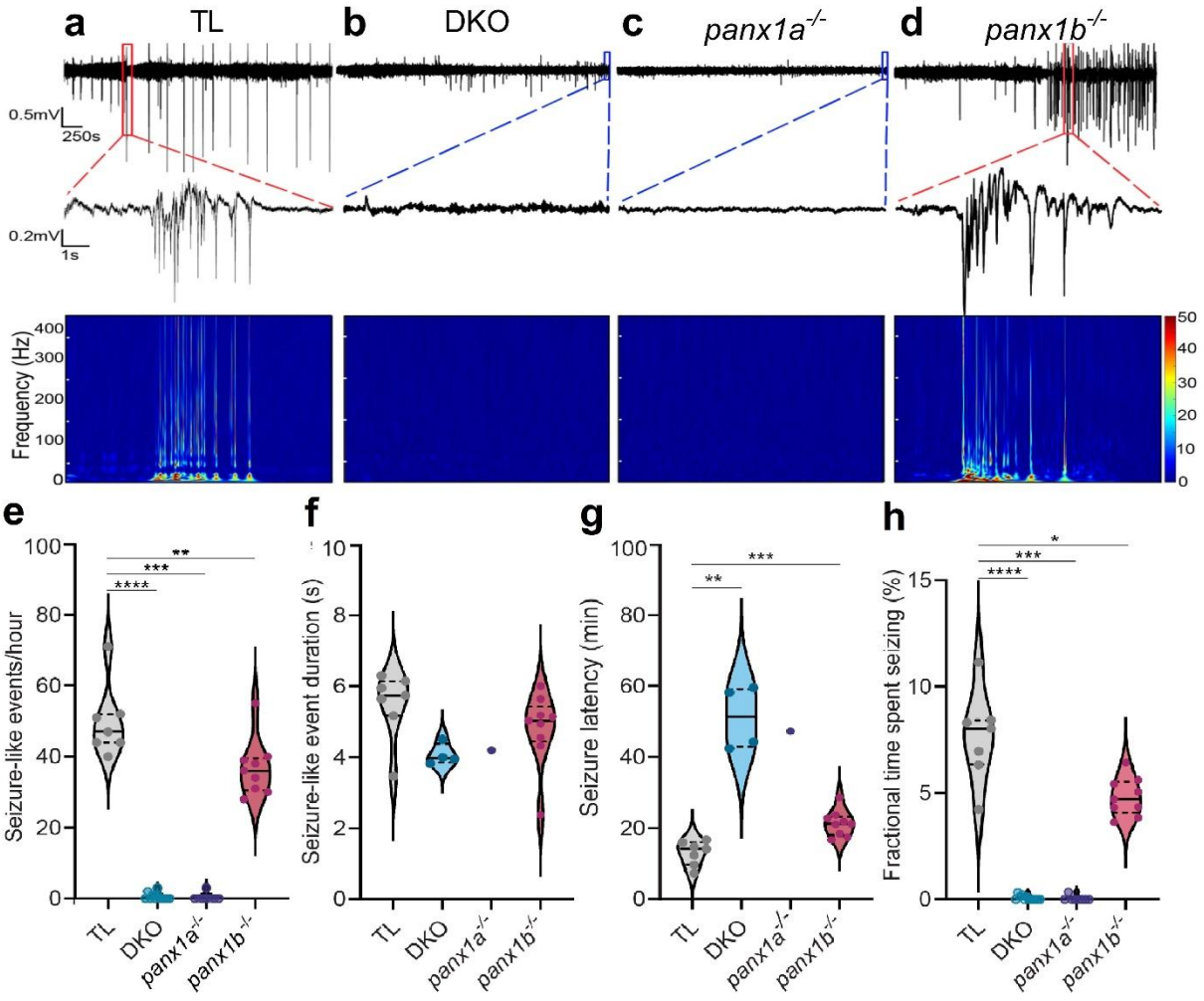

In-vivo LFP recordings were obtained from the optic tectum of 7dpf TL and *panx1* knockout larvae (n = 5-12) treated with 15mM PTZ. **a** LFP recording of a SLE (red) and a frequency spectrogram during the SLE obtained from TL. Large polyspiking was observed in the LFP signal and high and low frequency power increased during SLE. **b, c** characteristic SLE and increase in frequency power was not observed in DKO and *panx1a*$^{-/-}$ (blue). **d** *Panx1b*$^{-/-}$ exhibited SLEs like TL. **e** Total number of SLEs was highest in TL, followed by *panx1b*$^{-/-}$ ($p < 0.01$). **f** SLE duration did not differ between the genotypes. **g** SLE onset was delayed in *panx1a*$^{-/-}$ ($p < 0.01$) and *panx1b*$^{-/-}$ ($p < 0.001$). **h** Seizing frequency was the highest in TL compared to all the *panx1* knockouts. * - $p < 0.05$, ** - $p < 0.01$, *** - $p < 0.001$, **** - $p < 0.0001$. ***Data and graphs were generated by Paige Whyte-Fagundes and included in*** (Whyte-Fagundes et al., 2021) ***manuscript***.

5.2 Pharmacological targeting of Panx1 reduces seizure susceptibility

Genetic targeting of the *panx1* gene in a zebrafish seizure model elucidated the complex outcomes of knocking out *panx1a*, *panx1b* or both. Genetic targeting, although provides critical insight into the role of the *panx1* genes in the formation of the organism, its metabolism and ultimately its response to pathological conditions such as in the seizure model, the effects are difficult to distinguish from the global impact of the gene and correlated molecular pathways. As such, acute targeting of Panx1 was investigated via pharmacological blocking of the channel with a known Panx1 blocker Probenecid (Pb).

5.2.1 Standard pharmacological treatment of seizure-related activity with VPA

7dpf TL larvae were treated with valproic acid (VPA), a known anticonvulsant previously studied in zebrafish (Baraban et al., 2005), to establish the standard response of effective suppression of seizure-related behavior (**Fig. 15**). During the baseline activity of TL larvae (**Fig. 15a**), another group was treated with 5mM VPA (**Fig. 15b**; n = 60 per group). Treatment with VPA reduced larvae's activity significantly after 10 minutes compared to nontreated controls ($p < 0.05$; 11-29 minutes). After the application of 15mM PTZ, the hyperactivity curve observed in the PTZ only treated group was significantly reduced in magnitude in the VPA treated group throughout the entire hour ($p < 0.05$; 6-50, 52-60 minutes). Notably, none of the observed larvae treated with VPA and PTZ survived 24 hours after treatment (n = 24; 0%; not shown), and activity was reduced with VPA treatment alone. It is probable that the high concentration of VPA, although effective in suppressing seizure-associated behavior, may also pose toxicity on the larva's metabolism.

Fig. 15 PTZ-induced seizure-related hyperactivity in TL reduced with VPA treatment.

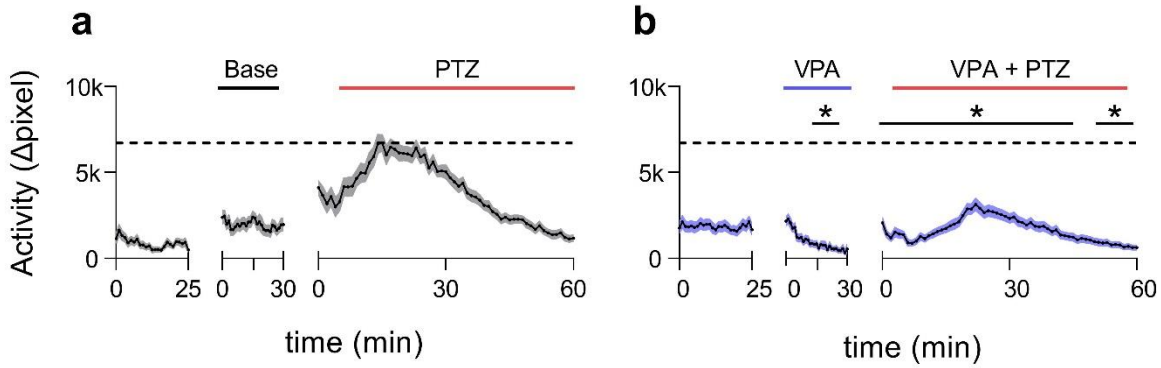

The activity was monitored in 15mM PTZ treated (**a**) and 5mM VPA and 15mM PTZ treated (**b**) TL larvae (n = 60). VPA alone reduced the locomotor activity of the larvae 10 minutes after application ($p < 0.05$). PTZ-induced hyperactivity was reduced in VPA treated larvae for almost the entire hour of treatment ($p < 0.05$). Dashed line indicates max average activity in PTZ treated TL larvae. * - $p < 0.05$. *Data and graphs generated by Daria Taskina and included in* (Whyte-Fagundes et al., 2021) *manuscript.*

5.2.2 Pharmacological targeting of Panx1 reduced seizure-associated behavioral and molecular outcomes

To elucidate the outcomes of acute targeting of the Panx1 channel in a zebrafish seizure model, Probenecid (Pb) was applied to the larvae before treatment with PTZ. Concentration was determined based on literature (de Marchi et al., 2019), and in-house dose-response analysis (**Supplementary Fig. S1**). TL larvae were recorded for resting activity and after 25 minutes either had E3 medium added into their wells (+ PTZ group) or 75µM Pb (Pb + PTZ group) (**Fig. 16a;** n = 36 per genotype). Larvae treated with Pb displayed a sharp and transient spike in locomotor activity ($p < 0.05$; 0-6 minutes) that returned to baseline within 30 minutes. With added PTZ treatment, Pb + PTZ group displayed an early onset of the activity peak around 5 to 15 minutes post-treatment that did not differ from the PTZ only group significantly. The activity of the Pb treated group substantially declined after the peak and returned to baseline for most of the remainder of the hour ($p < 0.05$; 14-52 minutes). AUC analysis revealed no significant differences between baseline and last 15 minutes of stabilized Pb treatment (**Fig. 16b left**, open points). AUC of the Pb + PTZ group's PTZ curve was significantly reduced compared to the PTZ only group (**Fig. 16b left**, closed points; $p < 0.0001$). When the mean activity of the last 15 minutes of Pb-only treatment was subtracted from the PTZ curve to find the sole effect of PTZ in

the group, the AUC remained significantly reduced compared to the group treated with PTZ alone (**Fig. 16b** right; $p < 0.0001$).

Seizure-associated stages II and III events were scored in Pb + PTZ treated larvae (n = 18) at 2-minute intervals for an hour and contrasted to the PTZ only treated group (**Fig. 16c**). Stage II onset occurred earlier in the Pb + PTZ group and ended in under 10 minutes ($p = 0.0057$, **Fig. 16c** bottom left), whereas in the PTZ-only group stage II activity peaked after 10 minutes of treatment (**Fig. 16c** upper left). Stage III manifested in the Pb + PTZ group similarly, with an early onset and small peak that declined substantially after 20 minutes ($p < 0.0001$; 20-60 minutes, **Fig. 16c** bottom right).

Differential expression of eight IEGs in the Pb and PTZ treated group was assessed against the group's control (Pb only treatment) (**Fig. 16d**; n = 30 per independent sample). Upregulation of *fosab* (54.61), *egr1* (6.09), *egr2b* (2.03) and *egr4* (96.97) was moderate in Pb + PTZ group compared to the + PTZ group. *Jun* (1.44) was not significantly upregulated in Pb treated larvae. Upregulation of *egr2a* (39.38) was higher in the Pb + PTZ group and *bdnf* (6.08) was comparable between the two groups. Incubation with Pb increased the survival (based on presence of circulation) in PTZ treated larvae, with 28% of larvae surviving to 24 hours post-treatment as opposed to the 1.3% of PTZ only treated larvae (**Fig. 16e**; n = 76 for Pb treated group; $p < 0.0001$).

Pharmacological targeting of Panx1 resulted in a phenotype that exhibits earlier onset of seizure-related activity that is also significantly reduced. Seizure-associated molecular markers indicated a reduced stress response and survival was improved in targeting the Panx1 channel in an acute seizure model.

Fig. 16 Pharmacological targeting of Panx1 improves behavioral and molecular outcomes of seizures.

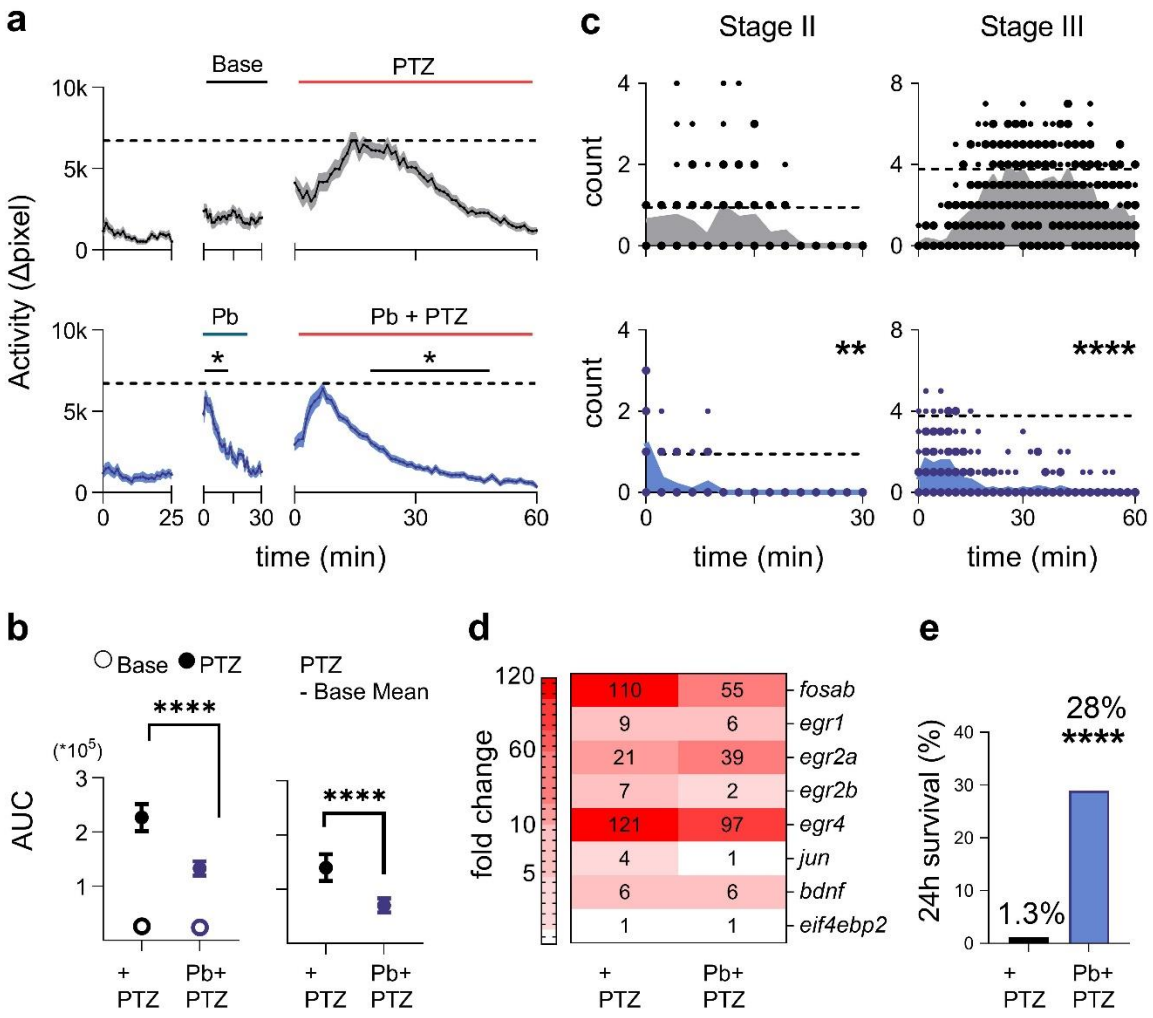

a Activity was measured in PTZ only treated (top), and 75μM Pb and PTZ treated (bottom) 7dpf TL larvae (n = 36). Pb treatment alone caused a short spike in activity, that returned to baseline within 30 minutes ($p < 0.05$, 0-6 minutes). PTZ-induced hyperactivity was reduced with Pb treatment; spike in activity occurred earlier with no significant difference from PTZ only treated group, and activity reduced significantly faster over the hour ($p < 0.05$, 14-52 minutes). Dashed line indicates max average activity in PTZ treated TL larvae. **b** AUC of baseline activity did not differ from Pb treatment (open points). Pb treatment significantly reduced the AUC of the PTZ activity ($p < 0.0001$, filled points). **c** Seizure-associated stages II ($p < 0.01$) and III ($p < 0.0001$) were significantly reduced with Pb treatment, while also exhibiting an earlier onset (n = 18). **d** Seizure associated IEG upregulation was reduced with Pb treatment. **e** Pb improved 24-hour survival of PTZ treated TL larvae (28%, n = 76, $p < 0.0001$). * - $p < 0.05$, ** - $p < 0.01$, *** - $p < 0.001$, **** - $p < 0.0001$. *Data and graphs were generated by Daria Taskina and included in* (Whyte-Fagundes et al., 2021) *manuscript.*

5.2.3 RNA-seq and RT-qPCR results signify potential coregulation of *panx1a* and *p2rx7*

The transcriptome of nontreated *panx1* knockout lines was analyzed via RNA-seq to uncover molecular processes regulated by the loss of *panx1* function (Whyte-Fagundes et al., 2021). The results had found downregulation of *p2rx7* in the *panx1a*$^{-/-}$ genotype, a well-established ATP-mediated interactor with the Panx1 channel. To elucidate the contribution of P2rx7 in the PTZ seizure model and its relationship with Panx1, pharmacological blocking of the purinergic receptor was examined.

5.2.4 Targeting of P2rx7 reduced seizure-related behaviors in TL and *panx1b*$^{-/-}$ larvae

Knocking out *panx1a* results in the downregulation of *p2rx7* in the zebrafish model, suggesting a potential interaction between the two. A P2rx7 blocker, A-438079 hydrochloride hydrate (A43; 100μM) was applied to PTZ treated TL and *panx1b*$^{-/-}$ larvae, to determine whether Panx1a or P2rx7 contribute to the seizure phenotype (**Fig. 17**). TL treated with A43 **(Fig. 17a**; n = 46) increased in activity slightly, but did not affect the baseline significantly, and returned to baseline within 30 minutes. Treatment with PTZ showed a reduction in seizure-related hyperactivity ($p < 0.05$; 8-12 minutes) relative to the PTZ only treated TL larvae (grey dotted line; n = 36). A43 treated TL had a reduced AUC for the PTZ activity (**Fig. 17b** left closed points; $p < 0.01$). Furthermore, removing the effect of A43 treatment by subtracting the mean activity of A43-only incubation, signified the reduction in the PTZ-induced curve (**Fig. 17b** right; $p < 0.05$). The occurrence of seizure-associated stage II events did not significantly differ with A43 treatment (**Fig. 17c**; n = 18; p = 0.1818). Stage III events were significantly reduced with A43 treatment ($p < 0.0001$) with the peak of activity spread widely across 20 to 40 minutes after PTZ treatment. A43 alone did not significantly raise activity in *panx1b*$^{-/-}$ (**Fig. 17d**; n = 46). Treatment with A43 reduced seizure-related hyperactivity in *panx1b*$^{-/-}$ larvae ($p < 0.05$; 21-24 minutes) compared to their PTZ only treated controls (magenta dotted line; n = 31). AUC analysis confirmed that AUC for PTZ treatment was significantly reduced with the addition of A43 treatment, with (**Fig. 17e** right; $p < 0.01$) and without (**Fig. 17e** left; $p < 0.001$) accounting for the small increase in activity during A43 incubation. Stage II ($p < 0.001$) and stage III events ($p < 0.0001$) were significantly reduced with A43 treatment without any apparent alterations to their onset time (**Fig. 17f;** n = 18). Overall, the pharmacological block of P2rx7 had an impact on both TL and *panx1b*$^{-/-}$ larvae's seizure-associated behaviors. Treatment had a marginally stronger effect on *panx1b*$^{-/-}$.

Fig. 17 Pharmacological targeting of P2rx7 improves seizure-related behavior in TL and *panx1b*$^{-/-}$.

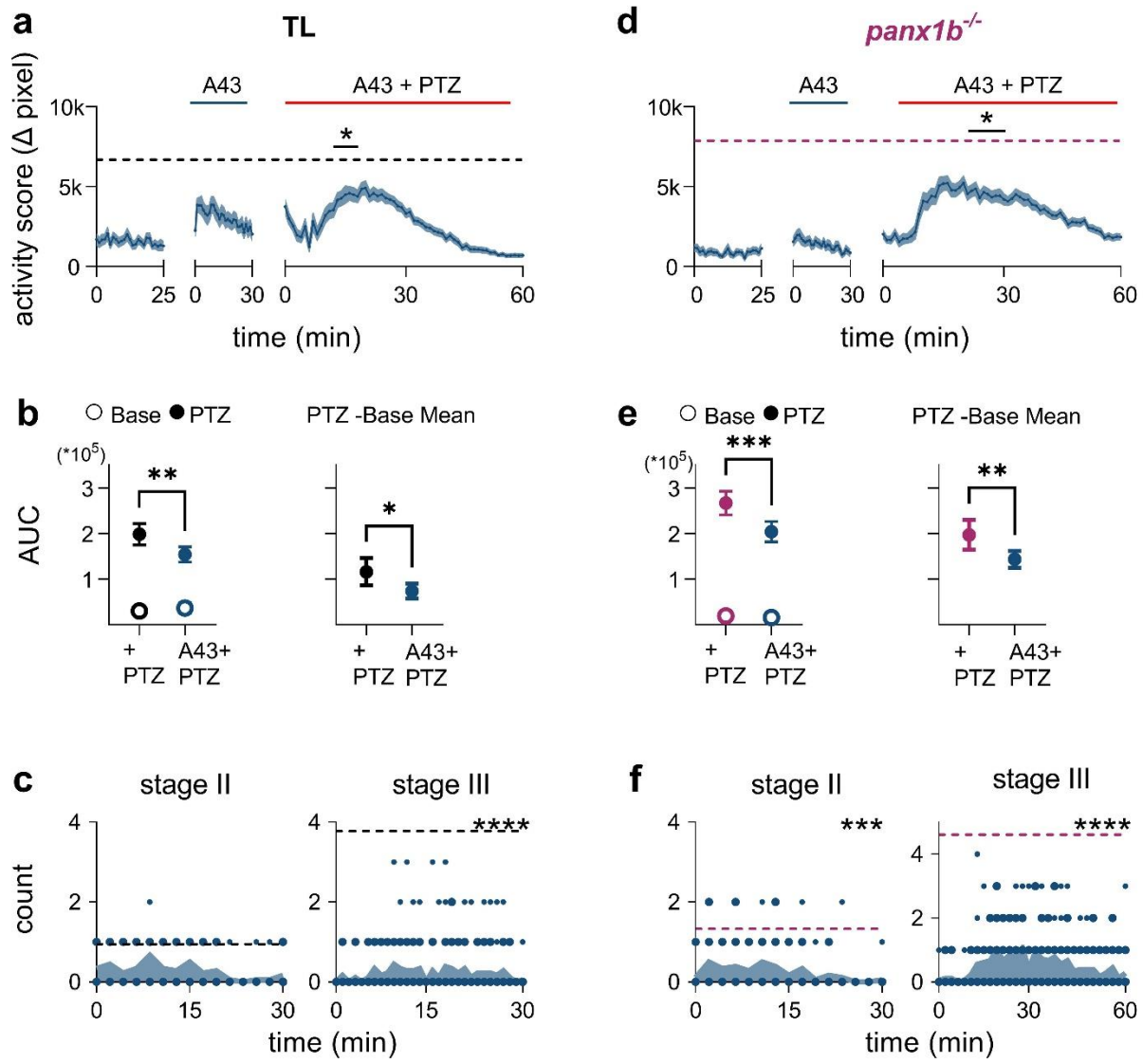

P2rx7 was blocked with A43 before PTZ treatment in 7dpf TL and *panx1b*$^{-/-}$ larvae. **a** Activity slightly increased with A43 treatment in TL larvae (n = 46), however, did not significantly differ from baseline. Seizure-related hyperactivity was moderately reduced in TL ($p < 0.05$, 8-12 minutes). The dashed line indicates max average activity in PTZ only group. **b** AUC of the PTZ activity was significantly reduced with A43 treatment. ($p < 0.001$ with A43 effect, $p < 0.01$ without A43 effect). A43 alone did not alter the AUC significantly. **c** Stage III, but not stage II, was significantly reduced with A43 treatment ($p < 0.0001$, n = 18). The dashed line represents max average stages II and III activity in PTZ only treated TL. **d** PTZ induced hyperactivity was reduced in A43 treated *panx1b*$^{-/-}$ ($p < 0.05$, n = 31, 21-24 minutes). The magenta dashed line indicates max average activity in PTZ only treated *panx1b*$^{-/-}$. **e** AUC of PTZ activity was reduced with accounting for the A43 treatment effect ($p < 0.01$, right) and not ($p < 0.01$, left filled points). **f** Both stages II ($p < 0.001$) and III ($p < 0.0001$) were reduced with A43 treatment in *panx1b*$^{-/-}$(n = 18). Magenta dashed line indicates max average stages II and III of PTZ only treated *panx1b*$^{-/-}$. * - $p < 0.05$, ** - $p < 0.01$, *** - $p < 0.001$, **** - $p < 0.0001$. *Data and graphs were generated by Daria Taskina and included in* (Whyte-Fagundes et al., 2021) *manuscript.*

5.2.5 SOM heatmaps for Pb or A43 and PTZ treated TL larvae reveal similarities with PTZ treated *panx1* knockouts

Pharmacologically treated TL larvae's behavior was evaluated with the previously described SOM method, to contrast acute blocking of Panx1 channel versus genetic targeting of the *panx1* gene (**Fig. 18**). Behavioral data for 75µM Pb treated (Panx1 blocker) or 100µM A43 treated (P2rx7 blocker) and 15mM PTZ induced TL larvae was clustered into the same four neurons for each behavioral parameter and calculated for average distance relative to the PTZ only treated genotypes. Pb treatment altered the behavioral response of TL larvae, as their response differed from the PTZ only treated group (**Fig. 18a; '**TL'). General activity, total duration of movement, number of freezing events, and burst duration were robustly altered with Pb treatment. Pb treatment in TL produced a phenotype resembling the PTZ treated *panx1a*$^{-/-}$, particularly in the activity, burst duration and average swimming duration parameters. Pb treatment produced a phenotype most dissimilar to *panx1b*$^{-/-}$, in terms of general activity, total and burst durations. Treatment with A43 resulted in a phenotype that was relatively dissimilar to any of the PTZ treated genotypes (**Fig. 18b**). Treatment affected normal swimming behavior, its duration and burst duration the most. *Panx1a*$^{-/-}$'s behavior had the most resemblance to the A43 treated TL, however, in comparison to Pb treatment the similarities were limited.

The results suggest that targeting Panx1 pharmacologically has the closest effect on the seizure-induced behavior in larvae as genetically knocking out *panx1a*. Treatment with A43 brought out PTZ induced behavior that was relatively dissimilar to any of the *panx1* genotypes, possibly due to targeting a different pathway.

Fig. 18 SOM heatmaps showed similarities between Pb or A43 and PTZ treated and PTZ only treated TL and *panx1* knockouts.

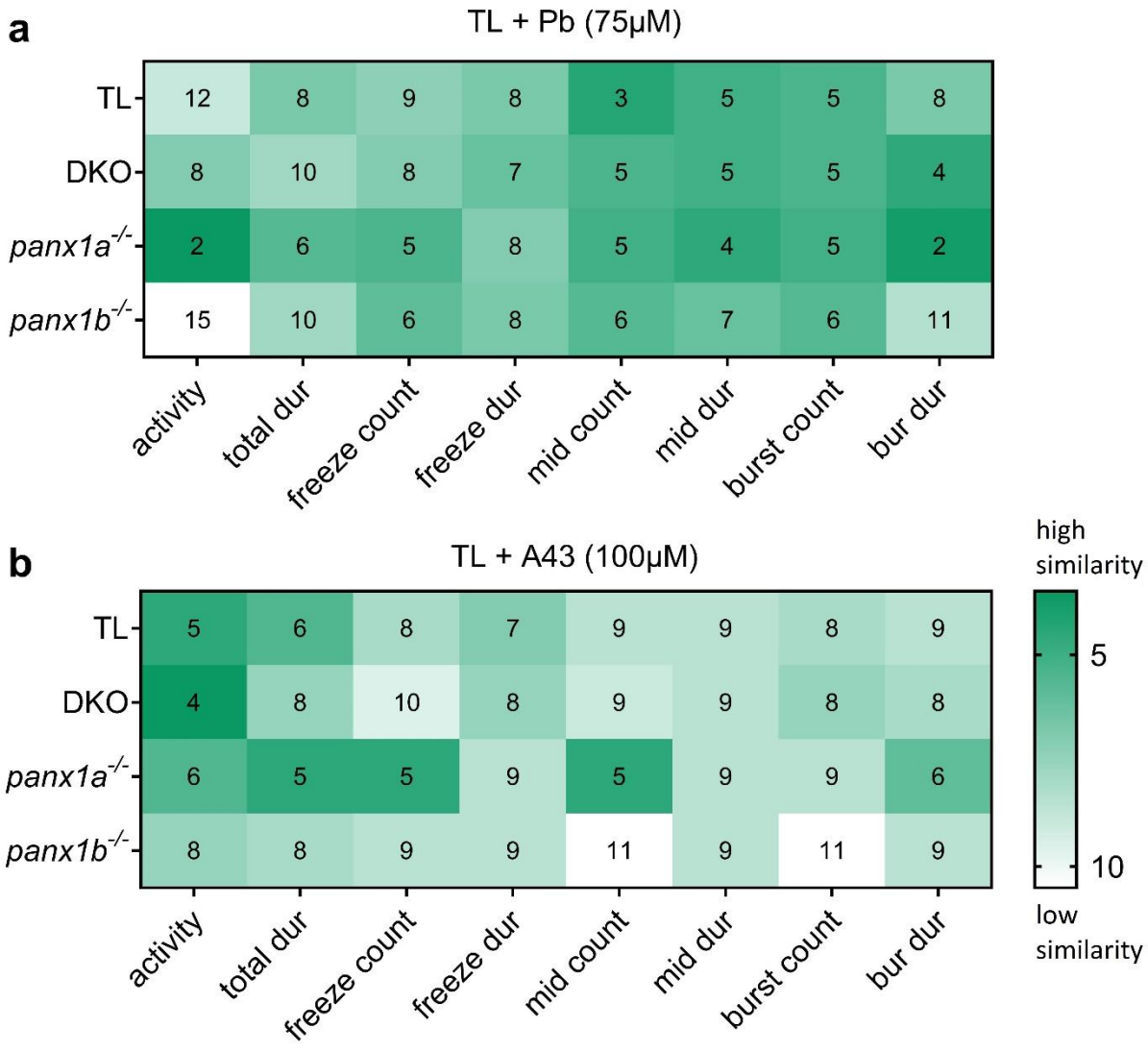

Heatmaps depict similarities between Pb + PTZ or A43 + PTZ treated TL and PTZ treated TL and *panx1* knockout larvae in eight behavioral parameters. High similarity is shown in green and with lower numbers. **a** Pb treatment altered the PTZ induced behavioral response, as the Pb + PTZ group shows dissimilarities with the 'TL' (PTZ only) group. Pb treatment produced behavior most similar to PTZ treated *panx1a*$^{-/-}$. **b** A43 treatment changed the PTZ induced response and was dissimilar to any of the PTZ treated genotypes. It was most similar to *panx1a*$^{-/-}$, however, the similarity was not greater than the Pb group.

5.2.6 SLEs were absent in Pb and PTZ treated TL larvae

LFP recordings in the right optic tectum of TL larvae (n =7) incubated with 75µM Pb 10 minutes before the application of 15mM PTZ did not exhibit any SLEs during the hour (**Fig. 19**). The frequency spectrogram did not elucidate any frequency power changes associated with a seizure event.

Fig. 19 Blocking of Panx1 eliminates SLEs in the optic tectum of PTZ treated TL larvae.

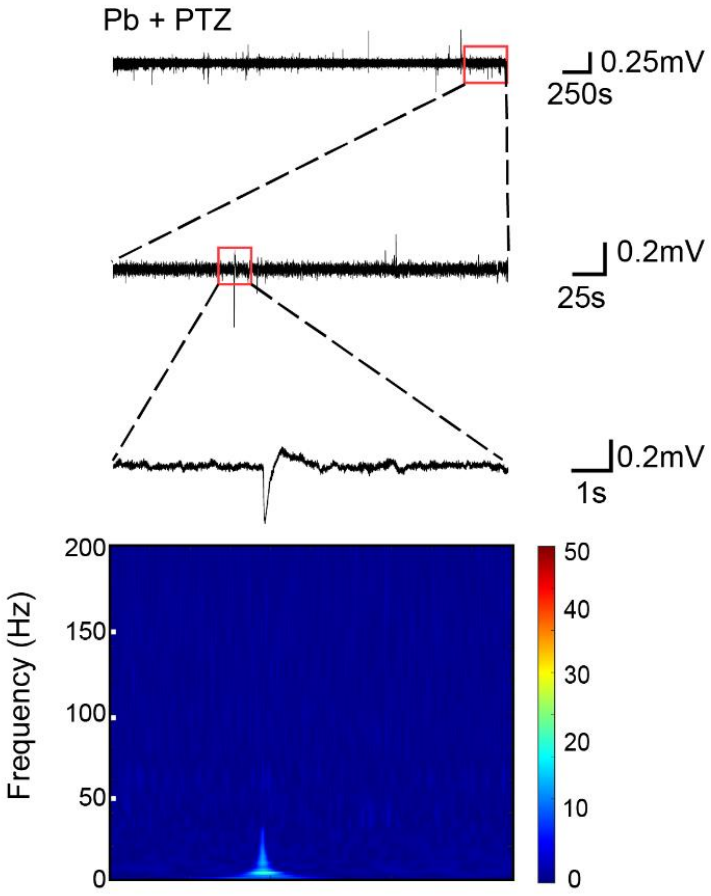

LFP recordings in the optic tectum of Pb incubated and PTZ treated TL larvae did not show any SLEs and the spectrogram did not show any frequency power increase associated with the SLE. Zoomed in trace depicts the largest LFP signal observed, which was not deemed to be an SLE. ***Data and graphs were generated by Paige Whyte-Fagundes and included in*** (Whyte-Fagundes et al., 2021) ***manuscript***.

5.2.7 GCaMP6 fluorescence intensity shifts through the brain during SLEs in TL larvae

5-7dpf GCaMP6 TL larvae were treated with 20mM PTZ and visualized for fluorescent calcium indicator for neuronal activity in the brain (**Fig. 20**). The addition of the PTZ medium did not alter the baseline fluorescence (**Fig. 20ab**). After 10 minutes, the larvae started to exhibit excessive fluorescence and SLEs in the LFP recordings (**Fig. 20cd**). Neuronal activity changes typically lasted for around 10 seconds for large SLE events. Fluorescence started off uniform in all the brain regions (**Fig. 20e**). As the SLE onset began, activity increased in the midbrain, optic tectum, cerebellum, and hindbrain regions, seen from the rise in fluoresce intensity. The increased activity lasted for several seconds while expanding into the periphery, into the forebrain and spinal cord. In the *panx1b*$^{-/-}$ with mosaic expression of GCaMP6, activity did not fluctuate during SLEs but increased over time with PTZ treatment (**Supplementary Fig. S2**).

Analysis of fluorescence intensity for each brain region over the course of the SLE illustrated the differences in their neuronal activity levels (n = 21 SLEs over 2 larvae) (**Fig. 21**). Larger SLEs typically had longer and stronger activity waves, starting high and gradually declining across all brain regions. Midbrain and optic tectum regions displayed the highest activity levels, activity in the cerebellum and the hindbrain was moderate, and in the forebrain and the spinal cord activity was the lowest throughout the SLE. 10 versus 5 second SLE and fluorescence showed some differences in the brain regions with the most neuronal activity, however, the overall pattern of radiating activity into the periphery remained the same.

GCaMP6 TL larvae (n = 2) were incubated with 75µM Pb before 20mM PTZ treatment, to elucidate the effects of blocking Panx1 on SLE associated brain activity (**Fig. 22**). Pb treatment alone did not elucidate any fluorescence that stood out from baseline (**Fig. 22a** ‘Pb’). Pb and PTZ treated larvae did not exhibit any SLEs in the optic tectum as previously reported. However, neuronal activity pattern similar to the one observed during SLEs in PTZ only treated group were present. These waves of activity manifested less often and typically lasted no longer than 3 to 5 seconds. The maximum fluorescence observed did not surpass the fluorescence intensity seen in the SLEs (**Fig. 22a** ‘Pb + PTZ’). They did not correlate with any abnormal activity in the LFP signals of the optic tectum. Fluorescence was less variant across brain regions, with most brain regions displaying close intensity. The spinal cord had the lowest fluorescence levels and did not differ from the baseline.

Fig. 20 GCaMP6 fluorescence intensifies with the onset of seizure-like events (SLEs) and dissociates into the periphery.

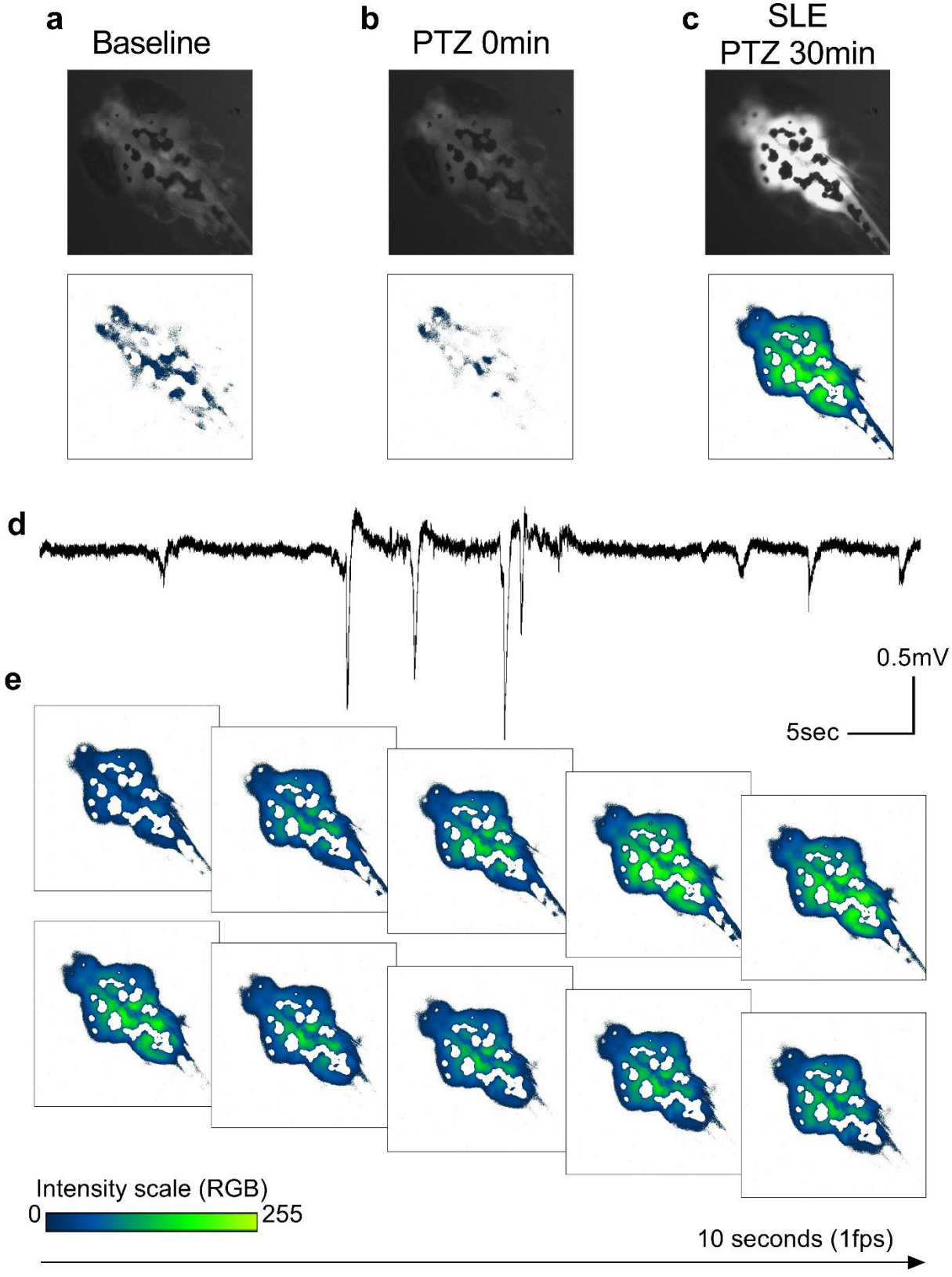

Representative fluorescence intensity in GCaMP6 TL larvae at baseline (**a**), immediately after 20mM PTZ treatment (**b**), and during a seizure-like event (SLE) after 30 minutes of PTZ treatment (**c**). Top images show fluorescence and bottom images are converted to threshold activity maps with lighter green representing more fluorescence. **d** LFP signal of the representative seizure-like event (SLE) in 20mM PTZ treated GCaMP6 TL larva recorded from the optic tectum. Depicted SLE lasted for ~10 seconds. **e** changes in fluorescence of the larva's brain during the above SLE obtained at 1fps.

Fig. 21 Fluorescence intensity differentially changes during SLEs across separate brain regions.

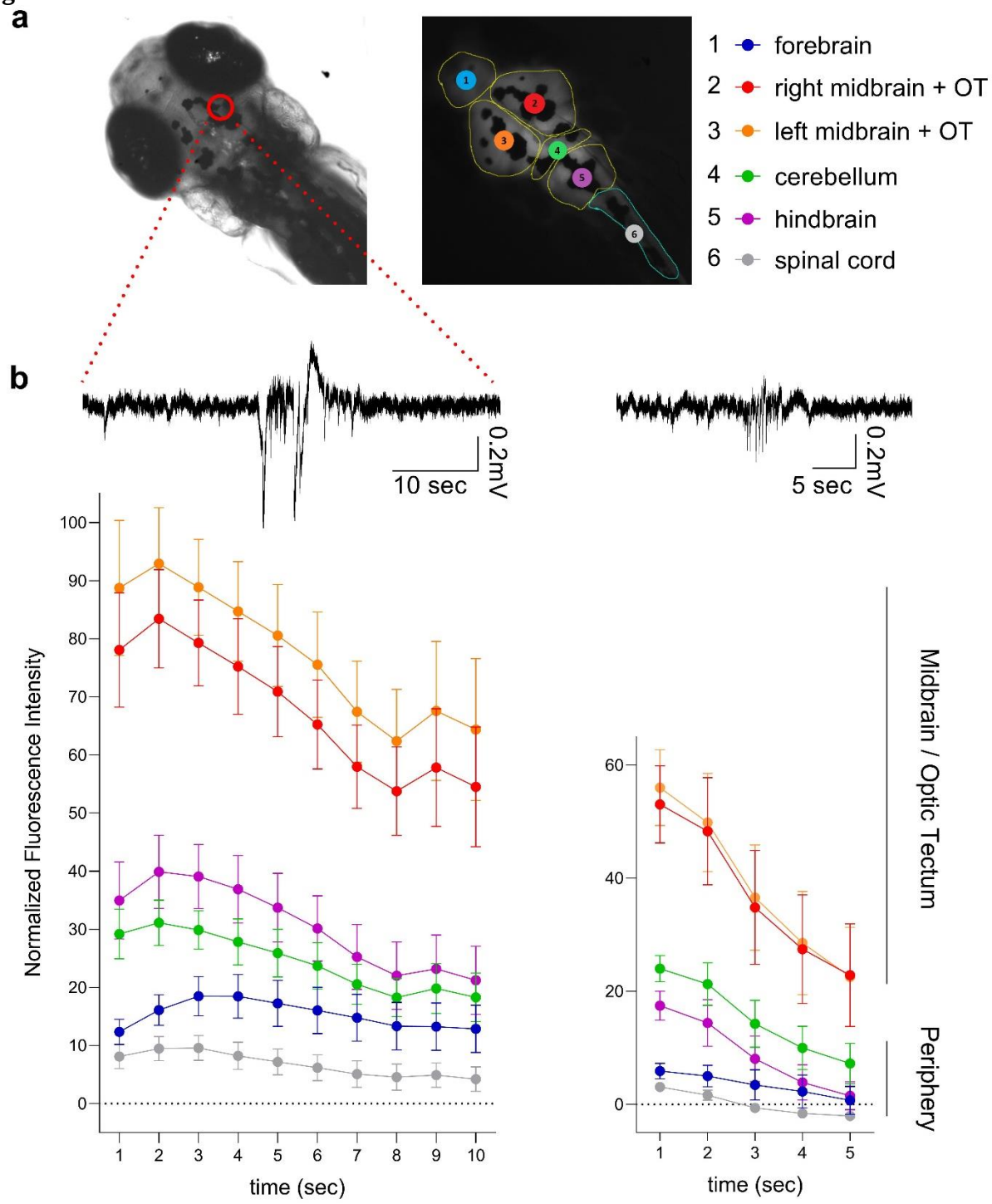

a Snapshot of larva (n = 2) recorded for LFP signal in the optic tectum (red circle) and the same larva's GCaMP6 fluorescent brain sectioned by brain regions. **b** LFP traces and fluorescence intensity changes across 10 second (n = 10) or 5 second (n = 11) SLEs. Fluorescence was normalized to the background and brain region-specific baseline fluorescence. Midbrain and optic tectum (OT) regions displayed the highest fluorescence intensity during SLEs, while the forebrain and the spinal cord were the lowest. All regions had high fluorescence with the onset of SLE that gradually declines over the 10 or 5 second period.

Fig. 22 GCaMP6 fluorescence intensity was reduced in Pb and PTZ treated TL larvae.

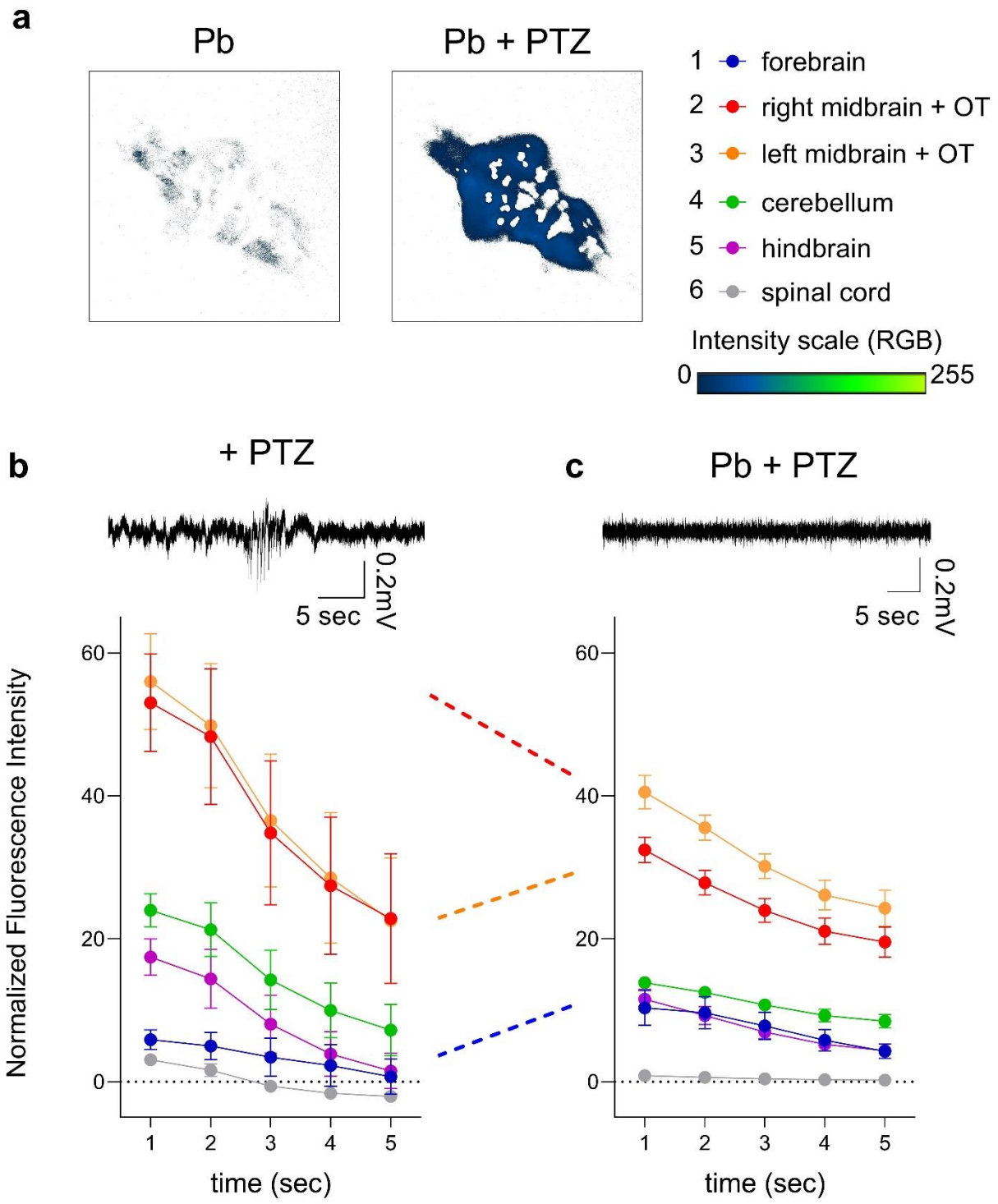

a GCaMP6 fluorescence threshold maps for 75μM Pb treatment alone (left) and maximum fluorescence intensity seen in Pb and PTZ treated larvae (right). **b** Changes in fluorescence intensity across different brain regions were reduced in magnitude and variance with Pb treatment (right; n = 10 over 2 larvae). All regions except the spinal cord displayed similar trendlines of activity across time, typically lasting no longer than 5 seconds, whereas the spinal cord's activity did not differ from the baseline.

5.3 Changes to extracellular ATP concentration after seizure induction differ among TL and *panx1* knockouts

Extracellular ATP concentrations (µM) in nontreated controls and one-hour PTZ treated *panx1* knockouts and Pb incubated TL larvae (n = 50 per sample) were measured (**Fig. 23**). Concentration values were normalized to the sample's protein content (mg/ml) and the TL control. DKO and *panx1b*$^{-/-}$'s initial ATP concentration was elevated compared to TL. TL, DKO and *panx1b*$^{-/-}$ exhibited a decrease in extracellular ATP after PTZ treatment ($p < 0.05$). *Panx1a*$^{-/-}$ and TL incubated with Pb started with a low extracellular ATP concentration and endured no significant changes after PTZ treatment.

Fig. 23 Extracellular ATP concentrations (µM) in PTZ treated *panx1* knockout and Pb treated TL larvae.

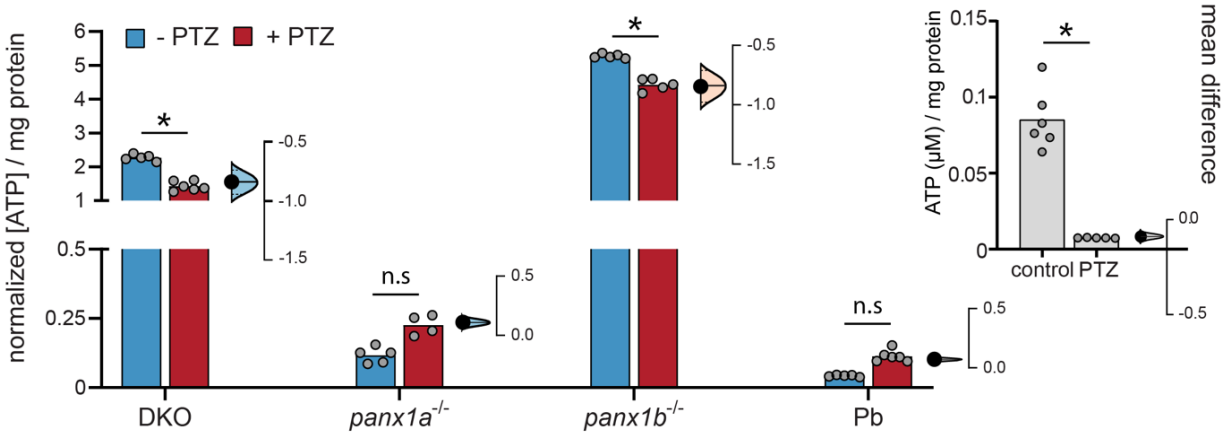

Extracellular ATP concentration (µM) was measured in nontreated controls and PTZ treated (one hour) *panx1* knockout and Pb incubated TL larvae. Concentrations were normalized to respective samples' protein content (mg/ml) and to ATP concentration in TL control. Estimation plots were used to visualize the variability in control and PTZ treated ATP concentration changes. TL, DKO and *panx1b*$^{-/-}$ exhibited reduced ATP concentration after PTZ treatment ($p < 0.05$). *- $p < 0.05$. ***Data and graphs were generated by Paige Whyte-Fagundes and included in*** (Whyte-Fagundes et al., 2021) ***manuscript***.

5.4 Molecular markers reveal potential mechanisms associated with Panx1 in seizures

To elucidate potentially associated pathways and molecular interactors with Panx1 in a PTZ induced seizure model, RT-qPCR was conducted on several genes of interest to investigate their differential expression after one hour of PTZ treatment in TL, *panx1* knockouts and Pb treated TL (n = 30 per sample, n = 3 biological replicates) (**Fig. 24**). Expression values were calculated based on fold change compared to nontreated controls.

Among purinergic receptors, *p2rx7* was downregulated in PTZ treated TL and upregulated in *panx1a*$^{-/-}$, which has previously been shown to exhibit downregulation of *p2rx7* under normal circumstances. *p2ry12* was down regulated in *panx1b*$^{-/-}$. ATP associated genes were not regulated for the most part, except for *entpd1*, encoding for CD39 that functions to hydrolyze ATP, which had shown a robust upregulation in all groups except the Pb treated. *Adora1b*, coding for A1 adenosine receptor, was upregulated in *panx1a*$^{-/-}$.

Solute carries, mediating Na^+ and Ca^{2+} transport, were mainly upregulated in *panx1a*$^{-/-}$ and Pb treated TL, and some downregulated in DKO and *panx1b*$^{-/-}$. Ca^{2+}/Na^+ antiporters *slc8a1b* and *slc8a2b* were upregulated in Pb treated TL, whilst *slc8a2b* was downregulated in DKO. *Slc8a1a* and Na^+ transporter *slco2b1* were upregulated in *panx1a*$^{-/-}$, and *slco2b1* was downregulated in *panx1b*$^{-/-}$ and Pb treated. *Scn4bb,* coding for Na^+ voltage-gated channel, was also downregulated in *panx1b*$^{-/-}$.

Cacna1da and *trpv6* were shown to be downregulated in *panx1a*$^{-/-}$ under non-pathological conditions (Safarian et al., 2020), and here, *trpv6* was shown to be upregulated as seen with *p2rx7*.

K^+ regulating channels were not regulated overall, except for *kcnc3a* that was upregulated in Pb treated TL. *Grin2bb*, NMDA receptor subunit, was upregulated in Pb treated larvae as well. Finally, *il1b* that codes for proinflammatory cytokine and is typically upregulated during inflammation and immune responses was upregulated in TL, *panx1a*$^{-/-}$ and *panx1b*$^{-/-}$, while no significant regulation of observed in the DKO and Pb treated.

Together, the differential expression in the selected genes depict overall high regulation in the *panx1a*$^{-/-}$, specifically for the solute carriers, and showcase the differential molecular response in *panx1a*$^{-/-}$ and *panx1b*$^{-/-}$.

Fig. 24 Gene regulation in several molecular pathways altered after PTZ treatment in *panx1* knockout and Pb treated TL larvae.

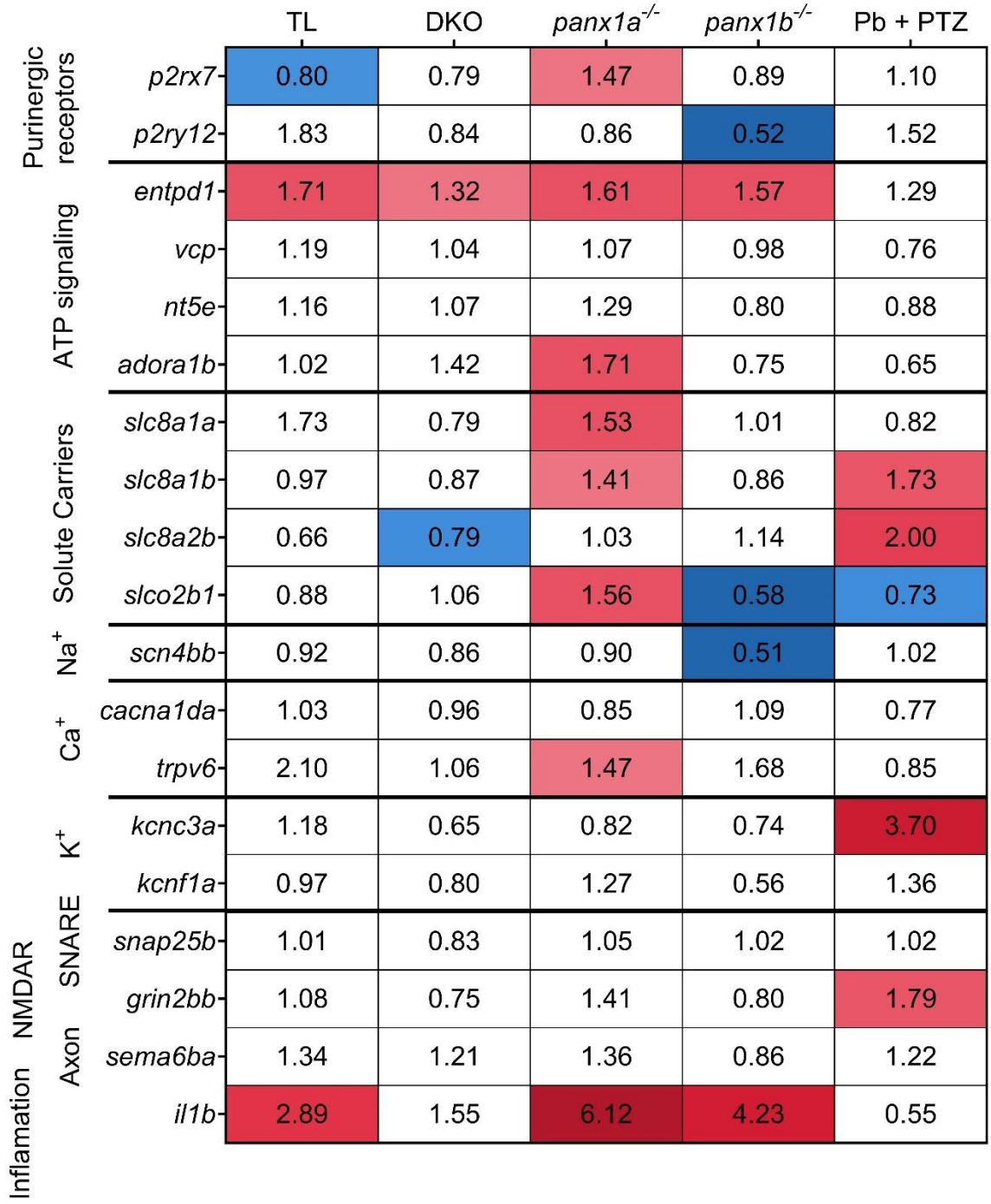

Gene regulation in several molecular pathways was altered after an hour of 15mM PTZ treatment in TL, *panx1* knockout and, Pb treated TL larvae. Expression values are fold change compared to nontreated controls, red color indicates upregulation and blue down regulation. Significant regulation – $p < 0.05$. Gene expression was assessed in purinergic, ATP signaling, and hydrolysis associated pathways, solute carriers and ion channels, genes associated with the synaptic density, inflammation, and axon regeneration. *Data and graph generated by Daria Taskina and partial data included in* (Whyte-Fagundes et al., 2021) *manuscript.*

6. Summary of results

6.1 Genetic targeting of *panx1 – Summary*

Panx1a and *panx1b* genes were knocked out in zebrafish lines, to investigate their involvement in seizures *in-vivo*. The loss of function of *panx1* was examined for its effect on the whole organism, from RNA sequencing analysis on 7dpf *panx1* knockout larvae to behavioral, molecular, and electrophysiological characterization of larvae chemically induced with seizures. Loss of *panx1a*, *panx1b* or both, have differential outcomes on the RNA makeup of developing zebrafish, indicative of altered balance in several molecular pathways (Safarian et al., 2020; Whyte-Fagundes et al., 2021). Such alterations in the molecular processes point to the differential response to chemically induced seizures in the three *panx1* knockouts. *Panx1a* knockout exhibited a phenotype least susceptible to seizures. The frequency and magnitude of seizure-like events in the optic tectum of the brain, seizure-related behavioral manifestations such as increased hyperactivity and convulsions were all suppressed significantly with the loss of *panx1a*. The larvae's survival and their IEG response to chemical induction had improved in *panx1a*$^{-/-}$, indicating a protective mechanism on the organism. Knocking out *panx1b* however, resulted in an opposed response to convulsant treatment. *Panx1b*$^{-/-}$ exhibited a robust seizure-like brain activity comparable to TL, coupled with heightened activity and occurrence of seizure-related behaviors. However, like *panx1a*$^{-/-}$, their survival is improved, and molecular stress and seizure-associated response is restricted. Notably, their behavioral response appears to be delayed in comparison to TL. Loss of function of both *panx1a* and *panx1b* genes resulted in an intermediate phenotype. Seizure-like events were significantly reduced in the DKOs, as well as the molecular response was contained. However, their behavioral response and survival were most similar to TL, rather than the other two knockouts. In summary, genetic targeting of *panx1* generates a mixed response in the *in-vivo* model for seizure investigation, with likely *panx1a* as the major contributor to the propagation of seizures.

Table 6. Summary of seizure phenotypes in *panx1* knockouts relative to TL.

Seizure phenotype relative to TL	*DKO*	*panx1a*$^{-/-}$	*panx1b*$^{-/-}$
LFP activity in optic tectum	33% seized; reduced seizure-like events (SLEs)	13% seized; reduced SLEs	100% seized; SLE occurrence comparable to TL
PTZ-induced hyperactivity	No significant difference	Reduced for most of the treatment duration	Increased shortly, non-significant when the baseline is subtracted
Stage II and III of seizure-associated behavior	Stage III reduced	Stage III reduced	Average stage III activity delayed
Seizure-associated IEGs upregulation	Reduced upregulation	Mixed response depending on IEG	Reduced upregulation
Fitness and survival	Reduced mobility	Reduced mobility; increased circulation	Increased circulation; less degradation
Similarity to TL phenotype (SOM model)	Most similar	Least similar	Intermediate

6.2 Pharmacological targeting of Panx1 – *Summary*

Next, the acute model of targeting Panx1 in the zebrafish seizure model was evaluated. Panx1 channel was targeted pharmacologically, with a known Panx1 inhibitor Probenecid, which have previously been shown to block the channel and attenuate ATP release (Dahl et al., 2013). This model allows for a distinctive characterization of the mechanism under which Panx1, and associated pathways are involved in seizure propagation. It addresses some of the limitations in the genetically targeted model; although the observed shift in several molecular mechanisms due to loss of *panx1* is a crucial finding with opportunity for further investigation, it creates difficulty in deciphering the isolated effects of the seizure model on the organism.

First, a known anticonvulsant, Valproic Acid was tested on PTZ-induced larvae to observe for the standard seizure-suppressing phenotype in age-matched zebrafish. Both behavioral and electrophysiological data had shown a lack of typical seizure-like brain activity or locomotor

response (Whyte-Fagundes et al., 2021). When Pb was applied to PTZ-induced larvae, a similar reduction in seizure activity was observed. Overall, behavioral response to PTZ treatment was reduced and the occurrence of stages II and III of seizure-associated behavior was limited. Interestingly, treatment with Pb had resulted in an accelerated onset of PTZ-induced hyperactivity, compared to a normal response curve in PTZ treated larvae. Additionally, stages II and III events commenced earlier with Pb treatment and subsided faster than with only PTZ treatment. Seizure-associated molecular responses were reduced, and survival improved. Recordings from the optic tectum had shown no seizure-like activity in terms of LFP signals, however, Ca^{2+} imaging did show a less robust activity that manifested similarly as during seizures. Blocking Panx1 may not fully eliminate a hyperexcitable state but reduces the magnitude by taking away a major contributor. Across all examined facets, Pb treatment improved the outcome of seizure induction in the organism.

Panx1 is known for its interaction with the purinergic pathway and its activation through the P2rx7 purinoreceptor (Iglesias et al., 2008). Interestingly, RNA sequencing data has shown downregulation of the *p2rx7* gene in the *panx1a*$^{-/-}$ model (Safarian et al., 2020). This finding suggests a potential coregulation of *panx1a* and *p2rx7* in the zebrafish. As such, the effect of pharmacologically targeting P2rx7 in TL, with both copies of *panx1*, and in *panx1b*$^{-/-}$ that carries only *panx1a* was examined, to decipher the role P2rx7 plays in seizure propagation and its involvement with Panx1a. Larvae were treated with P2rx7 blocker A43 before PTZ and examined for behavioral outcomes. A43 treatment suppressed seizure activity in both TL and *panx1b*$^{-/-}$, with PTZ-induced hyperactivity and seizure-associated behavior significantly reduced. These findings suggest that the P2rx7 is also involved in seizure propagation, potentially interacting with Panx1.

Table 7. Summary of seizure phenotypes in pharmacologically treated TL and *panx1b*$^{-/-}$ larvae.

Seizure phenotype relative to PTZ only treatment	*VPA (standard anticonvulsant)*	*Pb (Panx1 blocker)*	*A43 – TL (P2rx7 blocker)*	*A43 - panx1b*$^{-/-}$ *(P2rx7 blocker)*
LFP activity in optic tectum	No SLE	No SLE	-	-
PTZ-induced hyperactivity	Reduced for most of the treatment; similar activity curve	Reduced for most of the treatment; early onset of peak activity	Reduced during peak activity; similar activity curve	Reduced during peak activity; similar activity curve
Stage II and III of seizure-associate behavior	-	Stage II and III reduced; earlier onset	Stage III reduced, a similar timeline of onset	Stages II and III reduced, a similar timeline of onset
Seizure-associated IEGs upregulation	-	Reduced upregulation	-	-
Survival (presence of circulation)	Decreased survival at 24 hours	Increased survival at 24 hours	-	-
Similarity to TL or panx1 knockout phenotype (SOM model)	-	Most similar to *panx1a*$^{-/-}$	Not similar to any genotype	-

6.3 Machine Learning for characterization of behavior in *panx1* knockouts

Zebrafish offer a variety of advantages as a model organism for investigating diseases. They present a high-throughput and versatile platform for examining physiological, molecular, and behavioral outcomes of interference and efficient large-scale drug screening. In examining epilepsy and seizure associated mechanisms via zebrafish, a limited number of studies have taken advantage of machine learning to optimize the use of this animal model. Several groups have developed a sophisticated method of collecting and characterizing behavioral data, either with previously established behavioral attributes or with novel features extracted via unsupervised machine learning (Marques et al., 2018). Others have utilized machine learning in

electrophysiological recordings to automatically detect seizures (Hong et al., 2016; Hunyadi et al., 2017), phenotype specimens based on the efficacy of the antiepileptic drug (Eimon et al., 2018), and combine with Calcium imaging for high-throughput brain activity mapping (Lin et al., 2018). Such efforts serve to automatize data collection and standardize protocols across the field. Moreover, they provide unique perspectives in solving the research questions at hand. For example, although categorizing seizure-associated behaviors in zebrafish larvae in stages have been established via manual examination (Baraban et al., 2005), detailed characterization and quantification of these behaviors is unattainable manually. Machine learning techniques that automatically recognize these stages of behavior can systematically quantify, determine the frequency of occurrence and length of specified locomotor events.

Here, CNN was implemented to automatically score Stage III convulsive behavior in PTZ treated TL and *panx1* knockout larvae. The CNN model extracts distinctive features of the images and generates an optimal algorithm for categorizing images into specified groups. Extracting consecutive occurrences of 'convulsing' frames determined the frequency and duration of convulsions in PTZ treated larvae. The model was used to generate convulsion frequency plots during peak convulsive activity, with the highest frequency observed in *panx1b*$^{-/-}$, followed by TL, DKO and *panx1a*$^{-/-}$. Moreover, *panx1b*$^{-/-}$ experienced the longest convulsive events compared to the other genotypes. The results corresponded with the SLE frequency results obtained from the LFP recordings. These findings were qualitatively observed during manual scoring; however, the CNN model was able to standardize and quantify these results. Notably, when non-PTZ treated controls were analyzed with the model, the number of false positives was reasonably low, suggesting that the model can be trained on a specific behavioral attribute. The CNN model offers a novel systematic approach in examining the behavioral manifestations in the PTZ treated zebrafish model and can differentiate the unique outcomes of genetic targeting. The model poses the potential of being utilized in characterizing other zebrafish disease or genetically modified models.

In addition to establishing an automatized and uniform approach to analysing known behavior, machine learning can bring advantages in generating new data via unsupervised machine learning. SOM is a prime example of a relatively simple unsupervised clustering technique that can classify data free of the experimenter's bias or subjectivity. Several behavioral features

extracted from the ZebraLab software for PTZ treated *panx1* knockouts were analyzed via SOM, to determine how data for each genotype is distributed in relation to one another. Several behavioral attributes were identified that describe genotypes' similarities in response to treatment and attributes that are indicative of high variability between their responses. Additionally, the relationships between data distribution of genotypes revealed close similarity between TL and DKO, due to the presence of several key behavioral features with high similarity. *Panx1a*$^{-/-}$ was the least similar phenotype to any of the other, indicative of its unique response to PTZ. Finally, TL larvae treated with Pb or A43 before PTZ were contrasted against the PTZ treated *panx1* genotypes, to document similarities between genetically and pharmacologically targeting Panx1. Pb treatment produced a behavioral response most similar to *panx1a*$^{-/-}$, as expected from both of their lack of seizure phenotypes discovered previously. The SOM, however, provides a descriptive in-depth analysis into which behavioral attributes share this similarity. The model creates a foundation for breaking down and standardizing behavioral features that characterize differential responses to treatment. Taken further, it can allow contrasting new drug treatments or genetically modified genotypes against the existing model for phenotype matching.

7. Discussion

7.1 Panx1a drive seizures *in-vivo*

Research on the Panx1 channel has gained ground in the epilepsy field, as overexpression of the channel correlated to temporal seizures and cortices of epilepsy patients (Jiang et al., 2013; Li et al., 2017) and hippocampal seizure models in mice (Mylvaganam et al., 2010). Panx1 is proposed to contribute to seizure propagation through its function of extracellular ATP release (Dossi et al., 2018; Santiago et al., 2011). This mechanism is reinforced in the present pharmacological model, as treatment with a Panx1 blocker in an acute zebrafish seizure model attenuated the seizure phenotype. Complete loss of Panx1 function through genetic intervention has also exhibited a seizure rescue phenotype, although the outcome is comparatively mixed most likely due to compensatory mechanisms at work during the organism's formation and development. Furthermore, independent *panx1a* or *panx1b* loss-of-function proved genetic targeting of *panx1* to be even more complex as both pro- and anti-seizure properties were observed in their phenotypes.

The opposing mechanisms seen in the zebrafish Panx1s resemble the differential Panx1 function based on the location of its expression in the mouse model. Deletion of Panx1 in astrocytes resulted in an increased epileptiform activity while deletion of neuronal Panx1 attenuated it (Scemes et al., 2019; Suadicani et al., 2012). The antagonistic mechanism of Panx1, depending on its localization in a mouse model, may also reflect the relationship between the two Panx1s in the zebrafish model as the two channels show differential expression patterns. Panx1b is mainly expressed in the CNS, whilst Panx1a exhibits ubiquitous expression across various tissue types (Kurtenbach et al., 2013), providing a potential explanation for a pro-seizure phenotype in *panx1b*$^{-/-}$. Panx1a's global expression, localization on the plasma membrane, and similarities in conductive properties to mammalian Panx1 suggest that Panx1a functions similarly to Panx1 in the context of seizures.

7.2 ATP mediated Panx1 mechanism and related molecular processes

The proposed mechanism of Panx1 in seizures is mediated by ATP release. Mammalian Panx1 expression and activation has been tied to ATP release (Dahl, 2015; Narahari et al., 2021) and mutations or absence of Panx1 are shown to attenuate it (Suadicani et al., 2012). The experimental evidence in literature corresponds with *panx1a*$^{-/-}$ examined in this project, as extracellular ATP concentration was reduced in this genotype at baseline. Extracellular ATP concertation was also reduced when Panx1 was pharmacologically blocked. No change in extracellular ATP after convulsant treatment was observed in the two anti-seizure phenotypes, *panx1a*$^{-/-}$ and Pb treated. However, extracellular ATP concentration decreased in treated TL, *panx1b*$^{-/-}$ and DKO, effectively grouping similar phenotypes in opposition to the expected outcome (**Fig. 23**). This phenomenon could be attributed to the metabolism of ATP after its excessive release during the neuronal excitatory stage. An hour into the induction of acute seizures, ATPase activity may become more prominent than extracellular ATP release. An excessive amount of ATP during neuronal hyperexcitability prompts a negative feedback mechanism from the microglia via ATP-hydrolyzing ectoenzyme CD39 and adenosine receptor A_1R (Badimon et al., 2020). By this, in this model CD39 coding gene, *entpd1* was upregulated in TL and all *panx1* knockouts an hour into seizure induction, while *panx1a*$^{-/-}$ was also upregulated for A_1R coding gene *adora1b* (**Fig. 24**).

7.3 P2rx7 involvement with Panx1 and seizures

P2rx7 is well established as an interacting partner of Panx1, mediated by ATP release (Iglesias et al., 2008). In the zebrafish model, inhibition of P2rx7 attenuated the seizure phenotype, however, not to the same magnitude as the inhibition of Panx1. Such experimental outcome advocates for the involvement of P2rx7, however, signifies Panx1a as the predominant driver of seizures.

Additionally, *p2rx7* was shown to be downregulated with the loss of *panx1a* (Safarian et al., 2020), but upregulated after the induction of seizures in the genotype. Moreover, *p2rx7* is downregulated in seizure-induced TL, an antagonistic outcome to *panx1a*$^{-/-}$. P2rx7 has been shown to activate Panx1 through ATP release, and is involved in an ATP positive feedback while the concentration remains at a nonpathological level (Dahl, 2015). The channel and receptor have been shown to cluster with elevated levels of ATP (Boyce & Swayne, 2017). Thus, a potential explanation for no substantial change in the extracellular ATP in anti-seizure phenotypes, is that the lack of functioning Panx1a and the absence of a pathological condition allows for a leveled ATP release to subsist. Whereas, in genotypes with functioning Panx1a that exhibit the seizure phenotype, the initial abundance of ATP and an excessive ATP release has commenced the negative feedback mechanism, downregulating *p2rx7* and inhibiting Panx1a and further release of ATP over time.

The differences in the behavioral responses of blocking P2rx7 versus Panx1 in a zebrafish seizure model may attest to the feedback mechanism between the two. Inhibition of P2rx7 moderately reduced seizure-associated activity overall, with the curve of activity remaining the same. Treatment with Probenecid significantly reduced the seizure-associated response but exhibited a skewed activity curve that displayed an early onset of transient hyperactivity. If Panx1 activation is in part achieved by P2rx7, the initial burst of seizure-like activity could be explained by the initial activation of P2rx7 and ATP release that is not sustained when no functioning Panx1 is present. When P2rx7 is blocked, the main driver Panx1 is still able to drive ATP release and neuronal hyperexcitability without the reinforcement from P2rx7, resulting in a moderate seizure phenotype.

7.4 Significance of Panx1 channel structure

The resolved structure of the human Panx1 channel (Jin et al., 2020; Mou et al., 2020; Qu et al., 2020) has enabled its structural comparison and modeling of Panx1a and Panx1b (**Fig. 25**). Although the recent structural findings do not fully explain the mechanism of ATP permeation (Mim et al., 2021), two structural attributes have been experimentally tied to proper ATP permeation and release, W74 and R75 located on the extracellular pore (Qiu & Dahl, 2009). The W74 site is conserved in Panx1a but not Panx1b, which may serve as further evidence of Panx1a functioning similarly to mammalian Panx1 and permeating ATP. R75 was implicated to be involved in the negative feedback of ATP, as mutations to R75 have been shown to lack Panx1 current inhibition in the presence of excess ATP (Qiu & Dahl, 2009). R75 site is conserved in Panx1b but not Panx1a. This may be indicative of a disrupted negative feedback mechanism in Panx1a giving rise to the hyperactive locomotor state and increased extracellular ATP concentration at baseline in *panx1b*$^{-/-}$ and contributing to the observed seizure phenotype.

Fig. 25 Panx1a and Panx1b extracellular gate structure.

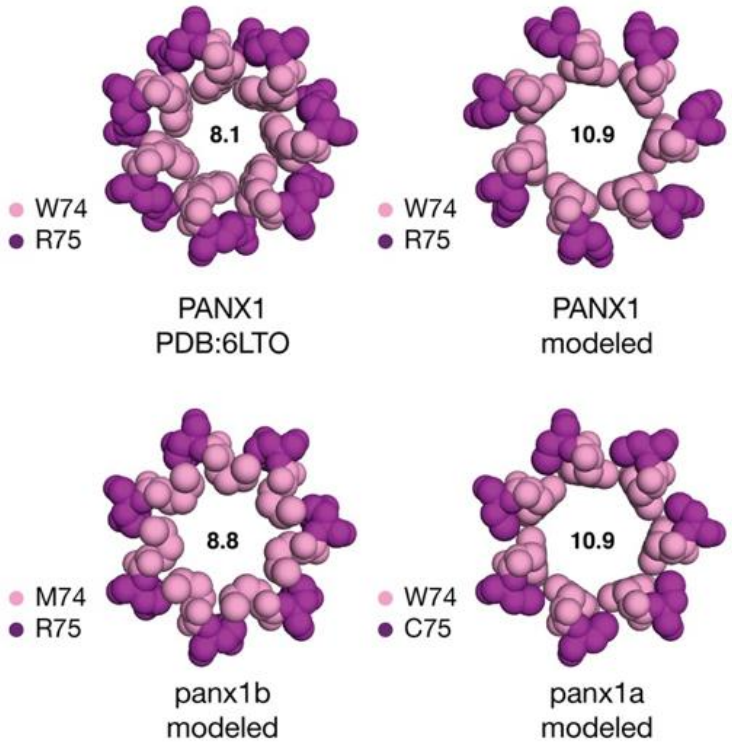

Human Panx1 (top left) was used to model and repack the extracellular gates of Panx1a and Panx1b. Human Panx1 under the same repacking protocol creates a larger pore (top right). Panx1b (bottom left) is conserved for site R75 but not W74 (M74), and Panx1a (bottom right) vice versa (C75). **Data and figures were generated by Dr. Logan W. Donaldson and include in the** (Whyte-Fagundes et al., 2021) **manuscript.**

7.5 Panx1-specific pharmacological inhibition preferentially targets Panx1a

Probenecid is a Panx1 inhibitor validated in the human and mouse models (de Marchi et al., 2019; Dossi et al., 2018). Treatment with Pb displayed an expected seizure suppressing outcome in the zebrafish model. The similarities in behavioral, survival, molecular and electrophysiological responses of *panx1a*$^{-/-}$ and Pb treated TL may point to Pb treatment working to block Panx1a rather than Panx1b. However, a comparison of pharmacological and genetic models is to be made with caution, as the exact metabolic effects of the two are unknown. The site of interaction between Pb and the Panx1 channel needs further investigation to elucidate the compound's effect in the zebrafish model. Advancements in machine learning technology, such as the AlphaFold software for prediction of protein structure, can serve as a powerful tool for drug-interactive site discovery (Tunyasuvunakool et al., 2021).

7.6 Points of consideration

The evidence provided for pro- or anti-seizure effects in the zebrafish model does not suggest that *panx1a* and *panx1b* are inherently seizure susceptible or resistance genes. The ubiquitous expression of Panx1 and its diverse function is characterized for involvement in several diseases (Penuela et al., 2014). However, mutations in human *panx1* have not been found to cause status epilepticus or disorders associated with symptoms of seizures (Sang et al., 2019), and *panx1b* knockouts do not endure spontaneous seizures. The purpose of the project was to elucidate the mechanistic involvement of Panx1a and Panx1b in the context of a hyperexcitable state of an intact neurocircuitry, to decipher the significance and functional relevance of their unique channel properties, and to identify molecular processes that interact with Panx1 in a seizure dynamic. Such assessments are achieved through genetic and pharmacological interventions; however, the two methods are not directly comparable. Genetic manipulation of live animal models results in a cascade of alterations to gene regulation and ultimately to molecular, morphological, and behavioral characteristics. The advantage of this is the ample amount of affected processes worthy of investigation. The disadvantage lies in the difficulty of deciphering a direct cause and effect in the mechanism of interest. Both genetic and pharmacological targeting of Panx1 provides insight into its mechanism. However, a comparison of the outcomes must be made accordingly.

7.7 Conclusion and novelty of findings

The novelty of this project is the characterization of anti- and pro- seizure phenotypes observed as a consequence of *panx1a* or *panx1b* loss-of-function. The most probable determinants of the seizure phenotype are the differences between the two channels' tissue-specific expression and membrane localization. These findings suggest the significance of examining astrocytes versus neuronal contributions to seizures. The differentially regulated genetic markers provide a preliminary snapshot of involved molecular pathways and structural differences potentially elucidate functional differences.

Another contribution of this project is evidence for Panx1's role in seizures that is mediated by ATP and involved with P2rx7, providing a focal point for further investigations. Taken together with the recent findings on Panx1 channel structure and its differences to the zebrafish Panx1s, key protein sites that differentially activate the channels and interact with ATP can be explored.

Finally, this project establishes a high-throughput *in-vivo* animal model for the investigation of Panx1a and Panx1b for their differential expression and localization, functional properties, and channels' structural differences. The interconnected attributes demonstrate an insight into the neofunctionalization of these channels over millions of years and the way that they affect the dynamic between molecular circuits today.

8. References

Afrikanova, T., Serruys, A. S. K., Buenafe, O. E. M., Clinckers, R., Smolders, I., de Witte, P. A. M., Crawford, A. D., & Esguerra, C. V. (2013). Validation of the Zebrafish Pentylenetetrazol Seizure Model: Locomotor versus Electrographic Responses to Antiepileptic Drugs. *PLoS ONE*, *8*(1), 1–9. https://doi.org/10.1371/journal.pone.0054166

Alfaro, J. M., Ripoll-Gómez, J., & Burgos, J. S. (2011). Kainate administered to adult zebrafish causes seizures similar to those in rodent models. *European Journal of Neuroscience*, *33*(7), 1252–1255. https://doi.org/10.1111/j.1460-9568.2011.07622.x

Aquilino, M. S., Whyte-Fagundes, P., Zoidl, G., & Carlen, P. L. (2017). Pannexin-1 channels in epilepsy. *Neuroscience Letters*, *695*, 71–75. https://doi.org/10.1016/j.neulet.2017.09.004

Badimon, A., Strasburger, H. J., Ayata, P., Chen, X., Nair, A., Ikegami, A., Hwang, P., Chan, A. T., Graves, S. M., Uweru, J. O., Ledderose, C., Kutlu, M. G., Wheeler, M. A., Kahan, A., Ishikawa, M., Wang, Y. C., Loh, Y. H. E., Jiang, J. X., Surmeier, D. J., … Schaefer, A. (2020). Negative feedback control of neuronal activity by microglia. *Nature*, *586*(7829), 417–423. https://doi.org/10.1038/s41586-020-2777-8

Bao, L., Locovei, S., & Dahl, G. (2004). Pannexin membrane channels are mechanosensitive conduits for ATP. *FEBS Letters*, *572*(1–3), 65–68. https://doi.org/10.1016/j.febslet.2004.07.009

Baraban, S. C., Dinday, M. T., Castro, P. A., Chege, S., Guyenet, S., & Taylor, M. R. (2007). A large-scale mutagenesis screen to identify seizure-resistant zebrafish. *Epilepsia*, *48*(6), 1151–1157. https://doi.org/10.1111/j.1528-1167.2007.01075.x

Baraban, S. C., Taylor, M. R., Castro, P. A., & Baier, H. (2005). Pentylenetetrazole induced changes in zebrafish behavior, neural activity and c-fos expression. *Neuroscience*, *131*(3), 759–768.

Baranova, A., Ivanov, D., Petrash, N., Pestova, A., Skoblov, M., Kelmanson, I., Shagin, D., Nazarenko, S., Geraymovych, E., Litvin, O., Tiunova, A., Born, T. L., Usman, N., Staroverov, D., Lukyanov, S., & Panchin, Y. (2004). The mammalian pannexin family is homologous to the invertebrate innexin gap junction proteins. *Genomics*, *83*(4), 706–716. https://doi.org/10.1016/j.ygeno.2003.09.025

Barbe, M. T., Hormuzdi, S. G., Herb, A., Bruzzone, R., & Monyer, H. (2003). Pannexins, a family of gap junction proteins expressed in brain. *Proceedings of the National Academy of Sciences*, *100*(23), 13644–13649. https://doi.org/10.1073/pnas.2233464100

Barkmeier, D. T., Senador, D., Leclercq, K., Pai, D., Hua, J., Boutros, N. N., Kaminski, R. M., & Loeb, J. A. (2012). Electrical, molecular and behavioral effects of interictal spiking in the rat. *Neurobiology of Disease*, *47*(1), 92–101. https://doi.org/10.1016/j.nbd.2012.03.026

Berghmans, S., Hunt, J., Roach, A., & Goldsmith, P. (2007). Zebrafish offer the potential for a primary screen to identify a wide variety of potential anticonvulsants. *Epilepsy Research*, *75*(1), 18–28.

Best, J. D., Berghmans, S., Hunt, J. J. F. G., Clarke, S. C., Fleming, A., Goldsmith, P., & Roach,

A. G. (2008). Non-associative learning in larval zebrafish. *Neuropsychopharmacology*, *33*(5), 1206–1215. https://doi.org/10.1038/sj.npp.1301489

Bilotta, J., & Saszik, S. (2001). The zebrafish as a model visual system. *International Journal of Developmental Neuroscience*, *19*(7), 621–629. https://doi.org/10.1016/S0736-5748(01)00050-8

Boassa, D., Ambrosi, C., Qiu, F., Dahl, G., Gaietta, G., & Sosinsky, G. (2007). Pannexin1 channels contain a glycosylation site that targets the hexamer to the plasma membrane. *Journal of Biological Chemistry*, *282*(43), 31733–31743. https://doi.org/10.1074/jbc.M702422200

Bond, S. R., Wang, N., Leybaert, L., & Naus, C. C. (2012). Pannexin 1 ohnologs in the teleost lineage. *Journal of Membrane Biology*, *245*(8), 483–493. https://doi.org/10.1007/s00232-012-9497-4

Boyce, A. K. J., & Swayne, L. A. (2017). P2X7 receptor cross-Talk regulates ATP-induced pannexin 1 internalization. *Biochemical Journal*, *474*(13), 2133–2144. https://doi.org/10.1042/BCJ20170257

Breier, B., & Onken, A. (2019). Analysis of Video Feature Learning in Two-Stream Cnns on the Example of Zebrafish Swim Bout Classification. *ArXiv*, *2018*, 1–18.

Budaszewski Pinto, C., de Sá Couto-Pereira, N., Kawa Odorcyk, F., Cagliari Zenki, K., Dalmaz, C., Losch de Oliveira, D., & Calcagnotto, M. E. (2021). Effects of acute seizures on cell proliferation, synaptic plasticity and long-term behavior in adult zebrafish. *Brain Research*, *1756*, 147334. https://doi.org/10.1016/j.brainres.2021.147334

Carlen, P. L. (2012). Curious and contradictory roles of glial connexins and pannexins in epilepsy. *Brain Research*, *1487*, 54–60. https://doi.org/10.1016/j.brainres.2012.06.059

Carpio, Y., & Estrada, M. P. (2006). Zebrafish as a genetic model organism. *Biotecnologia Aplicada*, *23*(4), 265–270.

Cenedese, V., De Graaff, W., Csikós, T., Poovayya, M., Zoidl, G., & Kamermans, M. (2017). Pannexin 1 is critically involved in feedback from horizontal cells to cones. *Frontiers in Molecular Neuroscience*, *10*, 403. https://doi.org/10.3389/fnmol.2017.00403

Cepeda, C., Chang, J. W., Owens, G. C., Huynh, M. N., Chen, J. Y., Tran, C., Vinters, H. V., Levine, M. S., & Mathern, G. W. (2015). In rasmussen encephalitis, hemichannels associated with microglial activation are linked to cortical pyramidal neuron coupling: A possible mechanism for cellular hyperexcitability. *CNS Neuroscience and Therapeutics*, *21*(2), 152–163. https://doi.org/10.1111/cns.12352

Chekeni, F. B., Elliott, M. R., Sandilos, J. K., Walk, S. F., Kinchen, J. M., Lazarowski, E. R., Armstrong, A. J., Penuela, S., Laird, D. W., Salvesen, G. S., Isakson, B. E., Bayliss, D. A., & Ravichandran, K. S. (2010). Pannexin 1 channels mediate "find-me" signal release and membrane permeability during apoptosis. *Nature*, *467*(7317), 863–867. https://doi.org/10.1038/nature09413

Chen, T. W., Wardill, T. J., Sun, Y., Pulver, S. R., Renninger, S. L., Baohan, A., Schreiter, E. R., Kerr, R. A., Orger, M. B., Jayaraman, V., Looger, L. L., Svoboda, K., & Kim, D. S. (2013).

Ultrasensitive fluorescent proteins for imaging neuronal activity. *Nature*, *499*(7458), 295–300. https://doi.org/10.1038/nature12354

Chiu, Y. H., Jin, X., Medina, C. B., Leonhardt, S. A., Kiessling, V., Bennett, B. C., Shu, S., Tamm, L. K., Yeager, M., Ravichandran, K. S., & Bayliss, D. A. (2017). A quantized mechanism for activation of pannexin channels. *Nature Communications*, *8*(1), 1–15. https://doi.org/10.1038/ncomms14324

Chiu, Y. H., Schappe, M. S., Desai, B. N., & Bayliss, D. A. (2018). Revisiting multimodal activation and channel properties of Pannexin 1. *Journal of General Physiology*, *150*(1), 19–39. https://doi.org/10.1085/jgp.201711888

Cong, L., Wang, Z., Chai, Y., Hang, W., Shang, C., Yang, W., Bai, L., Du, J., Wang, K., & Wen, Q. (2017). Rapid whole brain imaging of neural activity in freely behaving larval zebrafish (Danio rerio). *ELife*, *6*, 1–20. https://doi.org/10.7554/eLife.28158

Create Simple Deep Learning Network for Classification. (2020). In *MATLAB R2020a*. The Mathworks, Inc., Natick, Massachusetts, United States. https://www.mathworks.com/help/deeplearning/ug/create-simple-deep-learning-network-for-classification.html

Dahl, G. (2015). ATP release through pannexon channels. *Philosophical Transactions of the Royal Society B: Biological Sciences*, *370*(1672), 20140191. https://doi.org/10.1098/rstb.2014.0191

Dahl, G., Qiu, F., & Wang, J. (2013). The bizarre pharmacology of the ATP release channel pannexin1. *Neuropharmacology*, *75*, 583–593. https://doi.org/10.1016/j.neuropharm.2013.02.019

de Marchi, F. O., Cruz, F. F., Menezes, F. P., Kist, L. W., Bogo, M. R., & Morrone, F. B. (2019). P2X7R and PANX-1 channel relevance in a zebrafish larvae copper-induced inflammation model. *Comparative Biochemistry and Physiology Part - C: Toxicology and Pharmacology*, *223*, 62–70. https://doi.org/10.1016/j.cbpc.2019.05.012

Desmond, D., Kyzar, E., Gaikwad, S., Green, J., Riehl, R., Stewart, A. M., & Kalueff, A. V. (2012). Zebrafish Protocols for Neurobehavioral Research: Assessing Epilepsy-Related Behavioral Phenotypes in Adult Zebrafish. *Chemosphere*, *66*(Chapter 24), 312–324. https://doi.org/10.1007/978-1-61779-597-8

Dodd, A., Curtis, P. M., Williams, L. C., & Love, D. R. (2000). Zebrafish: Bridging the gap between development and disease. *Human Molecular Genetics*, *9*(16), 2443–2449. https://doi.org/10.1093/hmg/9.16.2443

Dossi, E., Blauwblomme, T., Moulard, J., Chever, O., Vasile, F., Guinard, E., Le Bert, M., Couillin, I., Pallud, J., Capelle, L., Huberfeld, G., & Rouach, N. (2018). Pannexin-1 channels contribute to seizure generation in human epileptic brain tissue and in a mouse model of epilepsy. *Science Translational Medicine*, *10*(443), 1–14. https://doi.org/10.1126/scitranslmed.aar3796

Eimon, P. M., Ghannad-Rezaie, M., De Rienzo, G., Allalou, A., Wu, Y., Gao, M., Roy, A., Skolnick, J., & Yanik, M. F. (2018). Brain activity patterns in high-throughput

electrophysiology screen predict both drug efficacies and side effects. *Nature Communications*, *9*(1). https://doi.org/10.1038/s41467-017-02404-4

Green, J., Collins, C., Kyzar, E. J., Pham, M., Roth, A., Gaikwad, S., Cachat, J., Stewart, A. M., Landsman, S., Grieco, F., Tegelenbosch, R., Noldus, L. P. J. J., & Kalueff, A. V. (2012). Automated high-throughput neurophenotyping of zebrafish social behavior. *Journal of Neuroscience Methods*, *210*(2), 266–271. https://doi.org/10.1016/j.jneumeth.2012.07.017

Guilbeault, N. C., Guerguiev, J., Martin, M., Tate, I., & Thiele, T. R. (2021). BonZeb: open-source, modular software tools for high-resolution zebrafish tracking and analysis. *Scientific Reports*, *11*(1), 1–21. https://doi.org/10.1038/s41598-021-85896-x

Hong, S. G., Lee, P., Baraban, S. C., & Lee, L. P. (2016). A Novel Long-term, Multi-Channel and Non-invasive Electrophysiology Platform for Zebrafish. *Scientific Reports*, *6*(June), 1–10. https://doi.org/10.1038/srep28248

Hortopan, G. A., Dinday, M. T., & Baraban, S. C. (2010). Spontaneous seizures and altered gene expression in GABA signaling pathways in a mind bomb mutant zebrafish. *Journal of Neuroscience*, *30*(41), 13718–13728. https://doi.org/10.1523/JNEUROSCI.1887-10.2010

Hosseini, S., Simianer, H., Tetens, J., Brenig, B., Herzog, S., & Sharifi, A. R. (2019). Efficient phenotypic sex classification of zebrafish using machine learning methods. *Ecology and Evolution*, *9*(23), 13332–13343. https://doi.org/10.1002/ece3.5788

Huang, R. Q., Bell-Horner, C. L., Dibas, M. I., Covey, D. F., Drewe, J. A., & Dillon, G. H. (2001). Pentylenetetrazole-induced inhibition of recombinant γ-aminobutyric acid type A (GABAA) receptors: Mechanism and site of action. *Journal of Pharmacology and Experimental Therapeutics*, *298*(3), 986–995.

Hunyadi, B., Siekierska, A., Sourbron, J., Copmans, D., & de Witte, P. A. M. (2017). Automated analysis of brain activity for seizure detection in zebrafish models of epilepsy. *Journal of Neuroscience Methods*, *287*, 13–24. https://doi.org/10.1016/j.jneumeth.2017.05.024

Iglesias, R., Locovei, S., Roque, A., Alberto, A. P., Dahl, G., Spray, D. C., & Scemes, E. (2008). P2X7 receptor-Pannexin1 complex: Pharmacology and signaling. *American Journal of Physiology - Cell Physiology*, *295*(3), 752–760. https://doi.org/10.1152/ajpcell.00228.2008

Ishaq, O., Negri, J., Bray, M. A., Pacureanu, A., Peterson, R. T., & Wahlby, C. (2013). Automated quantification of Zebrafish tail deformation for high-throughput drug screening. *Proceedings - International Symposium on Biomedical Imaging*, 902–905. https://doi.org/10.1109/ISBI.2013.6556621

Ishaq, O., Sadanandan, S. K., & Wählby, C. (2017). Deep Fish: Deep Learning-Based Classification of Zebrafish Deformation for High-Throughput Screening. *Journal of Biomolecular Screening*, *22*(1), 102–107. https://doi.org/10.1177/1087057116667894

Jaillon, O., Aury, J. M., Brunet, F., Petit, J. L., Stange-Thomann, N., Maucell, E., Bouneau, L., Fischer, C., Ozouf-Costaz, C., Bernot, A., Nicaud, S., Jaffe, D., Fisher, S., Lutfalla, G., Dossat, C., Segurens, B., Dasilva, C., Salanoubat, M., Levy, M., … Roest Crollius, H. (2004). Genome duplication in the teleost fish Tetraodon nigroviridis reveals the early vertebrate proto-karyotype. *Nature*, *431*(7011), 946–957.

https://doi.org/10.1038/nature03025

Jiang, T., Long, H., Ma, Y., Long, L., Li, Y., Li, F., Zhou, P., Yuan, C., & Xiao, B. (2013). Altered expression of pannexin proteins in patients with temporal lobe epilepsy. *Molecular Medicine Reports*, *8*(6), 1801–1806. https://doi.org/10.3892/mmr.2013.1739

Jin, Q., Zhang, B., Zheng, X., Li, N., Xu, L., Xie, Y., Song, F., Bhat, E. A., Chen, Y., Gao, N., Guo, J., Zhang, X., & Ye, S. (2020). Cryo-EM structures of human pannexin 1 channel. *Cell Research*, *30*(5), 449–451. https://doi.org/10.1038/s41422-020-0310-0

Kalueff, A. V., Gebhardt, M., Stewart, A. M., Cachat, J. M., Brimmer, M., Chawla, J. S., Craddock, C., Kyzar, E. J., Roth, A., Landsman, S., Gaikwad, S., Robinson, K., Baatrup, E., Tierney, K., Shamchuk, A., Norton, W., Miller, N., Nicolson, T., Braubach, O., … Schneider, H. (2013). Towards a comprehensive catalog of zebrafish behavior 1.0 and beyond. *Zebrafish*, *10*(1), 70–86. https://doi.org/10.1089/zeb.2012.0861

Kalueff, A. V., & Stewart, A. M. (2012). *Zebrafish Protocols in Neurobehavioral Research*. New York: Humana Press.

Kari, G., Rodeck, U., & Dicker, A. P. (2007). Zebrafish: An emerging model system for human disease and drug discovery. *Clinical Pharmacology and Therapeutics*, *82*(1), 70–80. https://doi.org/10.1038/sj.clpt.6100223

Khalili, A., Peimani, A. R., Safarian, N., Youssef, K., Zoidl, G., & Rezai, P. (2019). Phenotypic chemical and mutant screening of zebrafish larvae using an on-demand response to electric stimulation. *Integrative Biology : Quantitative Biosciences from Nano to Macro*, *11*(10), 373–383. https://doi.org/10.1093/intbio/zyz031

Kim, J. E., & Kang, T. C. (2011). The P2X7 receptor-pannexin-1 complex decreases muscarinic acetylcholine receptor-mediated seizure susceptibility in mice. *Journal of Clinical Investigation*, *121*(5), 2037–2047. https://doi.org/10.1172/JCI44818

Kurtenbach, S., Prochnow, N., Kurtenbach, S., Klooster, J., Zoidl, C., Dermietzel, R., Kamermans, M., & Zoidl, G. (2013). Pannexin1 Channel Proteins in the Zebrafish Retina Have Shared and Unique Properties. *PLoS ONE*, *8*(10), 1–19. https://doi.org/10.1371/journal.pone.0077722

Lenning, M., Fortunato, J., Le, T., Clark, I., Sherpa, A., Yi, S., Hofsteen, P., Thamilarasu, G., Yang, J., Xu, X., Han, H. D., Hsiai, T. K., & Cao, H. (2018). Real-time monitoring and analysis of zebrafish electrocardiogram with anomaly detection. *Sensors (Switzerland)*, *18*(1), 1–16. https://doi.org/10.3390/s18010061

Li, S., Zang, Z., He, J., Chen, X., Yu, S., Pei, Y., Hou, Z., An, N., Yang, H., Zhang, C., & Liu, S. (2017). Expression of pannexin 1 and 2 in cortical lesions from intractable epilepsy patients with focal cortical dysplasia. *Oncotarget*, *8*(4), 6883–6895. https://doi.org/10.18632/oncotarget.14317

Lin, X., Duan, X., Jacobs, C., Ullmann, J., Chan, C. Y., Chen, S., Cheng, S. H., Zhao, W. N., Poduri, A., Wang, X., Haggarty, S. J., & Shi, P. (2018). High-throughput brain activity mapping and machine learning as a foundation for systems neuropharmacology. *Nature Communications*, *9*(1), 1–12. https://doi.org/10.1038/s41467-018-07289-5

Liu, J., & Baraban, S. C. (2019). Network properties revealed during multi-scale calcium imaging of seizure activity in Zebrafish. *ENeuro*, *6*(1). https://doi.org/10.1523/ENEURO.0041-19.2019

Locovei, S., Bao, L., & Dahl, G. (2006). Pannexin 1 in erythrocytes: Function without a gap. *Proceedings of the National Academy of Sciences of the United States of America*, *103*(20), 7655–7659. https://doi.org/10.1073/pnas.0601037103

Locovei, S., Wang, J., & Dahl, G. (2006). Activation of pannexin 1 channels by ATP through P2Y receptors and by cytoplasmic calcium. *FEBS Letters*, *580*(1), 239–244. https://doi.org/10.1016/j.febslet.2005.12.004

Lösing, P., Niturad, C. E., Harrer, M., Reckendorf, C. M. Z., Schatz, T., Sinske, D., Lerche, H., Maljevic, S., & Knöll, B. (2017). SRF modulates seizure occurrence, activity induced gene transcription and hippocampal circuit reorganization in the mouse pilocarpine epilepsy model. *Molecular Brain*, *10*(1), 1–22. https://doi.org/10.1186/s13041-017-0310-2

Marques, J. C., Lackner, S., Félix, R., & Orger, M. B. (2018). Structure of the Zebrafish Locomotor Repertoire Revealed with Unsupervised Behavioral Clustering. *Current Biology*, *28*(2), 181–195. https://doi.org/10.1016/j.cub.2017.12.002

MATLAB and Deep Learning Toolbox Release 2020a. (2020). The Mathworks, Inc., Natick, Massachusetts, United States.

Mearns, D. S., Donovan, J. C., Fernandes, A. M., Semmelhack, J. L., & Baier, H. (2020). Deconstructing Hunting Behavior Reveals a Tightly Coupled Stimulus-Response Loop. *Current Biology : CB*, *30*(1), 54-69.e9. https://doi.org/10.1016/j.cub.2019.11.022

Michalski, K., Syrjanen, J. L., Henze, E., Kumpf, J., Furukawa, H., & Kawate, T. (2020). The Cryo-EM structure of a pannexin 1 reveals unique motifs for ion selection and inhibition. *ELife*, *9*, 1–14. https://doi.org/10.7554/eLife.54670

Mim, C., Perkins, G., & Dahl, G. (2021). Structure versus function: Are new conformations of pannexin 1 yet to be resolved? *The Journal of General Physiology*, *153*(5), 1–17. https://doi.org/10.1085/jgp.202012754

Mou, L., Ke, M., Song, M., Shan, Y., Xiao, Q., Liu, Q., Li, J., Sun, K., Pu, L., Guo, L., Geng, J., Wu, J., & Deng, D. (2020). Structural basis for gating mechanism of Pannexin 1 channel. *Cell Research*, *30*(5), 452–454. https://doi.org/10.1038/s41422-020-0313-x

Mussulini, B. H. M., Leite, C. E., Zenki, K. C., Moro, L., Baggio, S., Rico, E. P., Rosemberg, D. B., Dias, R. D., Souza, T. M., Calcagnotto, M. E., Campos, M. M., Battastini, A. M., & de Oliveira, D. L. (2013). Seizures Induced by Pentylenetetrazole in the Adult Zebrafish: A Detailed Behavioral Characterization. *PLoS ONE*, *8*(1), 1–9. https://doi.org/10.1371/journal.pone.0054515

Mylvaganam, S., Ramani, M., Krawczyk, M., & Carlen, P. L. (2014). Roles of gap junctions, connexins, and pannexins in epilepsy. *Frontiers in Physiology*, *5*, 1–12. https://doi.org/10.3389/fphys.2014.00172

Mylvaganam, S., Zhang, L., Wu, C., Zhang, Z. J., Samoilova, M., Eubanks, J., Carlen, P. L., & Poulter, M. O. (2010). Hippocampal seizures alter the expression of the pannexin and

connexin transcriptome. *Journal of Neurochemistry*, *112*(1), 92–102. https://doi.org/10.1111/j.1471-4159.2009.06431.x

Narahari, A. K., Kreutzberger, A. J. B., Gaete, P. S., Chiu, Y. H., Leonhardt, S. A., Medina, C. B., Jin, X., Oleniacz, P. W., Kiessling, V., Barrett, P. Q., Ravichandran, K. S., Yeager, M., Contreras, J. E., Tamm, L. K., & Bayliss, D. A. (2021). Atp and large signaling metabolites flux through caspase-activated pannexin 1 channels. *ELife*, *10*, 1–21. https://doi.org/10.7554/ELIFE.64787

Nath, T., Mathis, A., Chen, A. C., Patel, A., Bethge, M., & Mathis, M. W. (2019). Using DeepLabCut for 3D markerless pose estimation across species and behaviors. *Nature Protocols*, *14*(7), 2152–2176. https://doi.org/10.1038/s41596-019-0176-0

Panchin, Y., Kelmanson, I., Matz, M., Lukyanov, K., Usman, N., & Lukyanov, S. (2000). A ubiquitous family of putative gap junction molecules. *Current Biology*, *10*(13), 473–474. https://doi.org/10.1016/S0960-9822(00)00576-5

Paudel, Y. N., Kumari, Y., Abidin, S. A. Z., Othman, I., & Shaikh, M. F. (2020). Pilocarpine induced behavioral and biochemical alterations in chronic seizure-like condition in adult Zebrafish. *International Journal of Molecular Sciences*, *21*(7). https://doi.org/10.3390/ijms21072492

Pelegrin, P., & Surprenant, A. (2006). Pannexin-1 mediates large pore formation and interleukin-1β release by the ATP-gated P2X7 receptor. *EMBO Journal*, *25*(21), 5071–5082. https://doi.org/10.1038/sj.emboj.7601378

Penuela, S., Bhalla, R., Gong, X. Q., Cowan, K. N., Celetti, S. J., Cowan, B. J., Bai, D., Shao, Q., & Laird, D. W. (2007). Pannexin 1 and pannexin 3 are glycoproteins that exhibit many distinct characteristics from the connexin family of gap junction proteins. *Journal of Cell Science*, *120*(21), 3772–3783. https://doi.org/10.1242/jcs.009514

Penuela, S., Gehi, R., & Laird, D. W. (2013). The biochemistry and function of pannexin channels. *Biochimica et Biophysica Acta - Biomembranes*, *1828*(1), 15–22. https://doi.org/10.1016/j.bbamem.2012.01.017

Penuela, S., Harland, L., Simek, J., & Laird, D. W. (2014). Pannexin channels and their links to human disease. *Biochemical Journal*, *461*(3), 371–381. https://doi.org/10.1042/BJ20140447

Pérez-Escudero, A., Vicente-Page, J., Hinz, R. C., Arganda, S., & De Polavieja, G. G. (2014). IdTracker: Tracking individuals in a group by automatic identification of unmarked animals. *Nature Methods*, *11*(7), 743–748. https://doi.org/10.1038/nmeth.2994

Pfaffl, M. W., Horgan, G. W., & Dempfle, L. (2002). Relative expression software tool (REST) for group-wise comparison and statistical analysis of relative expression results in real-time PCR. *Nucleic Acids Research*, *30*(9). https://doi.org/10.1093/nar/30.9.e36

Pineda, R., Beattie, C. E., & Hall, C. W. (2011). Recording the adult zebrafish cerebral field potential during pentylenetetrazole seizures. *Journal of Neuroscience Methods*, *200*(1), 20–28. https://doi.org/10.1016/j.jneumeth.2011.06.001

Pineda, R., Beattie, C. E., & Hall, C. W. (2013). Closed-loop neural stimulation for pentylenetetrazole-induced seizures in zebrafish. *DMM Disease Models and Mechanisms*,

6(1), 64–71. https://doi.org/10.1242/dmm.009423

Prochnow, N., Hoffmann, S., Dermietzel, R., & Zoidl, G. (2009). Replacement of a single cysteine in the fourth transmembrane region of zebrafish pannexin1 alters hemichannel gating behavior. *Experimental Brain Research*, *199*(3–4), 255–264. https://doi.org/10.1007/s00221-009-1957-4

Prochnow, N., Hoffmann, S., Vroman, R., Klooster, J., Bunse, S., Kamermans, M., Dermietzel, R., & Zoidl, G. (2009). Pannexin1 in the outer retina of the zebrafish, Danio rerio. *Neuroscience*, *162*(4), 1039–1054. https://doi.org/10.1016/j.neuroscience.2009.04.064

Qiu, F., & Dahl, G. (2009). A permeant regulating its permeation pore: Inhibition of pannexin 1 channels by ATP. *American Journal of Physiology - Cell Physiology*, *296*(2), 250–255. https://doi.org/10.1152/ajpcell.00433.2008

Qiu, F., Wang, J., & Dahl, G. (2012). Alanine substitution scanning of pannexin1 reveals amino acid residues mediating ATP sensitivity. *Purinergic Signalling*, *8*(1), 81–90. https://doi.org/10.1007/s11302-011-9263-6

Qu, R., Dong, L., Zhang, J., Yu, X., Wang, L., & Zhu, S. (2020). Cryo-EM structure of human heptameric Pannexin 1 channel. *Cell Research*, *30*(5), 446–448. https://doi.org/10.1038/s41422-020-0298-5

Rakhade, S. N., Yao, B., Ahmed, S., Asano, E., Beaumont, T. L., Shah, A. K., Draghici, S., Krauss, R., Chugani, H. T., Sood, S., & Loeb, J. A. (2005). A common pattern of persistent gene activation in human neocortical epileptic foci. *Annals of Neurology*, *58*(5), 736–747. https://doi.org/10.1002/ana.20633

Ruan, Z., Orozco, I. J., Du, J., & Lü, W. (2020). Structures of human pannexin 1 reveal ion pathways and mechanism of gating. *Nature*, *584*(7822), 646–651. https://doi.org/10.1038/s41586-020-2357-y

Safarian, N., Houshangi-Tabrizi, S., Zoidl, C., & Zoidl, G. R. (2021). Panx1b modulates the luminance response and direction of motion in the zebrafish. *BioRxiv*.

Safarian, N., Whyte-Fagundes, P., Zoidl, C., Grigull, J., & Zoidl, G. (2020). Visuomotor deficiency in panx1a knockout zebrafish is linked to dopaminergic signaling. *Scientific Reports*, *10*(1), 1–14. https://doi.org/10.1038/s41598-020-66378-y

Sang, Q., Zhang, Z., Shi, J., Sun, X., Li, B., Yan, Z., Xue, S., Ai, A., Lyu, Q., Li, W., Zhang, J., Wu, L., Mao, X., Chen, B., Mu, J., Li, Q., Du, J., Sun, Q., Jin, L., … Wang, L. (2019). A pannexin 1 channelopathy causes human oocyte death. *Science Translational Medicine*, *11*(485). https://doi.org/10.1126/scitranslmed.aav8731

Santiago, M. F., Veliskova, J., Patel, N. K., Lutz, S. E., Caille, D., Charollais, A., Meda, P., & Scemes, E. (2011). Targeting pannexin1 improves seizure outcome. *PLoS ONE*, *6*(9). https://doi.org/10.1371/journal.pone.0025178

Scemes, E., Velíšek, L., & Velíšková, J. (2019). Astrocyte and Neuronal Pannexin1 Contribute Distinctly to Seizures. *ASN Neuro*, *11*. https://doi.org/10.1177/1759091419833502

Scott, C. A., Marsden, A. N., & Slusarski, D. C. (2016). Automated, high-throughput, in vivo

analysis of visual function using the zebrafish. *Developmental Dynamics*, *245*(5), 605–613. https://doi.org/10.1002/dvdy.24398

Semmelhack, J. L., Donovan, J. C., Thiele, T. R., Kuehn, E., Laurell, E., & Baier, H. (2014). A dedicated visual pathway for prey detection in larval zebrafish. *ELife*, *3*, 1–19. https://doi.org/10.7554/eLife.04878

Singh, S. P., Janjuha, S., Chaudhuri, S., Reinhardt, S., Kränkel, A., Dietz, S., Eugster, A., Bilgin, H., Korkmaz, S., Zararsız, G., Ninov, N., & Reid, J. E. (2018). Machine learning based classification of cells into chronological stages using single-cell transcriptomics. *Scientific Reports*, *8*(1), 1–12. https://doi.org/10.1038/s41598-018-35218-5

Sosinsky, G. E., Boassa, D., Dermietzel, R., Duffy, H. S., Laird, D. W., MacVicar, B., Naus, C. C., Penuela, S., Scemes, E., Spray, D. C., Thompson, R. J., & Zhao, Hong-BoDahl, G. (2011). Pannexin channels are not gap junction hemichannels. *Channels*, *5*(3), 193–197. https://doi.org/10.4161/chan.5.3.15765

Suadicani, S. O., Iglesias, R., Wang, J., Dahl, G., Spray, D. C., & Scemes, E. (2012). ATP signaling is deficient in cultured pannexin1-null mouse astrocytes. *Glia*, *60*(7), 1106–1116. https://doi.org/10.1002/glia.22338

Teng, Y., Xie, X., Walker, S., Rempala, G., Kozlowski, D. J., Mumm, J. S., & Cowell, J. K. (2010). Knockdown of zebrafish lgi1a results in abnormal development, brain defects and a seizure-like behavioral phenotype. *Human Molecular Genetics*, *19*(22), 4409–4420. https://doi.org/10.1093/hmg/ddq364

Tiedeken, J. A., & Ramsdell, J. S. (2007). Embryonic exposure to domoic acid increases the susceptibility of zebrafish larvae to the chemical convulsant pentylenetetrazole. *Environmental Health Perspectives*, *115*(11), 1547–1552. https://doi.org/10.1289/ehp.10344

Tiedeken, J. A., & Ramsdell, J. S. (2009). DDT exposure of Zebrafish embryos enhances seizure susceptibility: Relationship to fetal p,p'-DDE burden and domoic acid exposure of California Sea Lions. *Environmental Health Perspectives*, *117*(1), 68–73. https://doi.org/10.1289/ehp.11685

Timonina, K., Kotova, A., & Zoidl, G. (2020). Role of an aromatic–aromatic interaction in the assembly and trafficking of the zebrafish panx1a membrane channel. *Biomolecules*, *10*(2). https://doi.org/10.3390/biom10020272

Tunyasuvunakool, K., Adler, J., Wu, Z., Green, T., Zielinski, M., Žídek, A., Bridgland, A., Cowie, A., Meyer, C., Laydon, A., Velankar, S., Kleywegt, G. J., Bateman, A., Evans, R., Pritzel, A., Figurnov, M., Ronneberger, O., Bates, R., Kohl, S. A. A., … Hassabis, D. (2021). Highly accurate protein structure prediction for the human proteome. *Nature*, 1–9. https://doi.org/10.1038/s41586-021-03828-1

Viader-Llargués, O., Lupperger, V., Pola-Morell, L., Marr, C., & López-Schier, H. (2018). Live cell-lineage tracing and machine learning reveal patterns of organ regeneration. *ELife*, *7*, 1–23. https://doi.org/10.7554/eLife.30823

Vladimirov, N., Mu, Y., Kawashima, T., Bennett, D. V., Yang, C. T., Looger, L. L., Keller, P. J.,

Freeman, J., & Ahrens, M. B. (2014). Light-sheet functional imaging in fictively behaving zebrafish. *Nature Methods*, *11*(9), 883–884. https://doi.org/10.1038/nmeth.3040

Wang, J., Ambrosi, C., Qiu, F., Jackson, D. G., Sosinsky, G., & Dahl, G. (2014). The membrane protein Pannexin1 forms two open-channel conformations depending on the mode of activation. *Science Signaling*, *7*(335), 1–9. https://doi.org/10.1126/scisignal.2005431

Weaver, J. L., Arandjelovic, S., Brown, G., Mendu, S. K., Schappe, M. S., Buckley, M. W., Chiu, Y. H., Shu, S., Kim, J. K., Chung, J., Krupa, J., Jevtovic-Todorovic, V., Desai, B. N., Ravichandran, K. S., & Bayliss, D. A. (2017). Hematopoietic pannexin 1 function is critical for neuropathic pain. *Scientific Reports*, *7*(1), 1–15. https://doi.org/10.1038/srep42550

Weilinger, N. L., Lohman, A. W., Rakai, B. D., Ma, E. M. M., Bialecki, J., Maslieieva, V., Rilea, T., Bandet, M. V., Ikuta, N. T., Scott, L., Colicos, M. A., Teskey, G. C., Winship, I. R., & Thompson, R. J. (2016). Metabotropic NMDA receptor signaling couples Src family kinases to pannexin-1 during excitotoxicity. *Nature Neuroscience*, *19*(3), 432–442. https://doi.org/10.1038/nn.4236

Whyte-Fagundes, P., Taskina, D., Safarian, N., Zoidl, C., Donaldson, L. W., & Zoidl, G. R. (2021). Panx1 channels promote both anti- and pro-seizure-like activities in the zebrafish via p2rx7 receptors and ATP signaling. *BioRxiv*, 1–40.

Winter, M. J., Redfern, W. S., Hayfield, A. J., Owen, S. F., Valentin, J. P., & Hutchinson, T. H. (2008). Validation of a larval zebrafish locomotor assay for assessing the seizure liability of early-stage development drugs. *Journal of Pharmacological and Toxicological Methods*, *57*(3), 176–187. https://doi.org/10.1016/j.vascn.2008.01.004

Wong, K., Stewart, A., Gilder, T., Wu, N., Frank, K., Gaikwad, S., Suciu, C., Dileo, J., Utterback, E., Chang, K., Grossman, L., Cachat, J., & Kalueff, A. V. (2010). Modeling seizure-related behavioral and endocrine phenotypes in adult zebrafish. *Brain Research*, *1348*, 209–215. https://doi.org/10.1016/j.brainres.2010.06.012

Zhang, H., Lenaghan, S. C., Connolly, M. H., & Parker, L. E. (2013). Zebrafish larva locomotor activity analysis using machine learning techniques. *Proceedings - 2013 12th International Conference on Machine Learning and Applications, ICMLA 2013*, *1*, 161–166. https://doi.org/10.1109/ICMLA.2013.35

Zoidl, G., Kremer, M., Zoidl, C., Bunse, S., & Dermietzel, R. (2008). Molecular diversity of connexin and pannexin genes in the retina of the zebrafish danio rerioc. *Cell Communication and Adhesion*, *15*(1–2), 169–183. https://doi.org/10.1080/15419060802014081

9. Supplementary information

9.1 Supplementary tables

Supplementary Table S1 RT-qPCR values (fold change) for IEG regulation in TL and *panx1* knockout larvae treated with PTZ for one hour. Expression values, respective to non-treated controls, are > 1 for upregulated IEGs and < 1 for downregulated IEGs. P-values in bold represent significant upregulation and $p < 0.05$.

Gene	**TL**	p-value	**DKO**	p-value	***panx1a*$^{-/-}$**	p-value	***panx1b*$^{-/-}$**	p-value
fosab	110.36	**0**	67.62	**0**	88.89	**0**	57.72	**0**
egr1	9.16	**0.001**	7.35	**0**	10.41	**0**	6.30	**0**
egr2a	21.42	**0**	44.20	**0**	17.28	**0**	7.98	**0**
egr2b	6.86	**0**	4.65	**0.002**	7.59	**0**	5.32	**0**
egr4	120.54	**0**	63.68	**0**	76.99	**0**	44.53	**0**
jun	4.17	**0**	4.57	**0**	9.38	**0**	5.34	**0**
bdnf	6.13	**0**	3.95	**0**	4.73	**0**	3.10	**0**
eif4ebp2	1.04	0.765	0.96	0.813	1.56	0.05	1.50	**0.01**

Supplementary Table S2 RT-qPCR values (fold change) for IEG regulation in TL larvae treated with PTZ for one hour (+ PTZ) or treated with Pb 30min before the PTZ treatment (Pb + PTZ). Expression values, respective to non-treated controls, are > 1 for upregulated IEGs and < 1 for downregulated IEGs. P-values in bold represent significant upregulation and $p < 0.05$.

Gene	**TL (+ PTZ)**	p-value	**TL (Pb + PTZ)**	p-value
fosab	110.36	**0**	54.61	**0**
egr1	9.16	**0.001**	6.09	**0.001**
egr2a	21.42	**0**	39.38	**0**
egr2b	6.86	**0**	2.03	**0**
egr4	120.54	**0**	96.97	**0**
jun	4.17	**0**	1.44	0.073
bdnf	6.13	**0**	6.08	**0**
eif4ebp2	1.04	0.765	0.76	0.056

Supplementary Table S3 RT-qPCR values (fold change) for gene regulation in PTZ treated (one hour) TL, DKO, *panx1a*$^{-/-}$, *panx1b*$^{-/-}$ and Pb pretreated TL larvae compared to their respective controls. Expression values are > 1 for upregulated genes and < 1 for downregulated genes. P-values in bold represent significant regulation and $p < 0.05$.

Gene	**TL**	p-value	**DKO**	p-value	***panx1a*$^{-/-}$**	p-value	***panx1b*$^{-/-}$**	p-value	**TL + Pb**	p-value
adora1b	1.02	0.959	1.42	0.133	1.71	**0.003**	0.75	0.474	0.65	0.331
cacna1da	1.03	0.859	0.96	0.582	0.85	0.45	1.09	0.216	0.77	0.091
entpd1	1.71	**0**	1.32	**0.02**	1.61	**0**	1.57	**0.003**	1.29	0.07
grin2bb	1.08	0.803	0.75	0.091	1.41	0.124	0.80	0.313	1.79	**0.02**
il1b	2.89	**0.007**	1.55	0.105	6.12	**0**	4.23	**0**	0.55	0.38
kcnc3a	1.18	0.319	0.65	0.311	0.82	0.216	0.74	0.104	3.70	**0.001**
kcnf1a	0.97	0.822	0.80	0.603	1.27	0.247	0.56	0.143	1.36	0.459
nt5e	1.16	0.184	1.07	0.628	1.29	0.077	0.80	0.082	0.88	0.499
p2rx7	0.80	**0.004**	0.79	0.378	1.47	**0.016**	0.89	0.654	1.10	0.645
p2ry12	1.83	0.187	0.84	0.526	0.86	0.577	0.52	**0.047**	1.52	0.12
scn4bb	0.92	0.632	0.86	0.128	0.90	0.334	0.51	**0**	1.02	0.936
sema6ba	1.34	0.204	1.21	0.461	1.36	0.068	0.86	0.262	1.22	0.277
slc8a1a	1.73	0.069	0.79	0.34	1.53	**0.042**	1.01	0.986	0.82	0.498
slc8a1b	0.97	0.895	0.87	0.302	1.41	**0.002**	0.86	0.211	1.73	**0**
slc8a2b	0.66	0.159	0.79	**0.029**	1.03	0.848	1.14	0.518	2.00	**0**
slco2b1	0.88	0.268	1.06	0.505	1.56	**0**	0.58	**0**	0.73	**0.008**
snap25b	1.01	0.946	0.83	0.346	1.05	0.659	1.02	0.779	1.02	0.9
trpv6	2.10	**0.181**	1.06	0.82	1.47	**0.028**	1.68	0.373	0.85	0.351
vcp	1.19	0.225	1.04	0.761	1.07	0.481	0.98	0.716	0.76	0.289

9.2 Supplementary figures

Supplementary Fig. S1 Probenecid concentration test on PTZ-induced 7dpf TL larvae

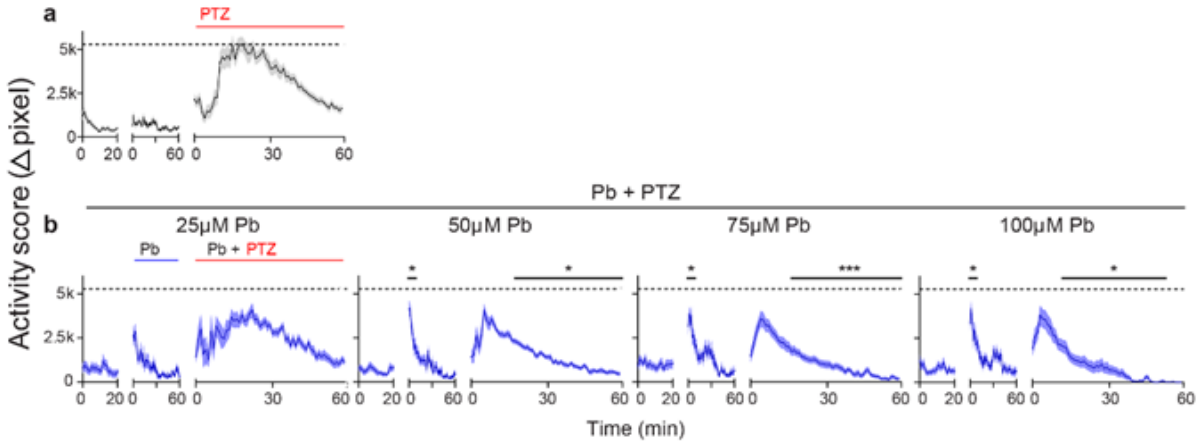

Probenecid's concertation dependant reduction of PTZ-induced hyperactivity was observed in 7dpf TL larvae (n = 18). Larvae were treated with 15mM PTZ (**a**) or incubated with 25, 50, 75 or 100µM Probenecid (Pb) for one hour and treated with 15mM PTZ (**b**). Pb significantly increased activity (Δpixel; mean +/- S.E.M.) for all concentrations tested compared to baseline, and significantly reduced PTZ-induced activity above 50µM. 75µM Pb was chosen for further investigation, as it significantly reduced seizure-related activity, without the evidence of substantial toxicity (activity level 0 within one hour). The dashed lines indicate max average activity for PTZ treated TL. *- $p < 0.05$, ***- $p < 0.001$. *Data and graphs were generated by Daria Taskina and included in the supplementary information for* (Whyte-Fagundes et al., 2021) *manuscript.*

Supplementary Fig. S2 Fluorescence in PTZ-induced *panx1b*$^{-/-}$ (F0 generation) with mosaic expression of GCaMP6.

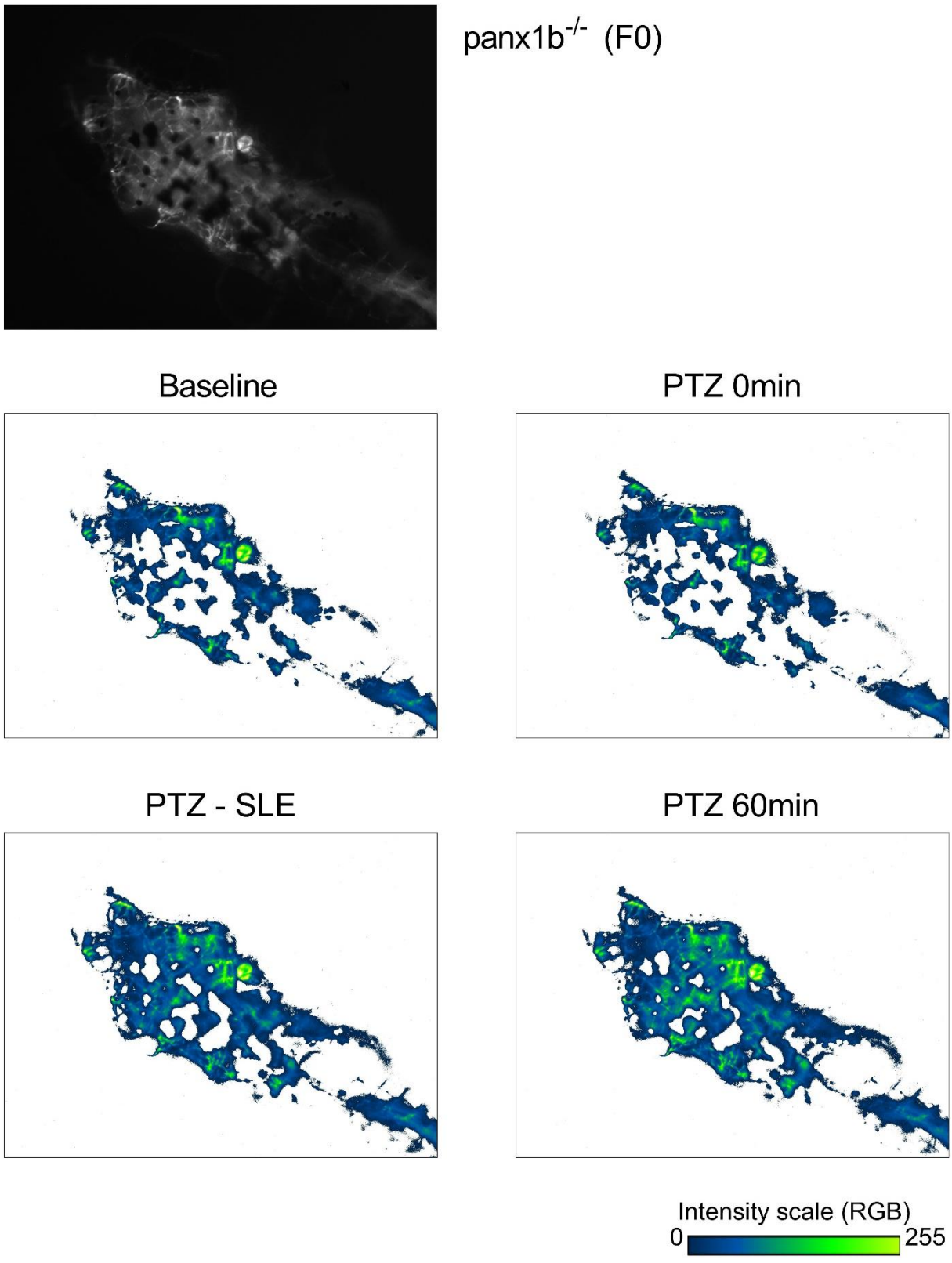

9.3 Statistical details

Figure	Treatment/ Group	Test	Comparison	P-value	Statistic value (F (DFn, DFd), t, Z, X2)	Sample size (N)	Star
7b Activity	Rest: TL - panx1b-/-	Two-way RM ANOVA	Genotype	<0.0001	F (1, 70) = 31.35	2 groups, n = 36 each	****
			Time	0.0015	F (11.71, 819.5) = 2.703; GG's epsilon = 0.4878	25	****
			Genotype x Time	0.7674	F (24, 1680) = 0.7787		
		Bonferroni's multiple comparison	Time	Rest : 8 - 13min		25 comparisons	*
	Base: TL - DKO	Two-way RM ANOVA	Genotype	0.0007	F (1, 70) = 12.71	2 groups, n = 36 each	***
			Time	0.484	F (11.31, 792.0) = 0.9591; GG's epsilon = 0.4041	29	
			Genotype x Time	0.0228	F (28, 1960) = 1.610		*
	Base: TL - panx1b-/-	Two-way RM ANOVA	Genotype	<0.0001	F (1, 70) = 39.15	2 groups, n = 36 each	****
			Time	0.6805	F (13.66, 956.1) = 0.7874; GG's epsilon = 0.4878	29	
			Genotype x Time	0.9665	F (28, 1960) = 0.5682		
		Bonferroni's multiple comparison	Time	Base : 1-9min, 20-25min		29 comparisons	*
	PTZ: TL - panx1a-/-	Two-way RM ANOVA	Genotype	<0.0001	F (1, 70) = 38.57	2 groups, n = 36 each	****
			Time	<0.0001	F (9.666, 676.6) = 53.27; GG's epsilon = 0.1638	60	****
			Genotype x Time	<0.0001	F (59, 4130) = 1.875		****
		Bonferroni's multiple comparison	Time	PTZ : 22 - 49min		60 comparisons	*
	PTZ: TL - panx1b-/-	Two-way RM ANOVA	Genotype	0.0013	F (1, 70) = 11.30	2 groups, n = 36 each	**
			Time	<0.0001	F (7.272, 509.0) = 72.37; GG's epsilon = 0.1233	60	****
			Genotype x Time	<0.0001	F (59, 4130) = 3.925		****
		Bonferroni's multiple comparison	Time	PTZ : 18 - 21min		60 comparisons	*
7c Area Under the Curve	Base	One-way ANOVA	All	<0.0001	F (3, 140) = 21.44	4 groups; 144 values	****
		Tukey's multiple comparison	TL - panx1b$^{-/-}$	<0.0001		36 values/group	****
	PTZ	One-way ANOVA	All	<0.0001	F (3, 140) = 28.44	"	****
		Tukey's multiple comparison	TL - panx1a$^{-/-}$	<0.0001		"	****
			TL - panx1b$^{-/-}$	0.0057		"	**
	PTZ-Base	One-way ANOVA	All	<0.0001	F (3, 140) = 7.596	"	****

		Tukey's multiple comparison	TL - panx1a$^{-/-}$	0.0002		"	***
10a Stage II count		Two-way RM ANOVA	TL - DKO	0.0982	Genotype F (1, 34) = 2.891	n = 18 per genotype	
		"	TL - panx1a$^{-/-}$	0.328	Genotype F (1, 34) = 0.9851	"	
		"	TL - panx1b$^{-/-}$	0.0804	Genotype F (1, 34) = 3.248	"	
10b Stage III count		"	TL - DKO	0.0149	Genotype F (1, 34) = 6.574	"	*
		"	TL - panx1a$^{-/-}$	0.0234	Genotype F (1, 34) = 5.635	"	*
		"	TL - panx1b-/-	0.105	Genotype F (1, 34) = 2.773	"	
10c Stage III total count/hour		Unpaired t test; two-tailed	TL - panx1b$^{-/-}$	0.105	t = 1.665, df =34	n = 18 per genotype	
10d Average St III count/2min		Paired t test (by time); two-tailed	TL - panx1b$^{-/-}$	0.0005	t = 3.931, df = 29	30 pairs	***
11a CNN conv freq		One-way ANOVA	TL - panx1a$^{-/-}$	< 0.0001	F (3,12) = 56.97	n = 6 values per group	****
			TL - panx1b$^{-/-}$	0.0004			***
11bCNN conv dur		One-way ANOVA	TL - panx1a$^{-/-}$	0.0409	F (3.12) = 37.99		*
			TL - panx1b$^{-/-}$	< 0.0001			****
13b Survival		Log-rank (Mantel-Cox)	TL - DKO	0.3848	Chi Square = 0.7553; df = 1	n = 80 per genotype	
			TL - panx1a$^{-/-}$	0.0088	Chi Square = 6.86; df = 1	"	**
			TL - panx1b$^{-/-}$	0.0081	Chi Square = 7.009; df = 1	"	**
15ab,16a Activity	Base : TL - TL + Pb	Two-way RM ANOVA	Treatment	0.0009	F (1, 70) = 12.13	2 groups, n = 36 each	***
			Time	<0.0001	F (12.76, 893.0) = 12.13; GG's epsilon = 0.4556	29	****
			Treatment x Time	<0.0001	F (28, 1960) = 9.434		****
		Bonferroni's multiple comparison	Time	Base : 0 - 6 min		29 comparisons	*
	Base : TL - TL + VPA	Two-way RM ANOVA	Treatment	<0.0001	F (1, 118) = 20.80	2 groups, n = 60 each	****
			Time	<0.0001	F (11.74, 1385) = 5.910; GG's epsilon = 0.4193	29	****
			Treatment x Time	<0.0001	F (28, 3304) = 3.988		****
		Bonferroni's multiple comparison	Time	Base : 11 - 29 min		29 comparisons	*
	PTZ : TL - TL + Pb	Two-way RM ANOVA	Treatment	<0.0001	F (1, 70) = 45.35	2 groups, n = 36 each	****
			Time	<0.0001	F (9.913, 693.9) = 60.74; GG's epsilon = 0.168	60	****
			Treatment x Time	<0.0001	F (59, 4130) = 18.40		****
		Bonferroni's multiple comparison	Time	PTZ : 14 - 52 min		60 comparisons	*
	PTZ : TL - TL + VPA	Two-way RM ANOVA	Treatment	<0.0001	F (1, 118) = 112.8	2 groups, n = 60 each	****

			Time	<0.0001	F (12.65, 1493) = 52.84; GG's epsilon = 0.2144	60	****
			Treatment x Time	<0.0001	F (59, 6962) = 11.64		****
		Bonferroni's multiple comparison	Time	PTZ: 6-50, 52-60min		60 comparisons	*
16b Area Under the Curve	Base	Unpaired t-test; two-tailed	PTZ - [Pb + PTZ]	0.502	t = 0.6748, df =70	2 groups; 72 values	
	PTZ	"	"	<0.0001	t = 6.73, df = 70	"	****
	PTZ-Base	"	"	<0.0001	t = 5.018, df = 70	"	****
16c Stage II count		Two-way RM ANOVA	PTZ - [Pb + PTZ]	0.0057	Treatment F (1, 34) = 8.695	n = 18 per treatment	**
16c Stage III count		Two-way RM ANOVA	PTZ - [Pb + PTZ]	<0.0001	Treatment F (1, 34) = 98.21	"	****
		Bonferroni's multiple comparison	Time	20-60min		30 comparisons	*
16e Survival		Barnard	+PTZ – Pb+PTZ	< 0.0001		n = 76 Pb+PTZ	****
17a Activity	TL + PTZ - TL + A43 + PTZ	Two-way RM ANOVA	Treatment	0.0021	F (1, 80) = 10.06	PTZ 36; A43+PTZ 46	**
			Time	<0.0001	F (9.402, 752.2) = 59.28; GG's epsilon = 0.1594	60	****
			Treatment x Time	<0.0001	F (59, 4720) = 6.136		****
		Bonferroni's multiple comparison	Time	PTZ : 8 -12 min		60 comparisons	*
17b Area Under the Curve	TL : Base	Mann-Whitney	PTZ - [A43 + PTZ]	0.9075	Mann-Whitney U = 815	PTZ 36; A43+PTZ 46	
	TL : PTZ	"	"	0.0024	Mann-Whitney U = 507	"	**
	TL : PTZ-Base	"	"	0.0448	Mann-Whitney U = 613.5	"	*
17c Stage II and III count	TL : stage II	Two-way RM ANOVA	PTZ - [A43 + PTZ]	0.1818	Treatment F (1, 34) = 1.858	n = 18 per treatment	
	TL : stage III	Two-way RM ANOVA	PTZ - [A43 + PTZ]	<0.0001	Treatment F (1, 34) = 116.7	"	****
		Bonferroni's multiple comparison	Time	16 - 52 min		30 comparisons	*
17d Activity	panx1b-/- + PTZ - panx1b-/- + A43 + PTZ	Two-way RM ANOVA	Treatment	0.0004	F (1, 75) = 13.51	PTZ 31; A43+PTZ 46	***
			Time	<0.0001	F (10.06, 754.6) = 42.79; GG's epsilon = 0.1705	60	****
			Treatment x Time	<0.0001	F (59, 4425) = 6.056		****
		Bonferroni's multiple comparison	Time	PTZ : 21 - 24 min		60 comparisons	*
17e Area Under the Curve	panx1b-/- : Base	Mann-Whitney	PTZ - [A43 + PTZ]	0.4053	Mann-Whitney U = 632	PTZ 31; A43+PTZ 46	
	panx1b-/- : PTZ	"	"	0.0005	Mann-Whitney U = 383	"	***
	panx1b-/- : PTZ-Base	"	"	0.0087	Mann-Whitney U = 462	"	**
17f Stage II and III count	panx1b-/- : stage II	Two-way RM ANOVA	PTZ - [A43 + PTZ]	0.0001	Treatment F (1, 34) = 18.77	n = 18 per treatment	***
	panx1b-/- : stage III	Two-way RM ANOVA	PTZ - [A43 + PTZ]	<0.0001	Treatment F (1, 34) = 133.5	"	****
		Bonferroni's multiple comparison	Time	22 - 60 min		30 comparisons	*

Supplementary figures							
S1 Pb Activity	**Base - Pb 50μM**	**Bonferroni's multiple comparison**	**Time**	**0 - 5 min**		**59 comparisons**	*
	Base - Pb 75μM	"	"	**0 - 5 min**		"	*
	Base - Pb 100μM	"	"	**0 - 4 min**		"	*
	PTZ - [Pb25μM + PTZ]	**Two-way RM ANOVA**	**Treatment**	**0.0154**	**F (1, 45) = 6.343**	**PTZ 30; Pb+PTZ 17**	*
	PTZ - [Pb50μM + PTZ]	**Two-way RM ANOVA**	**Treatment**	**<0.0001**	**F (1, 46) = 35.21**	**PTZ 30; Pb+PTZ 18**	****
		Bonferroni's multiple comparison	**Time**	**16 - 59 min**		**59 comparisons**	*
	PTZ - [Pb75μM + PTZ]	"	"	**<0.0001**	**F (1, 46) = 44.00**	**PTZ 30; Pb+PTZ 18**	****
		"	"	**16 - 59 min**		**59 comparisons**	***
	PTZ - [Pb100μM + PTZ]	"	"	**<0.0001**	**F (1, 46) = 50.74**	**PTZ 30; Pb+PTZ 18**	****
		"	"	**11 - 52 min**		**59 comparisons**	*